Fall 2013

Coupled Hydrologic And Hydraulic Models And Applications

Chi Chi Choi
University of Iowa

COUPLED HYDROLOGIC AND HYDRAULIC MODELS AND APPLICATIONS

by

Chi Chi Choi

A thesis submitted in partial fulfillment
of the requirements for the Master of
Science degree in Civil and Environmental Engineering
in the Graduate College of
The University of Iowa

December 2013

Thesis Supervisors: Associate Professor George Constantinescu
Adjunct Assistant Professor Ricardo Mantilla

Graduate College
The University of Iowa
Iowa City, Iowa

CERTIFICATE OF APPROVAL

_____

MASTER'S THESIS

_____

This is to certify that the Master's thesis of

Chi Chi Choi

has been approved by the Examining Committee
for the thesis requirement for the Master of Science
degree in Civil and Environmental Engineering at the December 2013
graduation.

Thesis Committee: _____
George Constantinescu, Thesis Supervisor

_____
Ricardo Mantilla, Thesis Supervisor

_____
Larry Weber

ACKNOWLEDGMENTS

I would like to acknowledge the invaluable guidance and encouragement of Dr. George Constantinescu and Dr. Ricardo in supervising this study. I would like to thank Dr. Larry Weber for taking time and effort to serve on my thesis committee. I would like to thank Dr. Witek Krajewski and Dr. Nathan Young for their valuable advice. I would like to acknowledge the financial support from Iowa Flood Center. The knowledge, skill and experience that I learnt here will be with me through my career. Lastly, I deeply thank my friends and especially my families for their unconditional support.

ABSTRACT

The use of hydraulic routing at regional scale was limited by the lack of accurate river topography and morphology, the high computation requirement and large amount of time setting up the hydraulic model. Since the advance development of LiDAR technology in recent centuries, it becomes feasible to extract the detailed river bathymetry directly in GIS environment.

In this study, automatic geo-processing tools are used to prepare the required river geometry input data to the hydraulic model. The developed hydraulic model solves the one dimensional Saint-Venant Equations (1D-SVE) by using the classical four-point weighted implicit Pressimann scheme. The 1D-SVE model is externally coupled with a link-based hydrological model, CUENCAS, to simulate 1D unsteady flow through a dendritic river networks. An application of the coupled H-H models is demonstrated in Clear Creek watershed, Iowa. Results are validated and calibrated with two USGS streamflow gauges and nine Iowa Flood Center (IFC) bridge sensors river stage measurements. Results show that the coupled H-H models improve the hydrologic predication capability and accuracy by adding more river stage measurements for model validation.

TABLE OF CONTENTS

LIST OF TABLES

LIST OF FIGURES

CHAPTER 1

INTRODUCTION

1.1 Motivation

Floods are one of the most common, costly natural disasters worldwide. For example in the US, floods caused 8.17 billion in damages and 89 deaths annually over the period 1983 to 2012 (NWS, 2012). Accurate flood prediction model can greatly reduce the flood damages costs. According to the National Weather Services (NWS, 2002), the total benefits from using the NWS hydrologic forecasts are 2.4 billion annually over the period 1981-2000 in US. Flood prediction and modeling refer to the processes of transformation of rainfall into a flood hydrograph throughout a watershed or any other hydrologic system (Ramirez, 2000). Accurate flood routing models provide explicit spatial and temporal information of flood peak attenuation and flood water levels that are crucial in flood forecasting operations and protection (Subramany, 2008).

The predicted flood water level can be used to generate flood inundation maps. These maps can help public, media, emergency mangers and others visualize the spatial extent and depth of flood waters (NWS, 2009). USGS Flood Inundation Mapping Program created static inundation map libraries at USGS stream gauges that are consisted of a set of flood extent and depth maps at various river stage intervals. A user can view real-time stage data and read the corresponding inundation maps to know the flood extent and depth. These maps are the simulation results from the steady-state hydraulic model based on pre-defined hydrologic inputs (e.g. design storm of a given recurrence interval) and does not represent actual storm event. An alternative to static map libraries is creation of dynamic inundation maps that are the simulation results from the unsteady-

state hydraulic model based on real-time hydrologic inputs (e.g. runoff generated from hydrologic model) derived from a realistic storm event.

Channel routing is a mathematical method (model) that can predict the timing of the peak, peak magnitude, and shape of a flood wave as it travels through a river network (Fread, D.L., 1985). Hydrologic and hydraulic routing are two common flow routing techniques that predict the spatial and temporal variation of a flood wave through a river network. Hydrologic routing is based on the continuity equation and storage-discharge relationships (typically empirical). It can reproduces a flood wave correctly when the assumed storage-discharge relationships are fitted relatively well to the actual flow dynamics characteristic in a river networks. Since these relationships are empirical-based that the river geometries are not considered, they cannot capture the dynamic properties of a flood wave which the channel/floodplain interaction and backwater effects due to downstream constriction are dominated. However, these flow dynamic characteristic can be well handled by hydraulic routing technique. Hydraulic routing attempts to solve the coupled continuity and momentum equations of one-dimensional Saint-Venant Equations (1D-SVE) which requires extensive physical-based data, such as river geometries and topographic information.

An important advantage of the 1D-SVE model is that it can calculate the flood propagation of river networks spatially and temporally, providing, simultaneously, predictions of stage and discharge, thus, stage measurements can be used to validate the flow propagation model and create both static and dynamic inundation maps. However, in order for the calculations associated to the 1D-SVE models to be accurate, the inflow/outflow boundary conditions, river bathymetric and topographic data must be

comparatively close to reality. In particular, the accuracy and availability of the topographic data has improved significantly with the advance of light detection and ranging systems (LiDAR) technology. However, LiDAR maps bathymetry do not capture the river bed features accurately (Cook, et al., 2009) which results in error prone riverbed profiles. These inaccuracies can lead to vertical offsets between the river stage measurement and the prediction. In addition, inflow boundaries (i.e. lateral runoff into channels) to the 1D-SVE model, following a rainfall event, are not measurable everywhere and they are driven by complex processes associated to hillslope surface runoff, soil water infiltration and the groundwater seepage. These uncertainties of river bathymetric and inflow boundaries limit the use of hydraulic routing in complex river networks. In additions, Hicks et al. (2005) suggested three reasons accounted for the limited use of hydraulic models for operational forecasting. First, there has not been strong evidence to convince officials to invest more funds for large-scale implementation of hydraulics modeling. Second, hydraulic models are more difficult to setup and model stability can be a concern. Third, forecasters have developed techniques to adjust hydrologic routing parameter to compensate for model inaccuracies.

Even with the aforementioned complications in mind, it is still attractive to solve the 1D-SVE because, in reality direct measurements of discharge are difficult and they form the basis for testing hydrologic routing methods. In contrast, the deployment of stream-stage gauges is easier and less expensive and they can provide dense, real-time river stage measurements at more locations within the river network. Therefore, these added measurement data can be used to evaluate the spatial and temporal accuracy of the runoff field generated from the hydrological model. Note that, in general, measurements

of river stage are converted to discharge by means of a rating curve. These indirect estimates of river discharge data are subject to uncertainties due to: (1) the error of stage and discharge measurements; (2) the hysteresis effect of a looped rating curve; and (3) the extrapolation of the rating curve beyond the measurement range (Fread, 1975; G Di Baldassarre et al., 2011). Moreover, the availability of the rating curves are usually limited to measured sites along the main stem of a river network which prohibits the direct comparison between the simulated discharge hydrographs from the hydrological model and river stage measurements that are primarily located on the tributaries. Another advantage of the 1D-SVE model is that the simulated stage-discharge relationship can be obtained for every computation nodes. The location of the nodes can be adjusted to provide an estimate of unknown rating curve for those river stage measurements locations.

The goal of the present work is to develop a physical-based 1D Saint-Venant PDEs solver that can be applied to calculate flood routing in river networks and can be coupled with the ODEs-based hydrological model for rainfall-runoff process. The hydrological model, CUENCAS, is used in the present work. Model parameters in CUENCAS are derived from the physical characteristic of the watershed and the measurement data (Cunha, 2012). A 1D-SVE model is developed with its set of GIS-based geo-processing tools that can simulate 1D unsteady flow through any dendritic river networks. The 1D-SVE model is validated with a test case and HEC-RAS. Furthermore, the runoffs generated from CUENCAS are used as the inflows (discharge) to the 1D-SVE model via the same geo-processing tools. The coupled hydrologic and hydraulic (H-H) model takes advantage of both stage and discharge data for model validation. It is implemented on a realistic rainfall event in the Clear Creek Watershed,

Iowa. After calibration of the coupled H-H models parameters, model is validated with measured data provided by IFC stream-stage sensor networks and USGS streamflow data. The coupled H-H models will be used to address some important research objectives that are discussed in the next section.

1.2 Research Objectives and Tasks

The overall objective of this study is to demonstrate the improved flood predictive capability of the coupled H-H models for a watershed with multiple stage gauging locations. To achieve this goal, two important objectives are identified:

1) Demonstrate that a 1D-SVE model is a better routing approach for some specific flow dynamics conditions (diffusive wave or dynamic wave).
2) Show that the results from the coupled H-H models can enhance hydrological model validation by providing a better spatial description of runoff field.

A series of research tasks have been identified to achieve the objectives mentioned above. These are listed below and specific progress in each one of them is presented in the main body of the document in Chapters 3 and 4. Specifically, the identified tasks are,

Task related to objective 1)

a) *Identify which streams require a 1D-SVE model*: A geo-processing tool is used to estimate the average bed slope for all the digitized streams for any selected watershed. These channel morphology data can be classified into three different flow regimes (kinematic, diffusive and dynamic) based on the slope regime classification recommended by National Weather Service (NWS, 2001). The flow dynamics characteristic of the 1D-SVE model is dynamic. One can infer the

spatial extent of the streams required for 1D-SVE model simulation, while the remaining streams can be modeled by the hydrological model.

Task related to objective 2)

a) *Evaluate the spatial accuracy of the runoff field generated by the hydrological model*: the simulated hydrographs (river stage and discharge) from the coupled H-H models and the measured values are compared to spatially evaluate the accuracy of the runoff generated from the hydrological model.

b) *Change parameters in the hydrological model (e.g. channel flow velocity, runoff coefficients) to better describe runoff generation fields*: Based on the results from step (a), the model parameters can be adjusted so as to have a better agreement of predicting the timing of the peak, peak value and the volume of a hydrograph with the measurement.

1.3 Outline and Contents

In Chapter 2 relevant literature related to the development and implementation of 1D-SVE models and coupled H-H models is reviewed. Chapter 3 describes the numerical algorithm implemented in the developed 1D-SVE model and the development of its own geo-processing tools needed to couple 1D-SVE model and the hydrological models (CUENCAS), and to set up simulations in natural watersheds. Chapter 4 discusses the results of various validation cases of different conditions for the 1D-SVE model. Finally, a real application of the coupled H-H models in the Clear Creek Watershed is presented. The accuracy of the hydrological model is compared with the coupled H-H models.

CHAPTER 2

LITERATURE REVIEW

The aim of this chapter is to discuss the development of the 1D-SVE model and the coupling with the hydrological model.

2.1 Governing Equations in the Hydraulic Model

The governing equations for the one-dimensional, unsteady, open-channel flow, known as, one-dimensional Saint-Venant equations (1D-SVE) can be written as,

Continuity:

$$\frac{\partial A}{\partial t} + \frac{\partial Q}{\partial x} - q = 0 \tag{2.1}$$

Momentum:

$$\frac{\partial Q}{\partial t} + \frac{\partial \left(\frac{\beta Q^2}{A}\right)}{\partial x} + gA\left(\frac{\partial h}{\partial x} + S_f\right) = 0 \tag{2.2}$$

where β = momentum correction factor, Q = discharge [m^3/s], A = flow area, g = gravitational acceleration [m/s^2], h = elevation of water surface measured from a horizontal datum [m], S_f = frictional slope, t = time [s] and x = distance measured along stream centerline [m]

The momentum equation 2.2 can also be written as a function of velocity, using $Q = AV$

$$\left(\frac{\partial A}{\partial t}\right) = \left(\frac{\partial A}{\partial y}\right)\left(\frac{\partial y}{\partial t}\right) = T\left(\frac{\partial y}{\partial t}\right); \left(\frac{\partial A}{\partial x}\right) = \left(\frac{\partial A}{\partial y}\right)\left(\frac{\partial y}{\partial x}\right) = T\left(\frac{\partial y}{\partial x}\right)$$

$y = h - z_b$; $S_0 = \frac{-\partial z_b}{\partial x}$, where T = top width of a cross section [m], y = flow depth [m], z_b = elevation of the channel bottom above the horizontal datum [m] and S_0 = channel bed slope

By multiplying both sides of equation 2.2 by g, the momentum equation can be written,

$$\frac{\partial V}{\partial t} + V\frac{\partial V}{\partial x} + g\frac{\partial y}{\partial x} - gS_0 + gS_f = 0 \qquad (2.3)$$

The first two terms in equation 2.3 are the local and convective acceleration. The third term is the pressure term. The fourth term is the gravity force term. The fifth term is the friction force term. The kinematic wave model considers the fourth and fifth terms. The diffusive wave model considers the third, fourth, and fifth terms. The dynamic wave model considers all the terms (Chow et al., 1988).

2.2 Use of Kinematic, Diffusive and Dynamic Wave Models

Two prime questions that needed to be addressed were, "*Where should we consider replacing storage-discharge-based hydrologic routing models with dynamic hydraulic models*?" and *"What accuracy should we expect from the hydraulic models?"* Some suggested answer to these questions are summarized (Reed, S., 2010). The selection of different simplified wave models depends mainly on the magnitude of bed slope (4^{th} term in equation 2.3). As a rule-of-thumb, United States Army Corp of Engineers (USACE, 1994) recommended the appropriate bed slope ranges and the total reach lengths for different wave models as shown in Table 2.1.

Table 2.1. Length of streams in different categories suggested by USACE (1994) classification

Category	Length (mi)	Percentage (%)	Rule-of-thumb Model Type
NWS hydraulic models	5501	6	
Slope <= 1 ft/mi (0.000189)	26236	22	Dynamic
1 ft/mi < Slope <= 10 ft/mi	71063	59	Diffusive
Slope > 10 ft/mi	17118	14	Kinematic

Table 2.1. Continued

Total	119916	100	

Source: Reed, S. (2010). Lessons Learned from Transitioning NWS Operational Hydraulic Models to HEC-RAS. Presented at the ASCE-EWRI World Water Congress 2010, Providence, RI.

Reed et al. (2010) used the above rule-of-thumb criterion to classify the rivers in the Contiguous United States (CONUS) as shown in Figure 2.1. Most National Weather Service (NWS) hydraulic models have been applied to rivers in the lowest slope regime (green lines) that represents only 21% of rivers with dynamic wave model necessity, but there are still many rivers in the medium slope regimes (brown lines) where the diffusive wave model are recommended. The accuracy of NWS hydraulics models applied to Tar River (T), Columbia River (C), Upper Mississippi (M), Ohio-Miss Cincinnati ORCM (O), and Lower Miss-Ohio Smithland (L) (Fig. 2.1) was assessed in comparisons with data shown in Figure 2.2. It was reported that the simulated river stage of the five hydraulic models is less than 5% root mean square errors disregarding to a different flood level. The details of each model's characteristics are given in Reed et al. (2010),

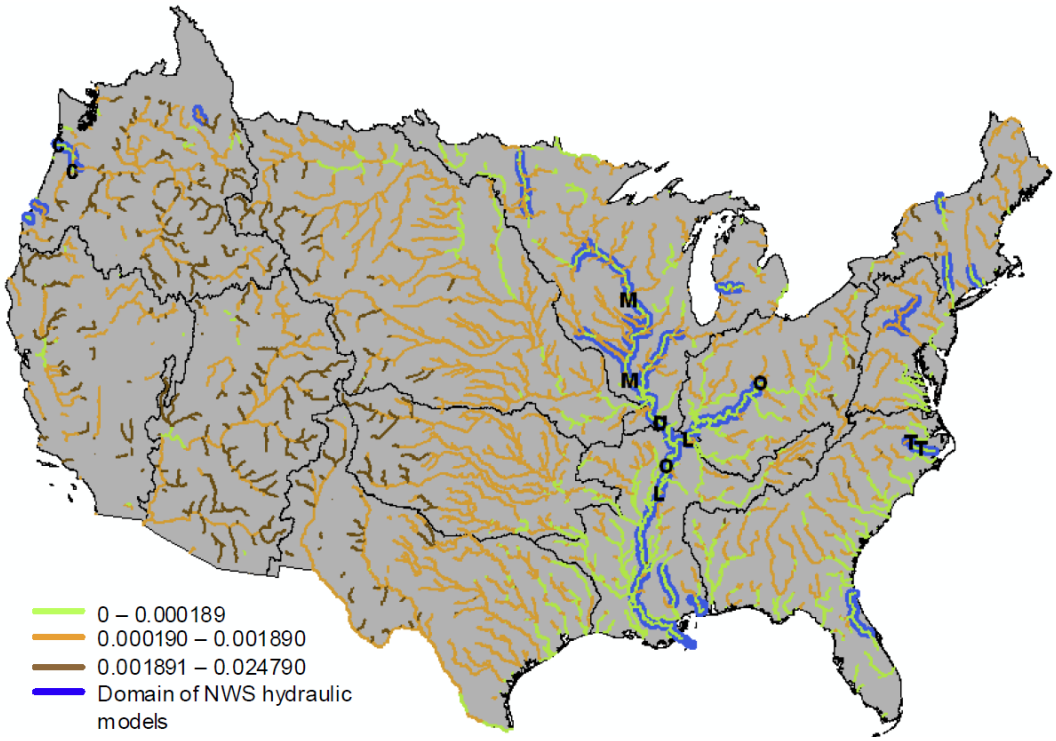

Figure 2.1. Slope regimes classification of rivers in CONUS

Source: Reed, S. (2010). Lessons Learned from Transitioning NWS Operational Hydraulic Models to HEC-RAS. Presented at the ASCE-EWRI World Water Congress 2010, Providence, RI.

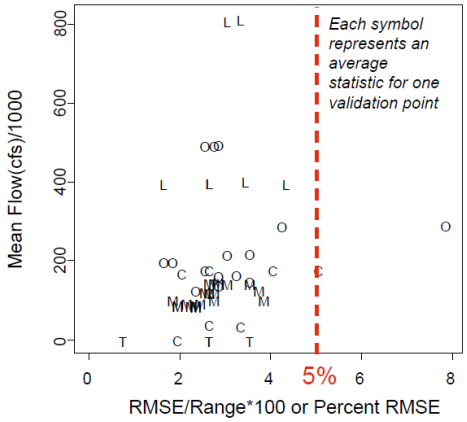

	Model Length (km)	Avg. cross-section spacing (km)
Tar River (T)	77	0.9
Columbia River (C)	304	2.8
Upper Mississippi (M)	724	4.6
Lower Miss-Ohio Smithland (L)	716	14.9
Ohio-Miss Cincinnati (O)	1320	1.4

Figure 2.2. Statistical analysis of the accuracy of five NWS hydraulic models

Source: Reed, S. (2010). Lessons Learned from Transitioning NWS Operational Hydraulic Models to HEC-RAS. Presented at the ASCE-EWRI World Water Congress 2010, Providence, RI.

Most of the streams characteristized by the steep slopes can be simulated with a simplified approach (e.g. kinematic wave model), while the dynamic or at least the diffusive wave model should be considered for streams with respect to the mild slopes to better capture the more complex flow dynamics characteristic, such as the backwater effect due to downstream constrictions (e.g. culverts, bridges and weirs).

Ponce et al. (1978; 1991) applied sinusoidal perturbations to the steady uniform flow with a wide rectangular shape, applicable to both the kinematic wave and diffusive models for flood routing within 95% accuracy. He recommended using the kinematic wave model if the inequality below holds:

$$\frac{T_r S_0 u_o}{d_0} > 85.5 \; for\ kinematic\ wave\ model \tag{2.4}$$

and diffusive wave model if the inequality below holds:

$$T_r S_0 \left(\frac{g}{d_0}\right)^{1/2} \geq 30 \text{ for diffusive wave model} \tag{2.5}$$

where T_r = time of rise of the flood wave [s]; S_0 = bed slope [m/m]; u_0 = mean flow velocity [m/s]; d_0 = flow depth; $\tau = \frac{T_r S_0 u_0}{d_0}$ = dimensionless wave period

Getirana et al. (2013) performed a large scale flow dynamics classification analysis in the Amazon Basin. It is based on the Moussa et al. (1996) method that depends on the magnitude of the dimensionless wave period (see equation 2.5) and the Froude number ($Fr = \frac{u_0}{\sqrt{g d_0}}$). These variables ($T_r, S_0, u_0, d_0$) are estimated either from the in-situ discharge measurement (T_r), the Shuttle Radar Topography Mission (SRTM)-derived bed elevation (S_0), and the Manning's equation with a rectangular river cross section assumption (u_0, d_0).

Although the criteria given by equations 2.4 and 2.5 are empirical and only validated for some particular cases, they were proved to be a fairly good first-order applicability criterion (Singh et al., 1996). By combining these criteria and the general rule-of-thumb described before, one can approximately determine where to use kinematic, diffusive and dynamic wave model to accurately predict flood propagation. The inflows of the 1D-SVE model are the runoff generated from either a hydrological model, or the design storm based on historical flood records with a different recurrence interval.

2.3 Numerical Method for Solving 1D-SVE

Since these nonlinear PDEs (equations 2.1 and 2.2) cannot be solved analytically, the approximate numerical solutions can be obtained by using either the method of characteristics (Strelkoff, 1970; Abbott, 1975; Ligget and Cunge, 1975; Abbott and Basco, 1989; Strelkoff and Falvey, 1993), the finite element method (Abbott and Basco, 1989; Lai, 1986), or the finite difference method (Ligget and Cunge, 1975; Abbott, 1979; Abbott and Basco, 1989; Cunge et al., 1980; Strelkoff and Falvey, 1993). The finite difference method outweighs the others due to its robustness and simplicity. Finite difference schemes are either explicit or implicit in time. Implicit schemes are more desirable than explicit schemes because they allow obtaining solution for higher Courant-Friedrich-Levy (CFL) conditions, which also allows for longer time steps in the simulation.

The four-point weighted implicit Preissmann scheme (box scheme) is the most popular scheme used in some of the most popular commercial and renewed codes based on 1D-SVE models, such as HEC-RAS (Brunner 2010a, 2010b), CCCHE1D (Wu and Vieira, 2000), DUFLOW (Clemmens et al., 1993) and others. The Preissmann scheme is

most suitable for relatively flat watersheds where bed slopes are less than 0.003, and no dry-bed conditions occur during the simulation (Ogden et al., 2002). It is valid for purely sub-critical or supercritical flow. The use of Preissmann scheme should be ended for applications where flow regime is trans-critical (Meselhe et al., 1997) because of the mismatch of boundary conditions requirements for different flow regimes. In order to overcome this problem, the suppression of the convective acceleration terms in the momentum equations (2^{rd} term in Equation 2.2) is used to ensure the flow does not leave the sub-critical regime (Havno et al., 1985; Abbott et al., 1991). The convective acceleration term is reduced by multiplying a factor which is expressed as a function of local average of Froude number in computational points (Kutija et al., 1993; Djordevic et al., 2004) which controls the flow to be subcritical. According to the recommendation for the implementation of 1D-SVE model for different bed slope regimes (Reed et al., 2010), this invalidity problem of the usage of Preissmann schemes becomes non-crucial as the flood routing among the steep mountain streams can be replaced by the much simpler, more efficient hydrologic routing method.

A large system of nonlinear PDEs is formed through the discretization of the 1D-SVE for a river network, using the Preissmann scheme with the addition of the interior boundaries and inflow/outflow boundaries. The nonlinear system is linearized over a discrete time Δt using the Newton-Raphson method. The Newton-Raphson method is used to obtain an approximate solution of the systems of nonlinear equations. The iterations are stopped once the computed residual of the solution is reduced below a preset tolerance. The implementation details of the Newton-Raphson method are given in

Chapter 3. The system of linear equations results from Newton-Raphson method is solved by either Gaussian-elimination or another matrix inversion method.

The double-sweep method takes advantage of the banded nature of the system of equations and is deemed the most efficient method for solving such systems of equations. For simulating flow in a river network, the addition of boundary conditions results in a non-banded sparse matrix that creates a large computation burden in storing and solving the matrix. Numerous studies have focused on how to improve the solution algorithm for such cases. Other studies (Choi et al., 1993; Nguyen et al., 1995) developed a specific node-numbering scheme to reduce the size of the coefficient matrix from 2N x 2N to 2N x 4, where N is the number of computation nodes. This method is applicable to non-looped channel networks containing junctions of up to four branches. Islam et al (2005), Sen and Garg (1998; 2002) adopted a three-phase algorithm to reduce the burden of the active matrix storage requirement to only 4M x 4M, where M is the number of branches. Zhu et al. (2011) proposed a junction-point water stage prediction and correction (JPWSPC) method to further enhance the solution algorithm by breaking up the computation individually, and thus avoiding the large computation effort required during the formation and solution of the global branch system of equations. They reported about 28 to 39% reductions in computation time over the solution algorithms used by Sen and Garg (2002) and Islam et al. (2005).

2.4 1D-SVE Model and the Coupling with a Hydrological Model

1D-SVE models have been widely applied in simulating unsteady flow in river reaches (e.g. Hicks et al., 2005) and river networks (e.g. see Paz et al., 2009; Pramanik et al., 2009). Although recent advance in the two (2D) and three dimensional (3D)

hydrodynamic modeling of flow in rivers, one dimensional SVE based hydrodynamic models are the most popular choice for solving large-scale river engineering problems owing to their reduced computational cost and data requirements compared to those for 2D and 3D models. The main assumptions of the 1D-SVE models are: (1) the flow is close to uniform over the cross section. (2) The streamline curvature is small and the hydrostatic pressure assumption is valid. (3) Boundary friction and turbulence can be accounted for by employing resistance laws analogous to those used for steady state flow (Chezy or Manning's equation). (4) The average channel bed slope is small (Zeng, 2006).

However, not much large-scale implementations of 1D-SVE models for high density networks are available in the literature. High density networks are referred to stream network with high branching complexities that usually have a large stream Horton-Strahler order. The smallest tributaries are classified as the first order streams. When two first order streams join, a second order stream is designated and so on for two, three, etc. When two streams of different order join, the stream keeps the order of the higher order stream. This classification is widely used and name as Strahler order. One possible reason is that the flow dynamics are site-specific, such that a simplified form of SVE (i.e. kinematic/diffusive) wave approximate are sufficiently accurate or backwater effects and floodplain storage are not significant. Another reason is the lack of accurate river topography at the regional or global scale which results in using parameterized cross-section shapes derived from the relatively coarse river topography data, SRTM Digital Elevation Model (DEM). Paz et al. (2009) proposed to use GIS-based automatic procedures to combine the detailed surveyed cross-sectional data related to the main channel and the elevation values related to the floodplain from the SRTM DEM. Bravo et

al. (2011) coupled 1D-SVE model of Paz et al. (2009) with a distributed large-scale hydrological model, MGB-IPH, to simulate the unsteady flow in the Upper Paraguay River Basin (UPRB) and reported satisfactory results. For simulating large river networks, such as the Amazon River (channel width up to 1.0-1.6 km at low stages), the assumption of a rectangular cross-section shape becomes acceptable, and the complex channel/floodplain interaction can be simplified as a dead storage area with zero flow velocity on the floodplain (Pavia et al., 2011, 2013a, b). Table 2.2 and 2.3 summarize some recent applications of 1D-SVE models and coupled H-H models to simulate unsteady flow in river networks.

Abshire (2012) coupled 1D-SVE model (HEC-RAS) with a distributed hydrological model, HLRDHM to simulate the unsteady flow in the Tar River Basin. Results verify that the coupled H-H models performance are relied on the accuracy of the boundary conditions provided by the hydrological model. Uncertainty from the boundary conditions may double the total uncertainty compared to the routing parameters alone (Scharrffenberg et al., 2011).

Table 2.2. Examples of 1D-SVE models used to simulate flood wave in river networks

Model Names, Citation	Location and Length	Model Setup	DEM-derived Cross-Section Description
HEC-RAS (Hicks et al., 2005) Four point implicit finite difference Preissmann scheme	Peace River, Canada, 1107 km	1 reach, 1107 cross sections, Δx=1km, Time step=6h, Boundary condition: Point discharge time series as lateral inflow River stage and discharge are validated at control points	57 surveyed cross sections with approximated rectangular shape and bed slope
HEC-RAS (Paz et al., 2009)	Upper Paraguay River, 4800 km	24 reaches, 1124 cross sections, Δx=5km, Time step=1h, Boundary conditions: Discharge time series Discharge are validated at control points	Composed SRTM DEM (90 m) and surveyed cross sections by the GIS-based automation procedures
MIKE-11 (Pramanik et al., 2009) Six point implicit finite difference Abbott-Ionescu scheme	Brahmani river basin, India, ~380 km	7 reaches, 40 cross sections, Δx=0.5-2km, Boundary conditions: upstream discharge and downstream stage time series No lateral inflows Stage and discharge are validated at control points	Modified the SRTM DEM (90 m) cross sections by a r.m.s.e. error of 127 survey's points and compared the computed conveyance for 4 measured cross-section profiles

Table 2.3. Summary of the recent examples of large-scale implementation of the coupled H-H models

Model Names, Citation	Location and Length	Model Setup	River Cross Sections Representation
MGB-IPH, hydrological model 1D-SVE model, Four point implicit finite difference Preissman scheme (Paiva et al., 2011, 2013a)	Solimoes, Amazon River basin, ~2.5 x 10^4 km	432 reaches, 2492 cross sections, Δx=10km, Time step=1h Stage and discharge are validated at control points	SRTM DEM (500 m), Rectangular, Width derived from $B = aA_d^b$, Floodplain storage model (Cunge et al., 1980)
Same as above (2013b)	Amazon River basin, ~ 1.0 x 10^5 km	1728 reaches, ~10,000 XS, Δx=10km, Time step=1h, Stage and discharge are validated at control points	Same as above (Paiva et al., 2013a)
MGB-IPH, hydrological model HEC-RAS (Bravo et al., 2011)	Entire UPRB, 4800 km	Same as (Paz., 2009), Δx=5 km, Time step=12h, Boundary conditions: Inflow and lateral inflow estimated by MGB-IPH model Discharge are validated at control points	Composed SRTM DEM (90 m) and surveyed XS by the GIS-based automation procedures
Eau-Dyssee, hydrological model HEC-RAS (Saleh et al., 2012)	Serein River, 89 km	1 reach, 20 cross sections, Δx=100m, Time step=0.5-3h, Boundary conditions: Inflow and lateral inflows by Eau-Dyssee	20 surveyed cross sections and the remaining are linearly interpolated
HLRDHM, hydrological model HEC-RAS (Abshire, 2012)	Tar River, 81 km	9 reaches, 800 cross sections, Δx=0.5-1km, Time step=1h, Stage and discharge are validated	Survey cross sections and interpolated cross sections

2.5 Modern Approach to Obtain Streambed Topography and Its Impact

The most common methods for obtaining river bathymetry are large-scale boat surveys and small-scale walking surveys. Walking surveys supplemented the boat surveys by providing the river bed measurements for shallow water area that is not navigable. The boat surveys use the boat-mounted acoustics, such as single or multi-beam SONAR (Sound Navigation and Ranging) and ADCP (Acoustic Doppler Current Profiler) linked with RTK GPS (Real Time Kinematic Global Positioning System) equipment to obtain the required position, the water surface elevations and the flow depth. The final river bathymetry is obtained through post-processing (Hilldale et al., 2008). For the walking surveys, the surveyor carries a survey rod mounted with a GPS receiver to measure the above variables directly without the need for post-processing.

In the applications of the remote-sensing technology in natural watersheds, LiDAR-derived DEM can be used to predict the streambed topography. It provides a much larger and denser coverage as compared with traditional land survey methods. However, LiDAR-derived measurements of streambed topography are sometimes, subject to significant errors, especially in regions where flow is relatively shallow. These errors can be attributed to the backscatter effect of LiDAR, non-distinguishable pulses returned from water surface and streambed. Hence, the LiDAR-derived longitudinal streambed profiles tend to underestimate the depth of the actual streambed profiles. The accuracy of Airborne LiDAR bathymetry (ALB) was investigated on the Yakima River in Washington State (Hilldale et al., 2007). The mean vertical error between the ALB and the surveyed data fell between 0.10 and 0.27 meter, while the standard deviation ranged from 0.12 to 0.31 m. This work coincides with my analysis in Clear Creek Watershed, Iowa. The difference in channel bottom elevations between the LiDAR-derived DEM and the surveyed cross sections (Lee, personal communcation) for eleven measured sites ranges from 0.1 to 1.8 meter (Fig. 4.14). It indicates that the precision of streambed topography estimated by LiDAR-derived DEM is subject to significant errors, and the accurate representation of bed elevation is critical in predicting the river stage through the hydraulic routing simulation. As the traditional surveying methods are time consuming and labor intensive. New methodologies were developed to take into account the difference between the LiDAR measurements and actual measurements.

Multiple corrections to these problems have been suggested. Pramanik et al. (2009) modified the river cross sections derived from Shuttle Radar Topographic Missing (SRTM) DEM data by subtracting the root mean square error (RMSE) value calculated

based on the elevation difference estimated at 127 sections between measured data form direct surveying and the corresponding measurements using SRTM. Hicks et al (1996) and Blackburn et al (2002) evaluated the reliability of a hydraulic routing model with limited field data over a long reach, Peace River, Canada. Limited field data was used to set up the simulation. They discuss in particular what are affected by errors in bathymetry. Since there is limited survey river cross-sectional data, the effective bed elevation was estimated by projecting the measured water surface slopes to where the projected water surface slope is as close as possible to the survey bed elevation. Saleh et al (2012) performed a similar study by evaluating the effect of bed elevation and cross-sectional shape on the simulated river stage on the Serein River in France. The length of the simulated river reach was 89 km. These studies concluded that the prediction of the local flood stage requires accurate prediction of bed elevation on a section-by-section basis. However, they found that the time at which the peak occurs and the relative change of river stage can still be captured with some vertical offset of which is due to the constant bed slope assumption. No significant effect on discharge prediction even the constant bed slope is assumed. Roughness and channel gradient controls the peak arrival time of discharge and stage, and these variables are not sensitive to the change of channel geometry.

2.6 Effect of the Floodplain Storage on Flood Attenuation

Floodplain storage is an essential process to consider predicting the peak flood attenuation in highly agricultural and urbanized areas. Consequently, 1D-SVE models should have the capability to account in a realistic way for floodplain storage during flood events. Many flood attenuation studies (Campbell et al., 1972; Wolff et al., 1994;

Woltemade et al., 1994; Acreman et al., 2003; Turner-Gillespie et al., 2003; Liu et al., 2004; Anderson et al., 2006; Ghavasieh et al., 2006; Sholtes et al., 2011) concluded that the peak discharge attenuation is affected by bed slope, floodplain width, and floodplain roughness. Most of their studies adopted the design inflow derived from historical flood records to investigate the impact of the main variables affecting peak discharge attenuation. Liu et al. (2004) measured the effects of increasing channel roughness and sinuosity of all first and second order streams with a distributed hydrological model.

CHAPTER 3

DEVELOPMENT OF 1D-SVE MODEL

3.1 Introduction

In the 1D-SVE code developed as part of the present work, the standard four-point weighted Preissmann scheme is used to solve the dynamic wave form of the 1D-SVE. The channel/floodplain interaction of the hydraulic routing was embedded in the modified 1D-SVE (Fread et al., 1976). There are two major assumptions associated with this approach. First, the water surface elevation is assumed to be the same across the channel and the floodplain. Second, the friction slopes in the channel and the floodplain are assumed to be equal. The reach lengths of the channel and the floodplain can be different, but in the present study they are assumed to be equal. Several test cases are used to validate the solution of the 1D-SVE solver in the present 1D-SVE model.

3.2 Numerical Algorithms used in the 1D-SVE Model

The steady state solution of the governing equations is found prior to performing unsteady state simulation. The discharge and stage variables at each computation node are assigned to be constant. The value of the baseflow at the outlet is estimated based on the variables from the observed hydrograph at the outlet. There are three options for setting the inflow boundaries: (1) Assign a constant value of inflows at each exterior reach, (2) Assign a constant value of lateral inflows along every reach, or (3) Assign inflow at each exterior reach supplemented by a lateral inflow along every reach. For all three options, the sum of the inflows should be equal to the estimated baseflow value at the outlet. Once the steady state solution is obtained, the discharge and stage values computed at each node become the initial conditions of the unsteady flow simulation.

The modified forms of the 1D-SVE (equations 2.1 and 2.2) that include the channel/floodplain interaction (Fread et al., 1976 and 78) are given below.

Continuity Equation for Channel:

$$\frac{\partial A_c}{\partial t} + \frac{\partial Q_c}{\partial x_c} = 0 \tag{3.1}$$

Momentum Equation for Channel:

$$\frac{\partial Q_c}{\partial t} + \frac{\partial \left(\frac{{Q_c}^2}{A_c}\right)}{\partial x_c} + gA_c\left(\frac{\partial h_c}{\partial x_c} + S_{fc}\right) = 0 \tag{3.2}$$

where Q = discharge [m^3/s], A = flow area, g = gravitational acceleration [m/s^2], h = elevation of water surface measured from a horizontal datum [m], S_f = friction slope, t = time [s] and x = displacement in the main flow direction [m]

Continuity Equation for Floodplain:

$$\frac{\partial A_f}{\partial t} + \frac{\partial Q_f}{\partial x_f} = 0 \tag{3.3}$$

Momentum Equation for Floodplain:

$$\frac{\partial Q_f}{\partial t} + \frac{\partial \left(\frac{{Q_f}^2}{A_f}\right)}{\partial x_f} + gA_f\left(\frac{\partial h_f}{\partial x_f} + S_{ff}\right) = 0 \tag{3.4}$$

The subscript, "c" denotes the variables pertaining to the river channel and the subscript, "f" denotes the variables pertaining to the floodplain

By adding equations 3.1 and 3.2 and respectively the equations 3.3 and 3.4, one obtains

$$\frac{\partial A_c}{\partial t} + \frac{\partial A_f}{\partial t} + \frac{\partial Q_c}{\partial x_c} + \frac{\partial Q_f}{\partial x_f} = 0 \tag{3.5}$$

or

$$\frac{\partial A}{\partial t} + \frac{\partial Q_c}{\partial x_c} + \frac{\partial Q_f}{\partial x_f} = 0 \tag{3.6}$$

and

$$\frac{\partial Q_c}{\partial t}+\frac{\partial Q_f}{\partial t}+\frac{\partial\left(\frac{{Q_c}^2}{A_c}\right)}{\partial x_c}+\frac{\partial\left(\frac{{Q_f}^2}{A_f}\right)}{\partial x_f}+gA_c\left(\frac{\partial h_c}{\partial x_c}+S_{fc}\right)+gA_f\left(\frac{\partial h_f}{\partial x_f}+S_{ff}\right)=0 \quad (3.7)$$

or

$$\frac{\partial Q}{\partial t}+\frac{\partial\left(\frac{{Q_c}^2}{A_c}\right)}{\partial x_c}+\frac{\partial\left(\frac{{Q_f}^2}{A_f}\right)}{\partial x_f}+gA_c\frac{\partial h_c}{\partial x_c}+gA_f\frac{\partial h_f}{\partial x_f}+gAS_{fc}=0 \quad (3.8)$$

where the total flow is the sum of the channel and floodplain flow ($Q_T = Q_c + Q_f$)

The ratio of $\frac{Q_c}{Q_T}$ is assumed to be equal to the ratio of the conveyance (equation 3.9)

$$\phi=\frac{Q_c}{Q_T}=\frac{K_c}{K_T}\rightarrow\frac{Q_c}{K_c}=\frac{Q_T}{K_T} \quad (3.9)$$

where K is the flow conveyance

$$1-\phi=\frac{Q_f}{Q_T}=\frac{K_f}{K_T}\rightarrow\frac{Q_f}{K_c}=\frac{Q_T}{K_T} \quad (3.10)$$

Using equations 3.9 and 3.10, one can show that

$$\frac{Q_c}{K_c}=\frac{Q_f}{K_f}=\frac{Q_T}{K_T}\rightarrow S_{fc}=S_{ff}=S_{fT} \quad (3.11)$$

which is a standout assumption in 1D-SVE equations applied for channels with floodplains

The continuity equation 3.6 and momentum equation 3.8 are discretized by using the implicit Preissmann scheme (Chaudhry, 1993). The discretized form of these equations is given below.

Continuity:

$$\frac{(A_{i+1}^{n+1}+A_i^{n+1})-(A_{i+1}^{n}+A_i^{n})}{2\Delta t}$$

$$+\theta\frac{(\phi_{i+1}Q_{i+1}^{n+1}-\phi_iQ_i^{n+1})}{\Delta x_c}+(1-\theta)\frac{(\phi_{i+1}Q_{i+1}^{n}-\phi_iQ_i^{n})}{\Delta x_c}$$

$$+\theta\frac{[(1-\phi_{i+1})Q_{i+1}^{n+1}-(1-\phi_i)Q_i^{n+1}]}{\Delta x_f}+(1-\theta)\frac{[(1-\phi_{i+1})Q_{i+1}^{n}-(1-\phi_i)Q_i^{n}]}{\Delta x_f}$$

$$=0 \qquad (3.12)$$

where θ is the temporal weighting coefficient, and the recommended ranges for accuracy and stability is, $0.55 \le \theta \le 0.6$ (Fread, 1975; Schaffranek et al., 1981)

Momentum:

$$\frac{(Q_{i+1}^{n+1}+Q_i^{n+1})-(Q_{i+1}^{n}+Q_i^{n})}{2\Delta t}$$

$$+\frac{\theta}{\Delta x_c}\left[\frac{(\phi_{i+1})^2(Q_{i+1}^{n+1})^2}{A_{c_{i+1}}^{n+1}}-\frac{(\phi_i)^2(Q_i^{n+1})^2}{A_{c_i}^{n+1}}\right]+\frac{(1-\theta)}{\Delta x_c}\left[\frac{(\phi_{i+1})^2(Q_{i+1}^{n})^2}{A_{c_{i+1}}^{n}}-\frac{(\phi_i)^2(Q_i^{n})^2}{A_{c_i}^{n}}\right]$$

$$+\frac{\theta}{\Delta x_f}\left[\frac{(1-\phi_{i+1})^2(Q_{i+1}^{n+1})^2}{A_{f_{i+1}}^{n+1}}-\frac{(1-\phi_i)^2(Q_i^{n+1})^2}{A_{f_i}^{n+1}}\right]$$

$$+\frac{(1-\theta)}{\Delta x_f}\left[\frac{(1-\phi_{i+1})^2(Q_{i+1}^{n})^2}{A_{f_{i+1}}^{n}}-\frac{(1-\phi_i)^2(Q_i^{n})^2}{A_{f_i}^{n}}\right]$$

$$+g\theta\frac{\left(A_{c_{i+1}}^{n+1}+A_{c_i}^{n+1}\right)}{2}\frac{(h_{i+1}^{n+1}-h_i^{n+1})}{\Delta x_c}$$

$$+g(1-\theta)\frac{\left(A_{c_{i+1}}^{n}+A_{c_i}^{n}\right)}{2}\frac{(h_{i+1}^{n}-h_i^{n})}{\Delta x_c}$$

$$+g\theta\frac{\left(A_{f_{i+1}}^{n+1}+A_{f_i}^{n+1}\right)}{2}\frac{(h_{i+1}^{n+1}-h_i^{n+1})}{\Delta x_f}$$

$$+g(1-\theta)\frac{\left(A_{f_{i+1}}^{n}+A_{f_i}^{n}\right)}{2}\frac{(h_{i+1}^{n}-h_i^{n})}{\Delta x_f}$$

$$+g\theta\frac{(A_{i+1}^{n+1}+A_i^{n+1})}{2}\frac{\left(S_{f_{i+1}}^{n+1}+S_{f_i}^{n+1}\right)}{2}+g(1-\theta)\frac{(A_{i+1}^{n}+A_i^{n})}{2}\frac{\left(S_{f_{i+1}}^{n}+S_{f_i}^{n}\right)}{2}$$

$$=0 \qquad (3.13)$$

$$S_f = \frac{n^2 P^{4/3} Q|Q|}{A^{10/3}}$$

$$\frac{\partial (S_f)_i}{\partial Q_i} = \frac{2n^2 {P_i}^{4/3} |Q_i|}{{A_i}^{10/3}}$$

$$\frac{\partial (S_f)_i}{\partial h_i} = \frac{n^2 Q_i |Q_i|}{{A_i}^{20/3}} \left(\frac{4}{3} {P_i}^{1/3} \frac{\partial P_i}{\partial h_i} {A_i}^{10/3} - \frac{10}{3} {A_i}^{7/3} \frac{\partial A_i}{\partial h_i} {P_i}^{4/3} \right)$$

When differentiating the continuity and momentum equations 3.12 and 3.13 with respect to $Q_i, Q_{i+1}, h_i, h_{i+1}$, one can estimate additional derivatives, $\frac{\partial C_i}{\partial Q_i}, \frac{\partial C_i}{\partial Q_{i+1}}, \frac{\partial C_i}{\partial h_i}, \frac{\partial C_i}{\partial h_{i+1}}, \frac{\partial M_i}{\partial Q_i}, \frac{\partial M_i}{\partial Q_{i+1}}, \frac{\partial M_i}{\partial h_i}, \frac{\partial M_i}{\partial h_{i+1}}$. Their expressions are given below.

Coefficient:

$$\frac{\partial C_i}{\partial Q_i} = \frac{-\phi_i \theta}{\Delta x_c} - \frac{(1-\phi_{i)}\theta}{\Delta x_f}$$

$$\frac{\partial C_i}{\partial h_i} = \frac{1}{2\Delta t} \frac{\partial A_{c_i}}{\partial h_i} + \frac{1}{2\Delta t} \frac{\partial A_{f_i}}{\partial h_i}$$

$$\frac{\partial C_i}{\partial Q_{i+1}} = \frac{\phi_{i+1} \theta}{\Delta x_c} + \frac{(1-\phi_{i+1)}\theta}{\Delta x_f}$$

$$\frac{\partial C_i}{\partial h_{i+1}} = \frac{1}{2\Delta t} \frac{\partial A_{c_{i+1}}}{\partial h_{i+1}} + \frac{1}{2\Delta t} \frac{\partial A_{f_{i+1}}}{\partial h_{i+1}}$$

$$\frac{\partial M_i}{\partial Q_i} = \frac{1}{2\Delta t} - \frac{2\theta Q_i \phi_i}{A_{c_i} \Delta x_c} - \frac{2\theta Q_i (1-\phi_i)}{A_{f_i} \Delta x_f} + g\theta \frac{(A_{i+1} + A_i)}{4} \frac{\partial (S_f)_i}{\partial Q_i}$$

$$\frac{\partial M_i}{\partial h_i} = \frac{\theta}{\Delta x_c} \frac{(Q_i)^2 (\phi_i)^2}{(A_{c_i})^2} \frac{\partial A_{c_i}}{\partial h_i} + \frac{\theta}{\Delta x_f} \frac{(Q_i)^2 (1-\phi_i)^2}{(A_{f_i})^2} \frac{\partial A_{f_i}}{\partial h_i} - g\theta \frac{(A_{c_{i+1}} + A_{c_i})}{2\Delta x_c}$$

$$- g\theta \frac{(A_{f_{i+1}} + A_{f_i})}{2\Delta x_f} + g\theta \frac{(h_{i+1} - h_i)}{2\Delta x_c} \frac{\partial A_{c_i}}{\partial h_i} + g\theta \frac{(h_{i+1} - h_i)}{2\Delta x_f} \frac{\partial A_{f_i}}{\partial h_i}$$

$$+ g\theta \frac{((S_f)_{i+1} + (S_f)_i)}{4} \frac{\partial A_i}{\partial h_i} + g\theta \frac{(A_{i+1} + A_i)}{4} \frac{\partial (S_f)_i}{\partial h_i}$$

$$\frac{\partial M_i}{\partial Q_{i+1}} = \frac{1}{2\Delta t} + \frac{2\theta Q_{i+1}\phi_{i+1}}{A_{c_{i+1}}\Delta x_c} + \frac{2\theta Q_{i+1}(1-\phi_{i+1})}{A_{f_{i+1}}\Delta x_f} + g\theta\frac{(A_{i+1}+A_i)}{4}\frac{\partial(S_f)_{i+1}}{\partial Q_{i+1}}$$

$$\frac{\partial M_i}{\partial h_{i+1}} = \frac{-\theta}{\Delta x_c}\frac{(Q_{i+1})^2(\phi_{i+1})^2}{(A_{c_{i+1}})^2}\frac{\partial A_{c_{i+1}}}{\partial h_{i+1}} - \frac{\theta}{\Delta x_f}\frac{(Q_{i+1})^2(1-\phi_{i+1})^2}{(A_{f_{i+1}})^2}\frac{\partial A_{f_{i+1}}}{\partial h_{i+1}}$$

$$+ g\theta\frac{(A_{c_{i+1}}+A_{c_i})}{2\Delta x_c} + g\theta\frac{(A_{f_{i+1}}+A_{f_i})}{2\Delta x_f} + g\theta\frac{(h_{i+1}-h_i)}{2\Delta x_c}\frac{\partial A_{c_{i+1}}}{\partial h_{i+1}}$$

$$+ g\theta\frac{(h_{i+1}-h_i)}{2\Delta x_f}\frac{\partial A_{f_{i+1}}}{\partial h_{i+1}} + g\theta\frac{((S_f)_{i+1}+(S_f)_i)}{4}\frac{\partial A_{i+1}}{\partial h_{i+1}}$$

$$+ g\theta\frac{(A_{i+1}+A_i)}{4}\frac{\partial(S_f)_{i+1}}{\partial h_{i+1}}$$

These coefficients are used to build the system of equations of the 1D-SVE. Finally, the Newton Raphson method is used to obtain the unknown discharge and stage at each timestep.

A five-branch river network example is used to explain how the system of equations is formulated and solved for networks containing multiple branches. Figure 3.1 depicts the river network schematic and the notation used.

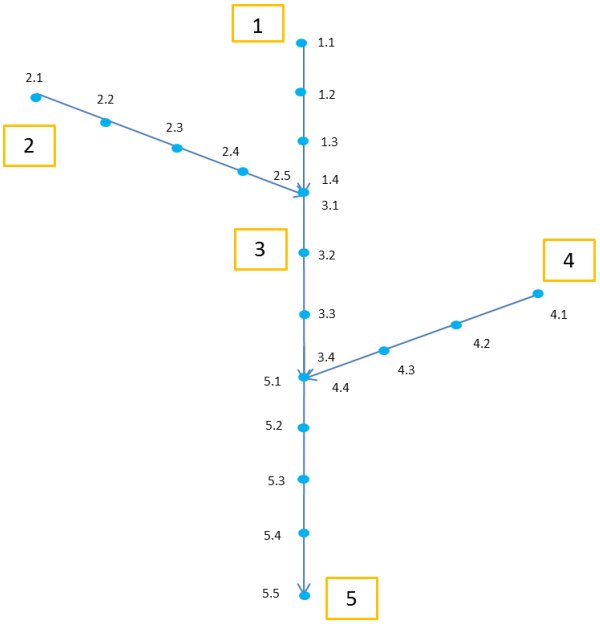

$$
\begin{aligned}
&B_{1.1}[Q_{1.1}^{n+1}, h_{1.1}^{n+1}] = 0 \\
(7)\quad &C_{1.1}[Q_{1.1}^{n+1}, h_{1.1}^{n+1}, Q_{1.2}^{n+1}, h_{1.2}^{n+1}] = 0 \\
&M_{1.1}[Q_{1.1}^{n+1}, h_{1.1}^{n+1}, Q_{1.2}^{n+1}, h_{1.2}^{n+1}] = 0 \\
&\vdots \\
(9)\quad &C_{1.N-1}[Q_{1.N-1}^{n+1}, h_{1.N-1}^{n+1}, Q_{1.N}^{n+1}, h_{1.N}^{n+1}] = 0 \\
&M_{1.N-1}[Q_{1.N-1}^{n+1}, h_{1.N-1}^{n+1}, Q_{1.N}^{n+1}, h_{1.N}^{n+1}] = 0 \\
&B_{2.1}[Q_{2.1}^{n+1}, h_{2.1}^{n+1}] = 0 \\
&\vdots \\
(7)\quad &B_{4.1}[Q_{1.1}^{n+1}, h_{1.1}^{n+1}] = 0 \\
&\vdots \\
&C_{4.3}[Q_{4.3}^{n+1}, h_{4.3}^{n+1}, Q_{4.4}^{n+1}, h_{4.4}^{n+1}] = 0 \\
&M_{4.3}[Q_{4.3}^{n+1}, h_{4.3}^{n+1}, Q_{4.4}^{n+1}, h_{4.4}^{n+1}] = 0 \\
(6)\quad &C_{3.1}[Q_{3.1}^{n+1}, h_{3.1}^{n+1}, Q_{3.2}^{n+1}, h_{3.2}^{n+1}] = 0 \\
&M_{3.1}[Q_{3.1}^{n+1}, h_{3.1}^{n+1}, Q_{3.2}^{n+1}, h_{3.2}^{n+1}] = 0 \\
&\vdots \\
&C_{3.N-1}[Q_{3.N-1}^{n+1}, h_{3.N-1}^{n+1}, Q_{3.N}^{n+1}, h_{3.N}^{n+1}] = 0 \\
&M_{3.N-1}[Q_{3.N-1}^{n+1}, h_{3.N-1}^{n+1}, Q_{3.N}^{n+1}, h_{3.N}^{n+1}] = 0 \\
(8)\quad &C_{5.1}[Q_{5.1}^{n+1}, h_{5.1}^{n+1}, Q_{5.2}^{n+1}, h_{5.2}^{n+1}] = 0 \\
&M_{5.1}[Q_{5.1}^{n+1}, h_{5.1}^{n+1}, Q_{5.2}^{n+1}, h_{5.2}^{n+1}] = 0 \\
&\vdots \\
(6)\quad &J[Q^{n+1}, h^{n+1}] = 0 \\
(1)\quad &B_{5.5}[Q_{5.5}^{n+1}, h_{5.5}^{n+1}] = 0
\end{aligned}
$$

44

Figure 3.1. River schematic of five-branch river network and the system of equations

In the example, there are a number of 44 or 2N (N=22, where N is the number of nodes) equations which are derived from the continuity and momentum equations, the boundary conditions, and the equations satisfied of the channel junctions (i.e. discharge continuity equations, same stage for all branches connecting a the junctions). Branches 1, 2, and 4 are defined as the exterior branches because their upstream end does not connect to other branches, while branches 3 and 5 are defined as the interior branches. The system of equations is listed from the exterior to the interior branches. Their sequential order of equations corresponding to each reach is ordered as follows,

[1.1,1.2,1.3,1.4,2.1,2.2,2.3,2.4,2.5,4.1,4.2,4.3,4.4,3.1,3.2,3.3,3.4,5.1,5.2,5.3,5.4,5.5]

In total there are 34 [2N-2B=2(22)-2(5)=34, where B is the number of branches] finite difference equations which are derived from the continutiy and momentum equations. The inflow boundary conditions at branches 1, 2, and 4 are the discharge time series, while the downstream boundary at branch 5 is the stage time series. At the junction nodes between 2 or more branches, two internal boundary conditions are imposed. The first is continuity at the junction node. The second is the stage at all nodes coming into the node is the same at the location of the node.

These interior boundary conditions are used to determine the coefficent of matrix locations. For example, the interior boundary conditions return multiple arrays [7,17,27], [8,18], …, etc,. that predict the coefficents [1,1,-1], [1,-1], …, etc,. matrix locations of the channel junctions (Fig. 3.2), and they are matched with the highlighted regions of the system of equations written in the matrix form as shown in Figure 3.3.

Interior boundary condition	$Q_{1.4} + Q_{2.5} - Q_{3.1} = 0$	⇒	[7,17,27]
	$h_{1.4} - h_{2.5} = 0$		[8,18]
	$h_{1.4} - h_{3.1} = 0$		[8,28]
	$Q_{4.4} + Q_{3.4} - Q_{5.1} = 0$		[25,33,35]
	$h_{4.4} - h_{3.4} = 0$		[26,34]
	$h_{3.4} - h_{5.1} = 0$		[34,36]

Figure 3.2. Interior boundary conditions of five-branch networks and the coefficient matrix location of the channel junctions

The Newton Raphson method is used to solve the system of equations (AX=C, where X is the vector column $(\Delta Q_i, \Delta h_i)$, see Fig 3.3) for the 2N unknowns, Q_i^{n+1} and h_i^{n+1} for i=1, 2, … , N. First, a set of initial values are assigned to the unknowns Q_i^{n+1} and h_i^{n+1} and the iteration (k) is equal to 1. The coefficient of the matrix on the left

hand side (A) and the residual column (C) on the right hand side is filled with the calculated values based on the initial values of the unknowns (Fig 3.3). The corrections ($\Delta Q_i, \Delta h_i$) that from column (X) are the solution of the system of linear equations (AX=C). The new values of the unknowns are calculated as $Q_i^{n+1}$and $h_i^{n+1}$for the next iteration (k+1) are expressed as follows:

$$(Q_i)_{k+1} = (Q_i)_k + (\Delta Q_i)_k$$

$$(h_i)_{k+1} = (h_i)_k + (\Delta h_i)_k$$

The iterative procedure terminates until the maximum value of corrections $\Delta Q_i, \Delta h_i$ column is reduced to the assigned threshold values.

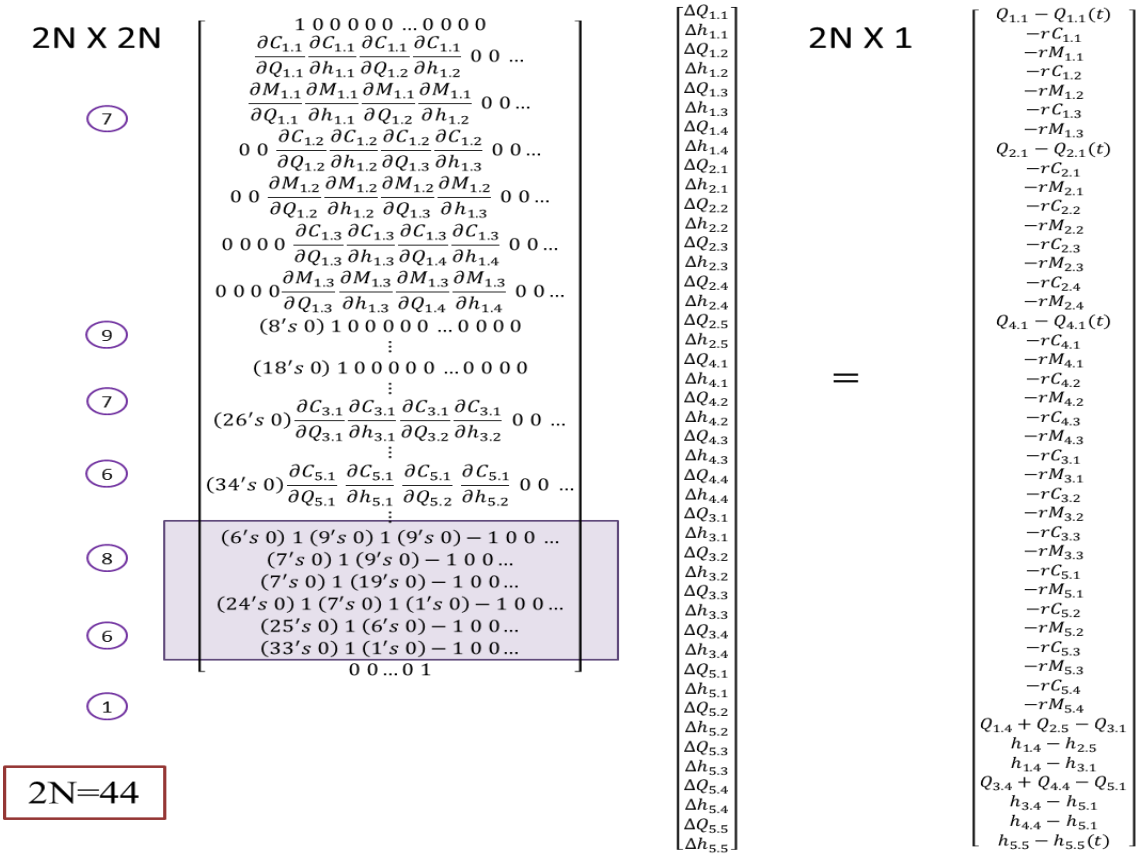

Figure 3.3. System of equations of five-branch river network

3.3 Development of the Geo-Processing Tools

Most commercial 1D-SVE codes have their own set of geo-processing tools, such as HEC-GeoRAS for HEC-RAS, MIKE11-GIS for MIKE-11, and TOPAZ for CCCHE1D. These tools are used to prepare the required river bathymetric data needed to perform 1D-SVE simulation. Since the goal of this study is to develop a complete hydraulic model that can be coupled with an external hydrological model, CUENCAS, a similar approach was adopted for the present model. Hence, automated geo-processing tools are developed to streamline the whole process.

First, the Manning's coefficient of each land cover type from the NLCD 2001 dataset (Fig 3.4) is assigned with the suggested Manning's roughness coefficients as shown in Table 3.1. These dataset are provided from the work completed by the Statewide Floodplain Mapping Project (Thomas, 2011).

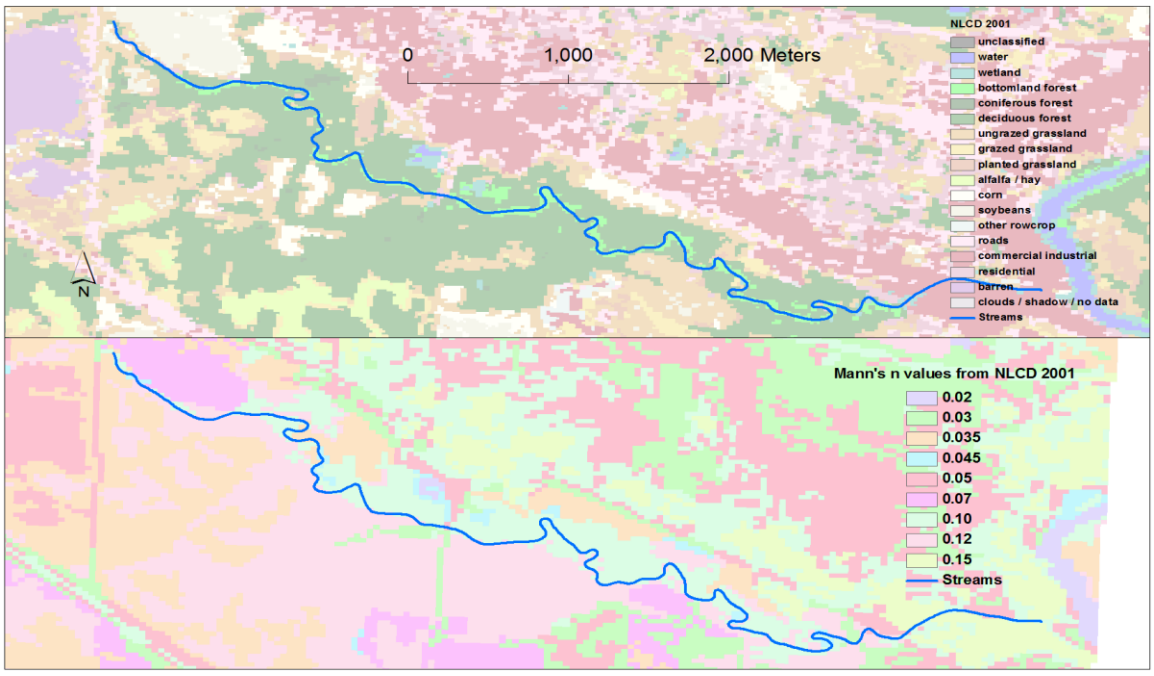

Figure 3.4. NLCD 2001 (top panel) Manning's roughness coefficients from NLCD 2001 (bottom panel)

Table 3.1. Roughness coefficients conversion from NLCD 2001

NLCD 2001 Classification	Manning's roughness coefficient
11 – Open Water	0.02
21 – Developed, Open Space	0.03
22 – Developed, Low Intensity	0.05
23 – Developed, Medium Intensity	0.1
24 – Developed, High Intensity	0.15
31 – Barren Land	0.05
41 – Deciduous Forest	0.12
42 – Evergreen Forest	0.12
43 – Mixed Forest	0.12
52 – Scrub/Shrub	0.08
71 – Grassland/Herbaceous	0.035
81 – Pasture/Hay	0.035
82 – Cultivated Crops	0.07
90 – Woody Wetlands	0.1
95 – Emergent Herbaceous Wetland	0.045

Source: Thomas, N. (2011). Standard Methods for the Iowa Statewide Floodplain Mapping Program.

Next, the geo-processing tools used to generate and prepare all needed inputs by the 1D-SVE solve are described into two sub-sections :) (1) Cross Sections Generator (2) Hydraulic Model Inputs Preparation

3.3.1 Cross Sections Generator

A GIS-based cross sections generator was developed in Python 2.5.1 environment, is part of the present work to generate river cross sections and extract the

river bathymetry data. The input data required by the tools includes the digitized streams centerline stored as Environmental Systems Research Institute (ESRI) shapefile format. The locations of the cross sections are identified along a reach based on the length of the digitized streams and the cross-sectional space interval (Fig 3.5a). A series of point perpendicular to the longitudinal streamwise direction are then generated for each cross section based on the cross-sectional width and the space interval at which points will be extracted (Fig 3.5b). Each river cross section represented by points is then used to extract values from the surface grids. The river topography and roughness coefficients of each cross section are extracted from the 1m-DEM grids and the roughness coefficients grids (Fig 3.5c and 3.5d). The floodplain roughness coefficients of the left and right overbank are the mean of the obtained values over the left and right floodplain width respectively. Each cross section is defined from left to right going downstream. Figure 3.5e depicts the cross section profile with the calculated floodplain roughness coefficients as shown in Figure 3.5d.

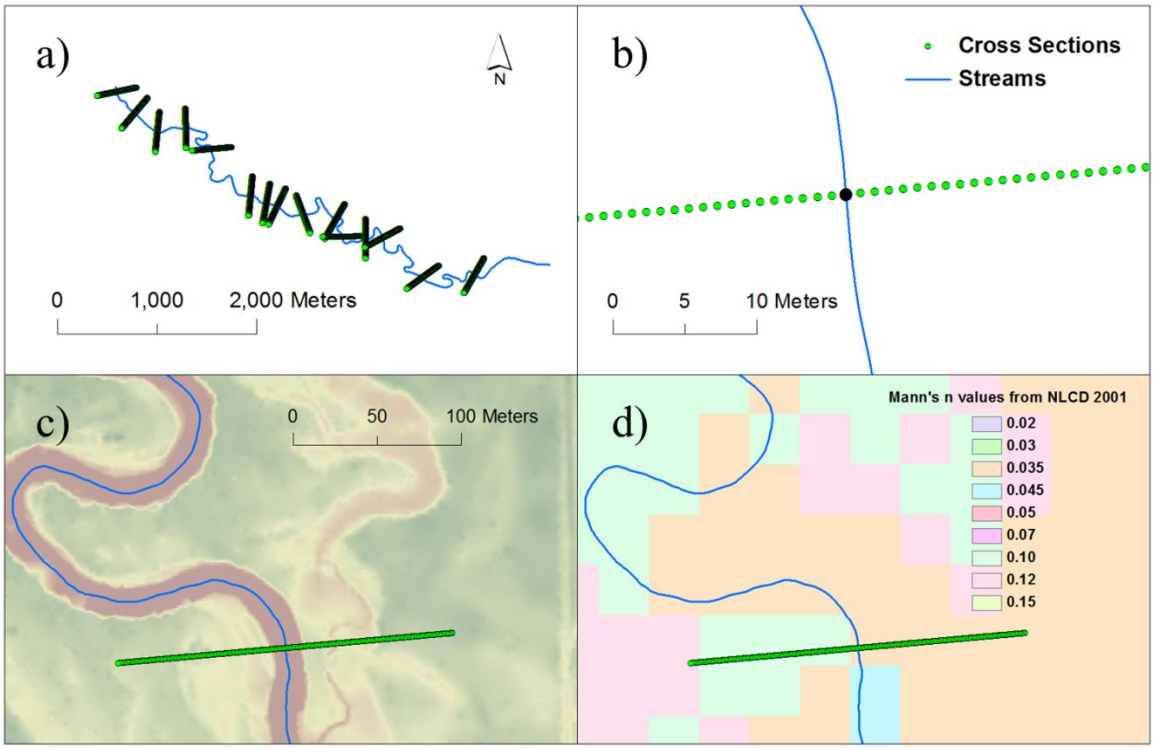

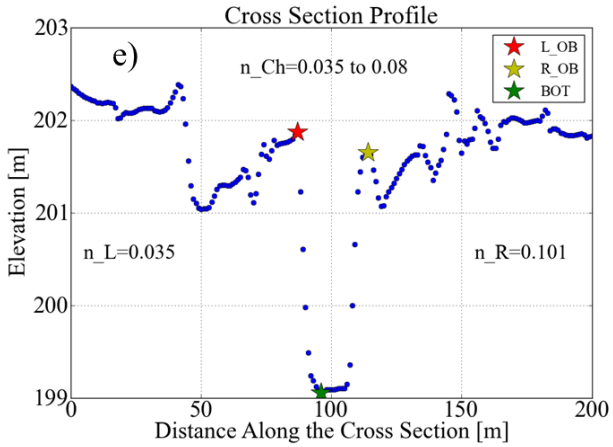

Figure 3.5. Example showing how floodplain roughness coefficients are extracted and import into cross-section geometry. a) Generate cross sections for a reach; b) Zoomed cross section diagram; c) Extract the river bathymetry from 1m-DEM grids; d) Extract the roughness coefficient from Manning's roughness coefficients grids from NLCD 2001; e) River cross section and calculated floodplain roughness coefficients.

3.3.2 Hydraulic Model Input Preparation

The developed geo-processing tools allow for: (1) Flexible cross section locations, (2) Identification of channel overbanks, (3) Control of ineffective flow area, and (4) Calculation of 1D-SVE model parameters. This section explains how the geo-processing tools achieve these tasks.

Cross sections locations are adjustable to any user specific requirements. For example, cross sections will not be cut near the river meandering. Some geometric strategies are used to avoid the river meandering where the channel conveyance cannot be accurately represented. This approach is consisted of the following steps:

1) Generate cross sections with user defined space interval (Fig 3.6a)

2) A stream buffer is created with a constant width (e.g. 20 m) (Fig 3.6b)

3) Delete the cross sections that are overlaid with the buffer polygon. Record the new locations length interval between cross sections (Fig 3.6c)

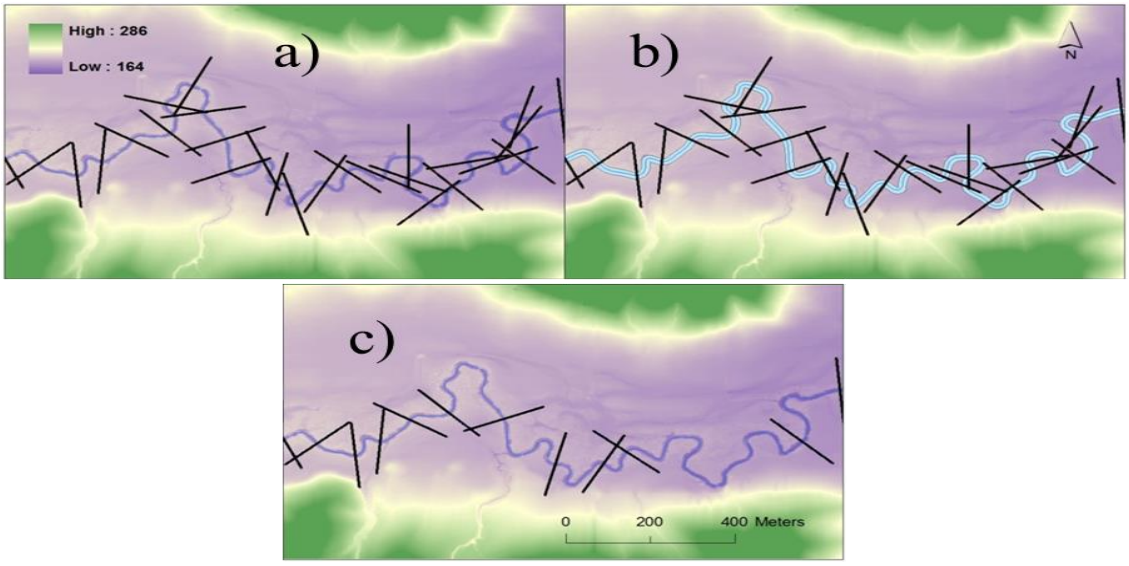

Figure 3.6. Strategy to avoid river meandering problem for a small reach. a) Generate cross sections; b) Create a stream buffer and select the overlaid cross sections; c) Delete the overlaid cross sections

A simple sorting rule is proposed to automate the process to identify the channel overbanks locations. The step-by-step procedure is illustrated in Figure 3.7.

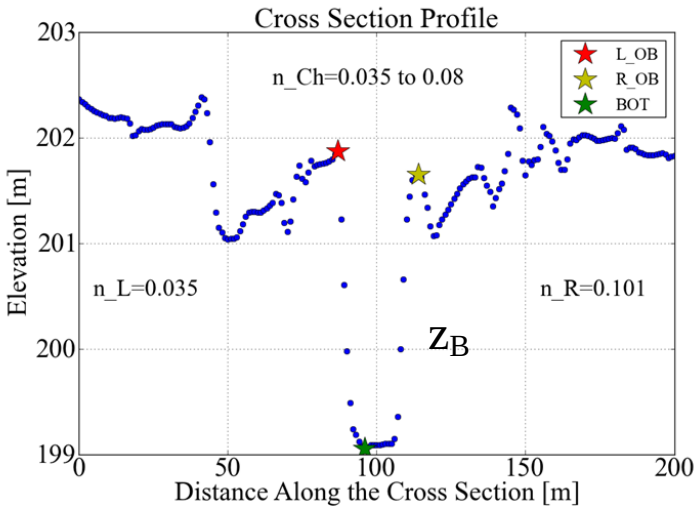

Figure 3.7. Cross section profile showing locations of overbanks of channel and floodplain

The main steps include:

1) Find the channel bottom location and elevation, and set it as the datum
2) Set a limit for the channel width (Ch_W = 40 m) and a stopping criteria for the change of the elevation (d_stop = 0.05 m)
3) Loop through the points-i from z_B to the left by Ch_W x 0.5 and z_B to the right by Ch_W x 0.5 respectively
4) Save the locations where there is a sharp change of the elevation (z_{i-5} - z_B >= 0 and $z_{i-6} - z_{i-5} <$ d_stop & $z_{i+5} - z_B > 0$ and $z_{i+6} - z_{i+5} <$ d_stop) as two arrays, BKL and BKR for the two overbanks
5) Select the location with the highest elevation from the BKL and BKR arrays
6) Identify the left overbank (L_OB) and the right overbank (R_OB) (see Fig. 3.7)

At some sections, the cross-sectional floodplain area is overestimated by including the ineffective flow area that a portion of cross section is not contributing in the

flow. Therefore, a variable, Z_TOL, is selected to control the in-effective flow area of the floodplain. The elevation of each point over the floodplain areas (i.e. y_horz < L_OB or y_horz > R_OB) is compared with the channel bottom elevation and Z_TOL (Fig. 3.8). The new bed elevations, z_i' are corrected as follows,

$$\text{if } Z_i < Z_B + Z\_TOL, \text{then } Z_i' = Z_B + Z\_TOL, \text{else } Z_i' = Z_i \quad (3.14)$$

The aim of this correction step is to reduce the overestimation of the ineffective flow area during the computation of the channel conveyance. The value of Z_TOL should be carefully chosen on a section-by-section basis so that it will not flatten the entire floodplain area, as that will result in sharp increase of the estimated wetted perimeter per unit increase of depth which can comprise the numerical stability of the simulation.

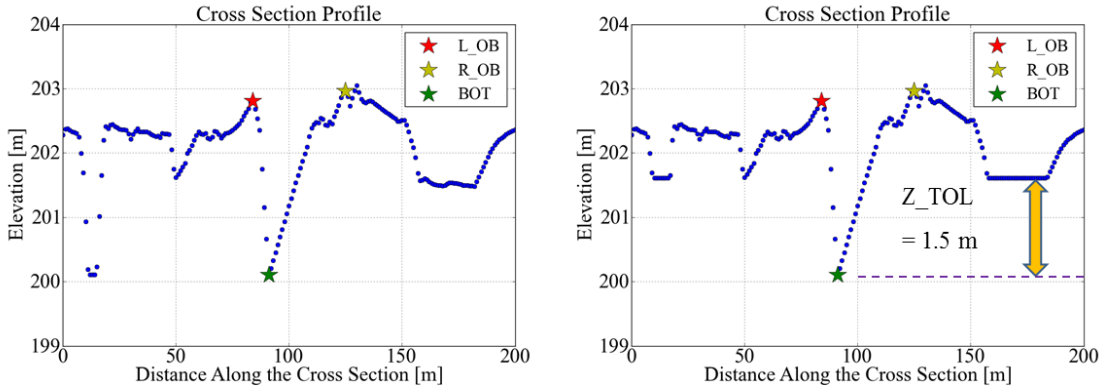

Figure 3.8. Raw cross section profile (left) and corrected cross section profile (right)

The required model parameters of each cross section, such as area (A), wetted perimeter (P) as a function of the flow depth are calculated based on the channel cross section and the value of the floodplain roughness coefficient (Fig. 3.9 and 3.10). The calculated values are then stored in a file to be used by the 1D-SVE solver.

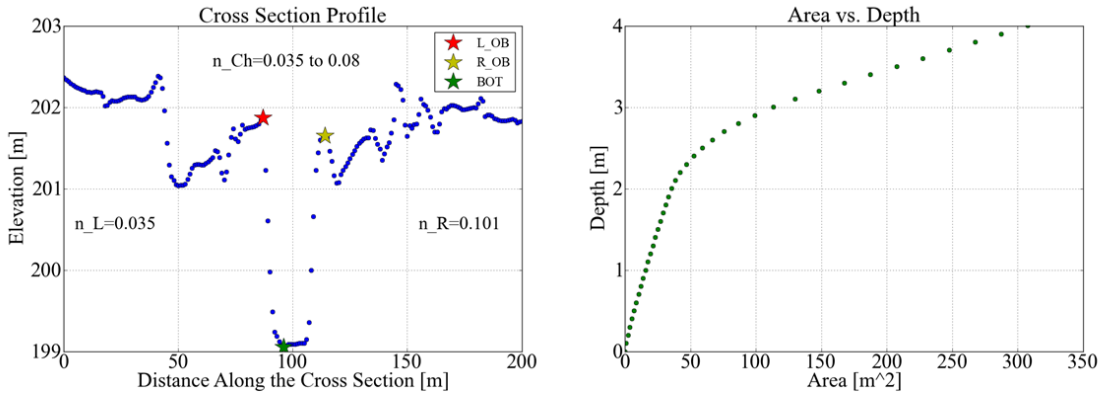

Figure 3.9. Computation of area (A) as a function of storage level based on the cross section profile

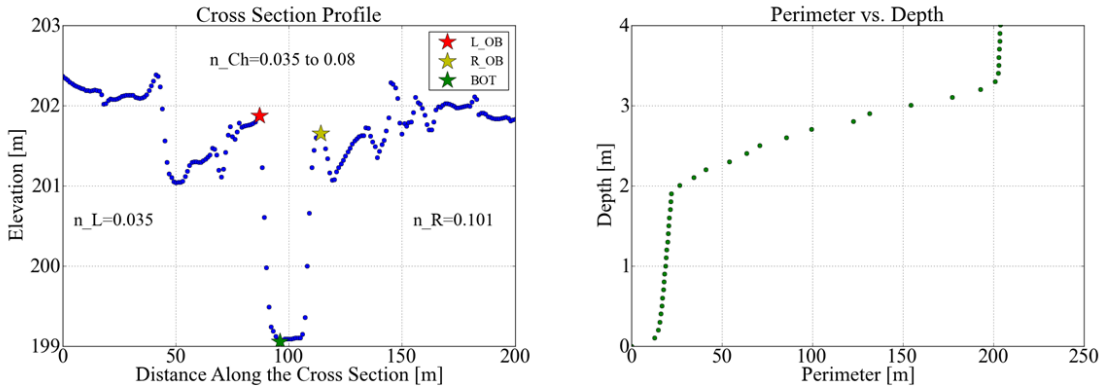

Figure 3.10. Computation of wetted perimeter (P) as a function of storage level based on the cross section profile

3.4 Comparison of the 1D-SVE Solver with a Test Case and HEC-RAS

We first consider a test case that was previously simulated by Choi et al. (1993). This test case considers the propagation of a flood wave through a river network. An eight-branch river networks is modeled in the 1D-SVE Solver. The model parameters are:

- Rectangular channel networks
- Manning's n value = 0.04, S_0 = 0.002, Channel width of branch 1, 2, 3, 4, 5 = 100 ft
- Channel width of main 1, 2, 3 = 200 , 400 and 500 ft
- Length of all the branches = 6 miles

- Downstream boundary: h = 3 ft
- Initial condition: Q = 100 CFS and h = 1 ft

The shapes of all inflow hydrograph are triangular with a constant baseflow of 500 CFS and a peak of 2300 CFS (Fig. 3.11). The simulated outflow hydrograph at main 3 by the present 1D-SVE solver is compared with the results from Choi et al. (1993) in Figures 3.12. The hydrograph shape, the timing of the peak, and the peak magnitude are very close.

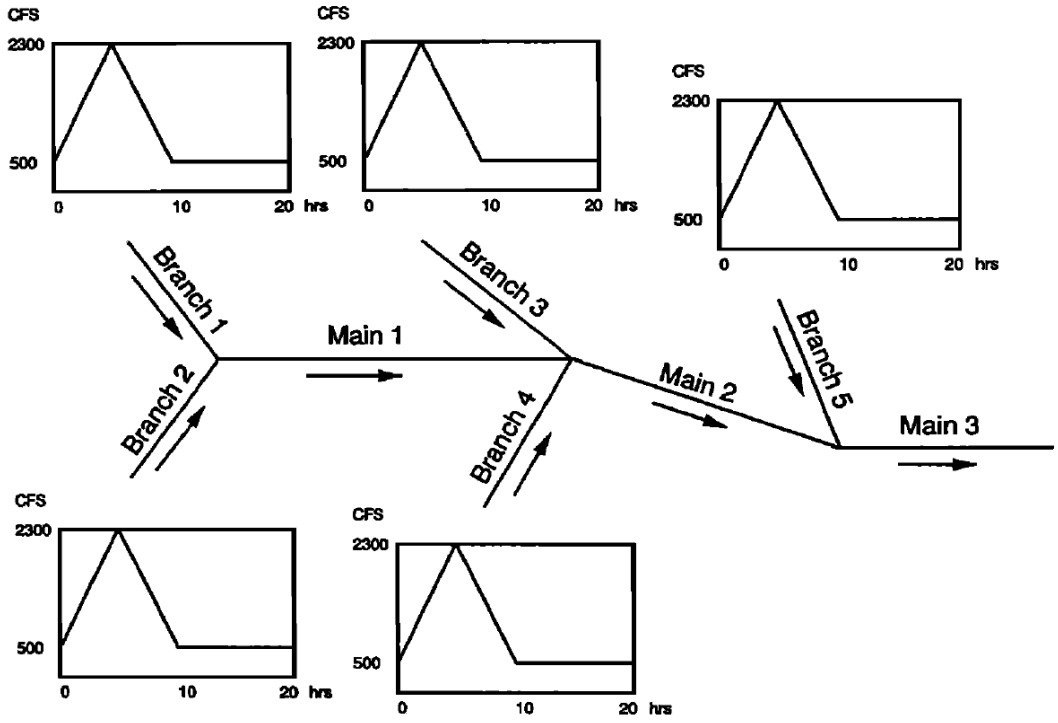

Figure 3.11. Eight-branch river network test case with five triangular inflow hydrographs

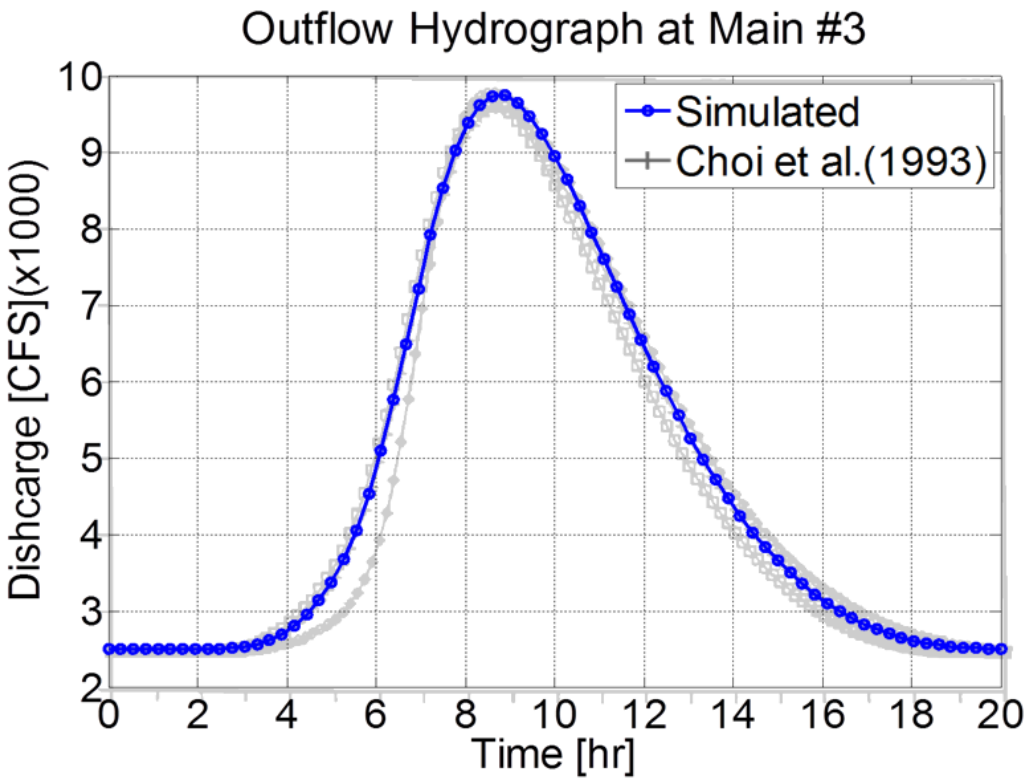

Figure 3.12. Comparison of outflow hydrographs predicted by Choi et al. (1993) (grey) and present model (blue)

Source: Choi, G. W., and A. Molinas. "Simultaneous solution algorithm for channel network modeling." Water resources research 29.2 (1993): 321-328.

We then consider a second case to validate the model accuracy in routing a river network with irregular cross-section geometries and real river morphology. A three-branch river network is modeled in both the 1D-SVE solver and HEC-RAS. This small river network is part of the Clear Creek Watershed, Iowa (Fig. 3.13a and 3.13b). The river cross-section geometries derived from the geo-processing tools and model parameters are replicated in the HEC-RAS simulation (Fig. 3.13c and 3.13d). Figure 3.13e and 3.13f show the calculated area and conveyance curve at one cross section. As expected, the curves used in the two simulations (1D-SVE model and HEC-RAS) are very close.

The model parameters and inflow conditions are:

- Three-branch, 26 cross sections, cross-section widths = 200 m, Time steps = 60s
- n=0.035 (Channel), n=0.05 (Floodplain)
- Downstream boundary stage: normal depth, friction slope = 0.0005
- Four CASES (#1 to #4) are simulated: Inflows at reach #A and #B = 10 CMS (baseflow) and Q_PEAK= 50, 100, 200 and 300 CMS
- Initial condition: 1m above channel bed (Stage level simulated)

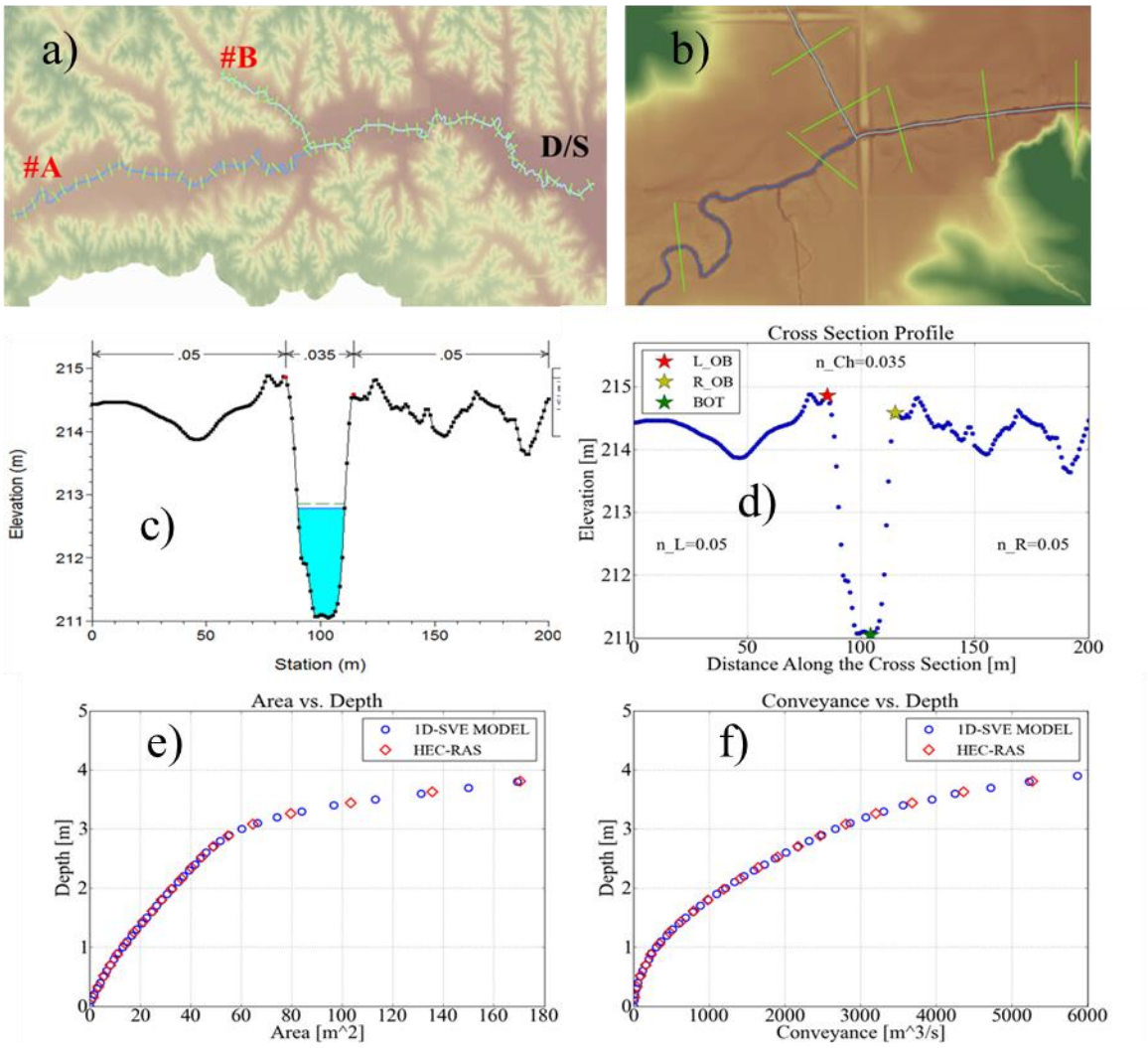

Figure 3.13. Second validation case of 1D-SVE model with HEC-RAS. a) River schematic of three-branch system; b) Zoomed river junction diagram; c) Cross section profile in HEC-RAS; d) Cross section profile in 1D-SVE model; e) Area as a function of flow depth in both models; f) Conveyance as a function of flow depth in both models.

The outflow hydrographs predicted by the 1D-SVE model and HEC-RAS for four different inflow hydrographs (CASE #1 to #4) are presented in Figure 3.14. The shape, the peak time, and the peak magnitude predicted by the two models for four simulation were sufficiently close to conclude that two models predict similar results.

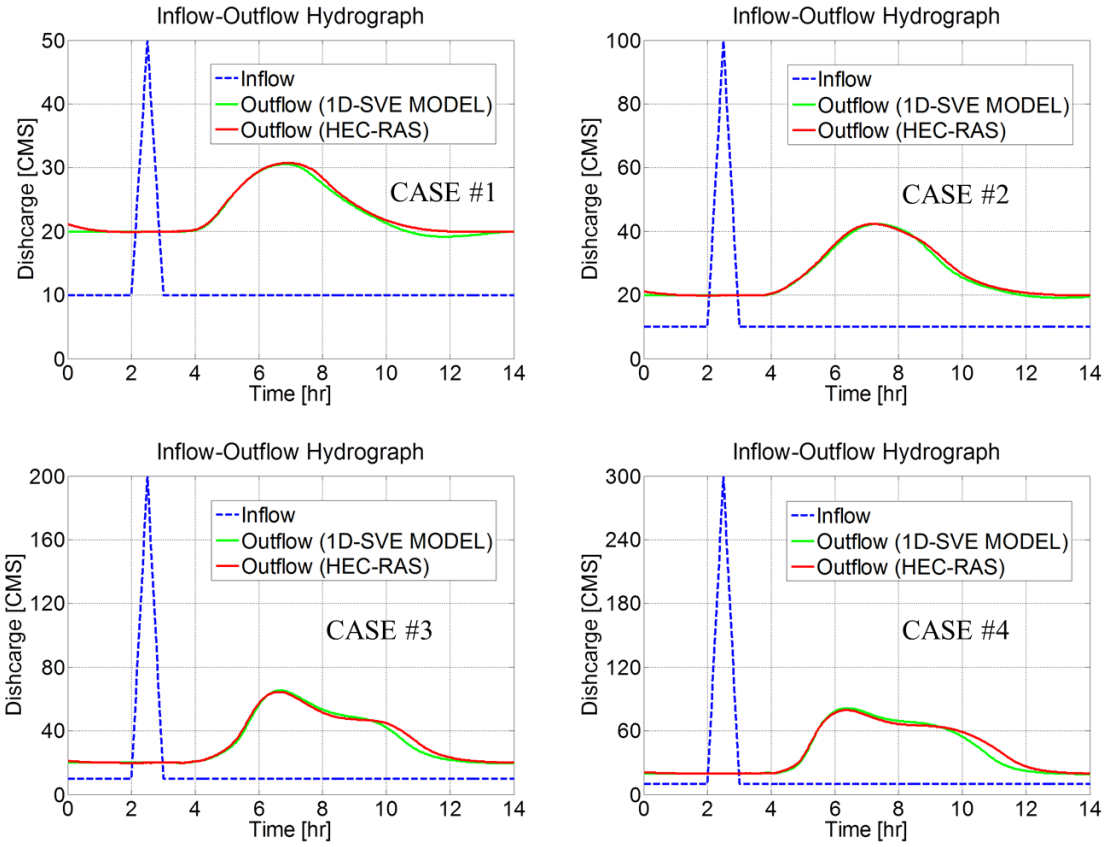

Figure 3.14. Outflow hydrographs predicted by present 1D-SVE model and HEC-RAS for four cases. a) Case #1, 50 CMS; b) Case #2, 100 CMS; c) Case #3, 200 CMS; d) Case #4, 300 CMS.

CHAPTER 4

COUPLED H-H MODELS RESULTS

4.1 Introduction

The methodology of connecting the 1D-SVE solver and CUENCAS, hydrological model used in this study is discussed. In the remaining of this chapter, the results towards the research objectives of this study described in Chapter 1 are discussed.

4.2 Coupling between the 1D-SVE Solver and CUENCAS

Ideally, hydraulic model uses the measured discharge hydrographs as boundary conditions which limits the uncertainty of boundary conditions to stage-discharge relationships. However, the availability of measured data is sparse in the un-gauges basin. This restricts the use of hydraulic model for a complex river network. To overcome the data scarcity, the simulated discharge hydrographs from hydrological model are used as the inflow boundary conditions of the hydraulic model. In this study, a realistic rainfall-runoff process is simulated by the hydrological model, CUENCAS, developed by IIHR, University of Iowa. The runoff generated from CUENCAS is used as the inflow (discharge) of the cross-section based 1D-SVE solver. The flow transport of river networks in CUENCAS is governed by a system of ODEs that uses the mass conservation equation for a link, e, (Mantilla et al., 2006) as follows:

$$\frac{dS(e,t)}{dt} = a_e R(e,t) + q(f_1,t) + q(f_2,t) - q(e,t) \quad (4.1)$$

where $S(e,t)$ is the storage in the link at time t, a_e is the total hillslope area of the draining into, $R(e,t)$ is the runoff intensity per unit area from the hillslope, $q(f_1,t) +$

$q(f_2, t)$ are the flow from the two upstream tributaries joining the link e, and $q(e, t)$ is the discharge at the outlet of the link

The channel storage, $S(e, t)$ and discharge, $q(e, t)$ can be written as $S(e, t) = l_e w_e d_e(t)$ and

$$q(e, t) = v_e(t) w_e d_e(t) = v_e(t) C_A \tag{4.2}$$

where w_e is the mean width of the link, $d_e(t)$ is the mean channel depth, C_A is the link average cross sectional area, $v_e(t)$ is the flow velocity and l_e is the link length, combing them gives,

$$S(e, t) = \frac{q(e, t) l_e}{v_e(t)}$$

Letting $v_e(t) = v_0 q^{\lambda_1} A^{\lambda_2}$ (4.3)

where v_0 is the initial velocity, λ_1 and λ_2 are the scaling exponents.

The channel storage, $S(e, t) = \frac{1}{v_0} q(e, t)^{1-\lambda_1} A^{\lambda_2} l_e$ as a function of discharge, then, equation 4.1 becomes,

$$\frac{dq(e, t)}{dt} = K\big(q(e, t)\big)[a_e R(e, t) + q(f_1, t) + q(f_2, t) - q(e, t)] \tag{4.4}$$

where $K\big(q(e, t)\big) = \frac{v_0 q(e,t)^{\lambda_1} A^{\lambda_2}}{(1-\lambda_1) l_e}$

A simplified version of the runoff production from hillslope is given by,

$$\frac{dS_p}{dt} = R_c p(t) - q_{pl} \tag{4.5}$$

$$\frac{dS_s}{dt} = (1 - R_c) p(t) - q_{sl} \tag{4.6}$$

$$R(e, t) = q_{pl} + q_{sl} \tag{4.7}$$

$$\frac{dS(e, t)}{dt} = a_e\big(q_{pl} + q_{sl}\big) + q(f_1, t) + q(f_2, t) - q(e, t) \tag{4.8}$$

where $q_{pl} = \frac{v_h L_l S_p}{A_h}$ and $q_{sl} = \frac{v_h L_l S_s}{A_h \times 290}$

R_c is the runoff coefficient, p(t) is the rainfall time series, q_{pl} is the surface storage, q_{sl} is the subsurface storage, v_h is the velocity of the hillslope [m/s] (0.01 m/s in this case), S_p is the storage volume from the surface [km^3], A_h is the area of hillslope drained to the link [km^2], S_s is the storage volume from the subsurface [km^3] and L_l is the link length [km].

The link-based mass conservation equation, 4.4, forms a system of M non-linear ODEs where M is the number of link in the networks. Since the spatial distribution of the river networks and the storage-discharge relationship of the ODEs systems used in CUENCAS are different than the PDEs systems used in the 1D-SVE solver, the geo-processing tools are used to convert the tributary inflows from the ODEs systems to the inflow to the 1D-SVE solver. A short river segment from the 1D-SVE solver is used to illustrate how these steps are proceeded as shown in Figure 4.1,

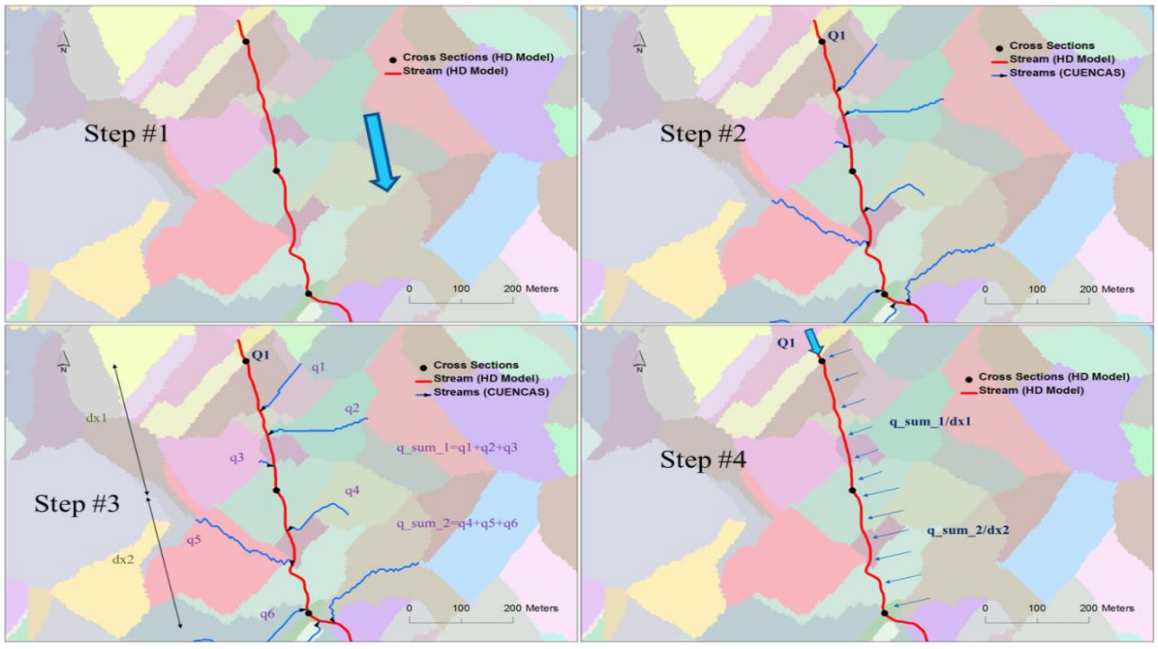

Figure 4.1. Schematic diagram showing the step-by-step procedures of converting inflow from CUENCAS to the 1D-SVE solver

The four main steps include:

1) Identify the corresponding LINK-ID of all the cross-section nodes
2) Find all the tributary inflows along the river segments
3) Sum up the tributary inflows, and find the length interval between two consecutive cross sections
4) Divide the sum of the tributary inflows over the length interval as the lateral inflows, and use the inflows at the exterior cross-section nodes directly

The tributary inflow is the flow contributions from the upstream area that drained to the desired location. According to equation 4.1, they are equal to the sum of the discharge released from the link storage and the discharge at the outlet of the link (i.e. $a_e R(e,t) + q(f_1,t) + q(f_2,t)$).

We consider an eleven-branch river network in Clear Creek Watershed (Fig 4.5) to verify the accuracy of the inflow boundary conditions of the 1D-SVE solver derived from the runoff and storage generated from CUENCAS. The calculated volume drained into each 1D-SVE solver branches (11 totals) were compared with the difference in hydrograph volume at the upstream and downstream cross section nodes calculated by CUENCAS. Then, the calculated volume was multiplied by a correction factor, KF, and called it adjusted volume as shown in equation 4.9 to ensure the mass conservation throughout the conversion process (Fig. 4.2).

$$\text{ADJUSTED VOL.} = \text{CALCULATED VOL.} \times \text{KF} = \text{VOL. DIFF. btw } {}^{U}/_{S} \text{ and } {}^{D}/_{S} \qquad (4.9)$$

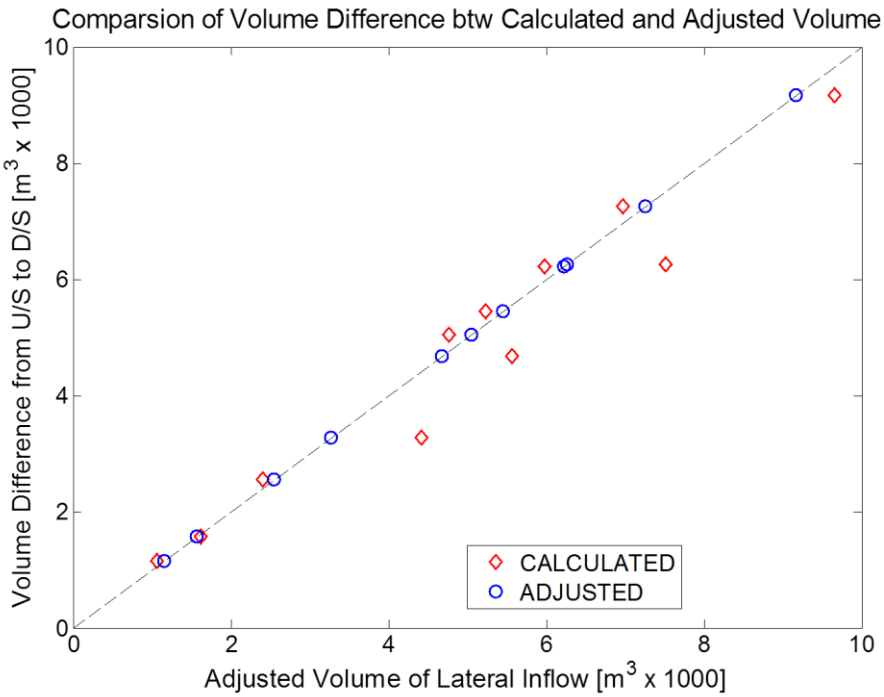

Figure 4.2. Validation of mass conservation between CUENCAS and the inflows to the 1D-SVE solver

This section describes the results related to the objectives described in Chapter 1.

The first objective is to *demonstrate that a 1D-SVE model is a better routing approach for some specific flow dynamics conditions (diffusive wave or dynamic wave).*

The primary question arises from achieving this objective is, '*Where should we use the dynamic hydraulic models*?' In order to determine the spatial extent of the streams network that needed to be modeled by 1D-SVE model, the flow dynamics classification approach recommended by NWS is used. The geo-processing tools are used to automate the average bed slope calculation for all of the digitized reaches within the Clear Creek Watershed provided by Iowa Statewide Mapping Project. There is a total of 293 digitized reaches that have upstream drainage area greater than the threshold value of one square mile. The average bed slope of each reach is linearly interpolated (1st degree polynomial)

for all the bed elevations derived from the extracted river cross sections as shown in Figure 4.3. The calculated average bed slopes for all the reaches are classified into three different flood wave model types based on the NWS slope regimes classification method (see Table 2.1), and Figure 4.4 is the spatial and statistical distribution of the calculated average bed slopes of all the reaches in the Clear Creek Watershed. About 20% (60 out of 293) of the reaches have the diffusive or dynamic flow dynamics characteristics, and they are mostly the main stem in a river network. Therefore, one can infer the suitability of the selected flood wave models and determine where the dynamic hydraulic models should be considered.

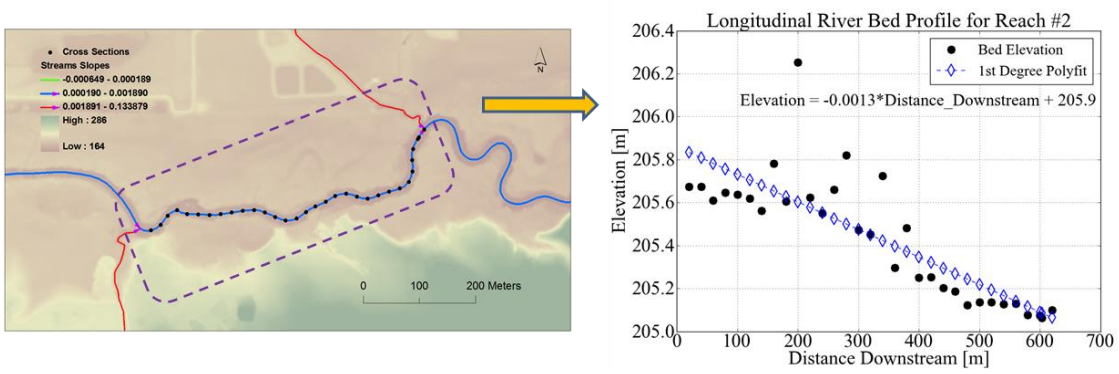

Figure 4.3. Average bed slope estimation by the 1st degree polynomial fit for a reach

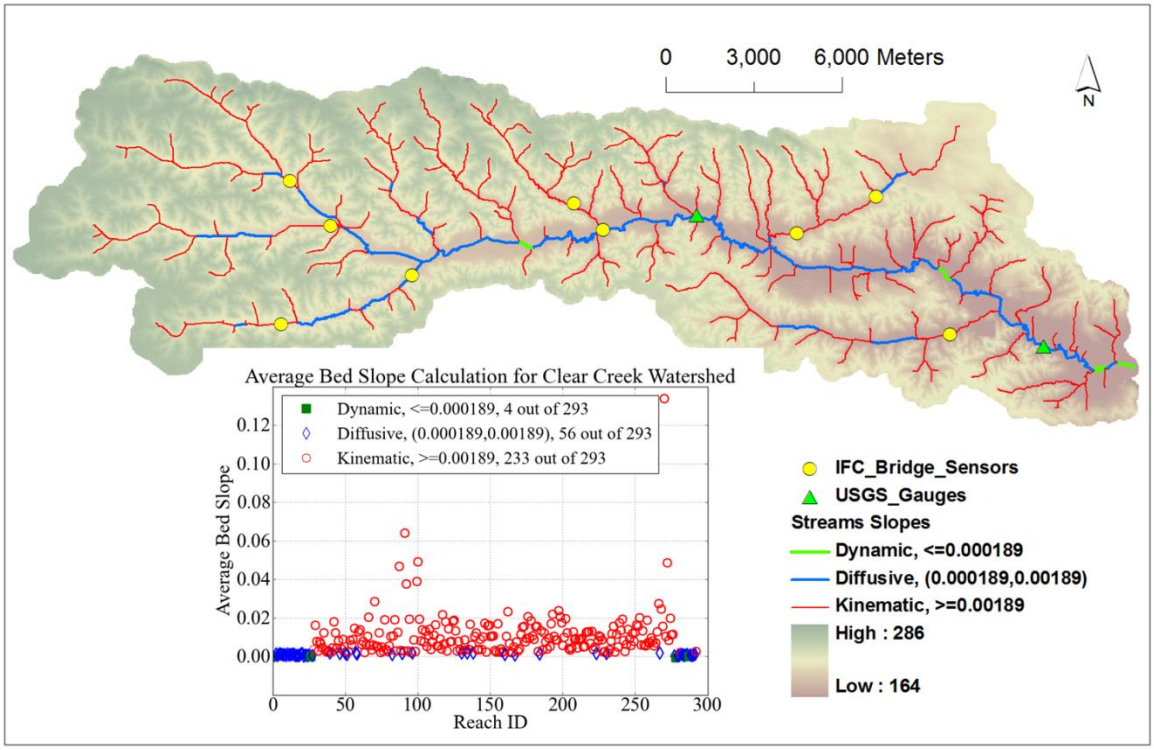

Figure 4.4. Spatial distribution of the flow dynamics classification based on the NWS slope regime classification for 293 reaches in the Clear Creek Watershed, Iowa (top panel); Average bed slopes statistics for 293 reaches in the Clear Creek Watershed, Iowa (bottom panel)

The second approach suggested by the empirical equation 2.4 is used to verify the first method. A simple check of the flow dynamics classification is performed on the two reaches that contain the two USGS streamflow gauges at Oxford and Coralville. The time of rise of the hydrograph and the flow depth are estimated from the USGS data. The average bed slopes are estimated from the LiDAR-derived cross sections at the upstream and downstream ends. The mean velocities are assumed to be 0.75 m/s. The inequalities for satisfying the kinematic wave model failed (see equation 2.4), but passed for satisfying the diffusive wave model for both study reaches (see equation 2.5). If the rule-of-thumb recommended from the NWS is also considered (see Table 2.1), the recommended way of flood routing are at least diffusive wave models, or even more

conservative dynamic wave model. Table 4.1 summarizes the predicted flow dynamics characteristics for these reaches.

Table 4.1. Predicted flow dynamics characteristics of the reaches where two USGS gauges are located

Gauge Location	$T_r[s]$	$S_0[^m/_m]$	$u_0[^m/_s]$	$d_0[m]$	$\frac{T_r S_0 u_0}{d_0}$	$T_r S_0 \left(\frac{g}{d_0}\right)^{1/2}$	Model (Eqns. 2.4 and 2.5)	Rule-of-thumb (NWS)
Oxford	25 x 3600	0.0009	0.75	4.5	13.5	119.6	Diffusive wave	Diffusive wave
Coralville	38 x 3600	0.0007	0.75	4.4	16.3	143.0	Diffusive wave	Diffusive wave

According to the results obtained from both approaches, the required streams for diffusive/dynamic wave models in Clear Creek Watershed are comprised of the main stem of the river network and several major tributaries. Therefore, a river network (11 in total) using this guidance is delineated as shown in Figure 4.5. The sum of the reach length is approximately equal to 53 miles, which is about 1/100 of the total reach length covered by the NWS hydraulic model (Table 2.1).

The second objective is to *show that the results from the coupled H-H models can enhance hydrological model validation by providing a better spatial description of runoff field.* Since this objective is closely related and heavily relied on the results obtained from the coupled H-H models, this section is organized as follows: (1) Model setup and model parameters selection; (2) Calibration of the coupled H-H models and (3) Results and discussion.

4.3 Model setup and model parameters selection

A flood event occurred on April, 2013 in Clear Creek Watershed, Iowa, was selected to validate the accuracy of the coupled H-H models. A LiDAR-derived DEM (1m resolution) topography data and 30-meter land use roughness data are used to extract the required river cross sectional geometries and the floodplain roughness coefficients of the coupled H-H models. The inflow boundary conditions of the coupled H-H models are provided from the runoff and storage release generated from CUENCAS. Two USGS measurements of stage and discharges at stations (Oxford, 05404220, upstream), (Coralville, 05454300, downstream) and nine IFC bridge sensors were used to measure stage hydrograph (Fig. 4.5). By using the eleven-branch river network (Fig 4.5) with the cross-section characteristics as shown in Table 4.2., a total of 229 cross sections were created by the geo-processing tool (Fig 4.5). The cross-section spacing is selected within a reasonable range (30 to 300 m) so that a relatively consistent river bathymetric can be obtained. The cross-section width is fixed at 400 meter which the channel-floodplain interactions are included. The cross-sectional locations are not situated in a river meandering region or keep 40 meter away from the channel junctions.

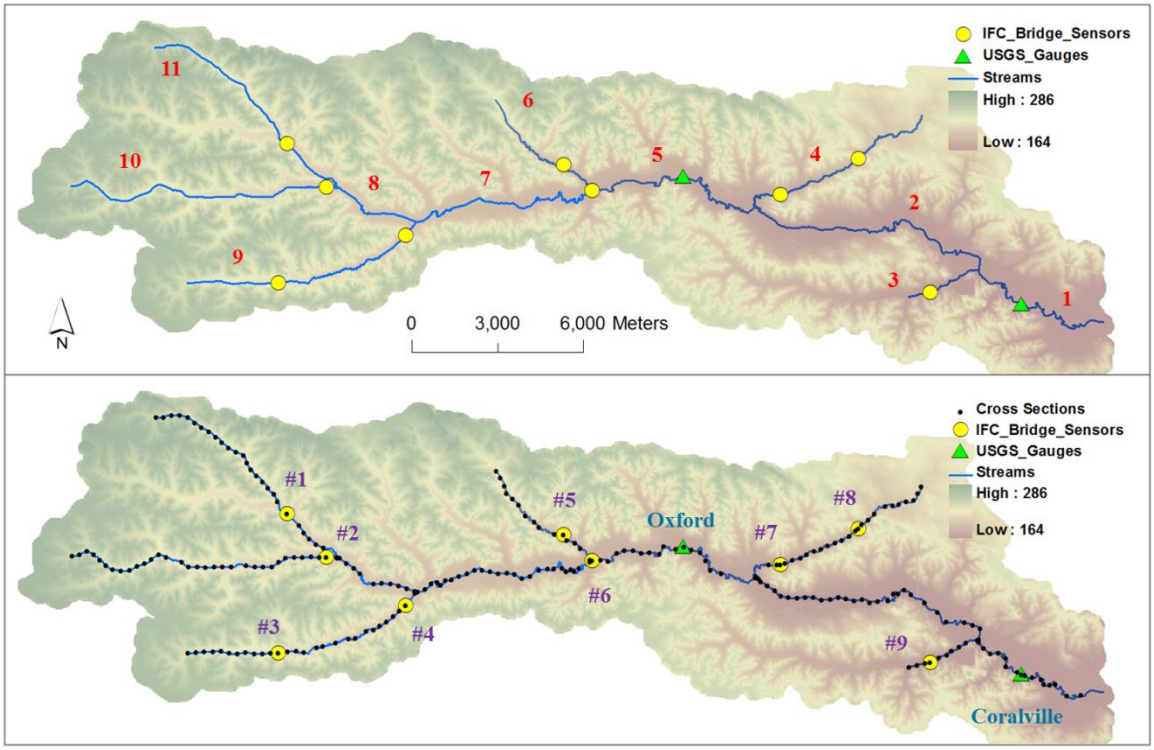

Figure 4.5. Simulated river networks superimpose on the Clear Creek Watershed: the branches numbers (top panel) and the location of USGS gauges and IFC stations (bottom panel).

Table 4.2. Model parameters and cross-section characteristics in the coupled H-H models

Cross-Section Characteristic	Description
Spacing	Fixed: 400 m
Width	○ If reach length < 300 m, Δx = 30 m ○ If 300 m < reach length < 500 m, Δx = 60 m ○ If reach length > 500 m, Δx = 300 m
Location	Avoid river meandering regions of the high curvature, at least one U/S and D/S XS at distance 40 m away from the end of streams
Bed Elevations	Constant bed slopes; 4 degree polynomial fit
Channel/Floodplain Roughness Coefficients	Channel: 0.045 Floodplain: NLCD 2001 derived

There are two methods of bed elevations approximation: (1) constant bed slope; and (2) n^{th} degree polynomial fit. For the first method, the bed slope for a reach is calculated as the change of bed elevation over the total longitudinal distance from the upstream to the downstream ends. Then, the bed elevations of all the cross sections are linearly interpolated along a reach by using the calculated bed slope and the known cross-sectional spacing, and this line should pass through the upstream and downstream bed elevations. For the second method, a 4^{th} degree polynomial (elevation vs. downstream distance) is used to fit the bed elevation of a reach. Once the polynomial is found, the bed elevations of all the cross sections are determined by substituting their downstream distances to the calculated polynomial. This process is then applied to all reaches. The final bed profiles of all the reaches except the outlet are adjusted so that the bed elevations at the upstream and downstream cross sections through the junctions are consistent. For example, if the flow is propagated from reach #2 to reach #1, the calculated bed elevation at the downstream cross section of the reach #2 from both approaches (dotted lines) are lowered from 201.9 m to 200.3 to match the bed elevation at the upstream cross section of the reach #1 (Fig.4.6). By comparing the performance of these methods, the accuracy of the 4^{th} degree polynomial fit method outweighs the constant bed slope method because it better retains original bed elevation curvature. Therefore, a 4^{h} degree polynomial fit method is used for bed elevation approximation for the rest of this study.

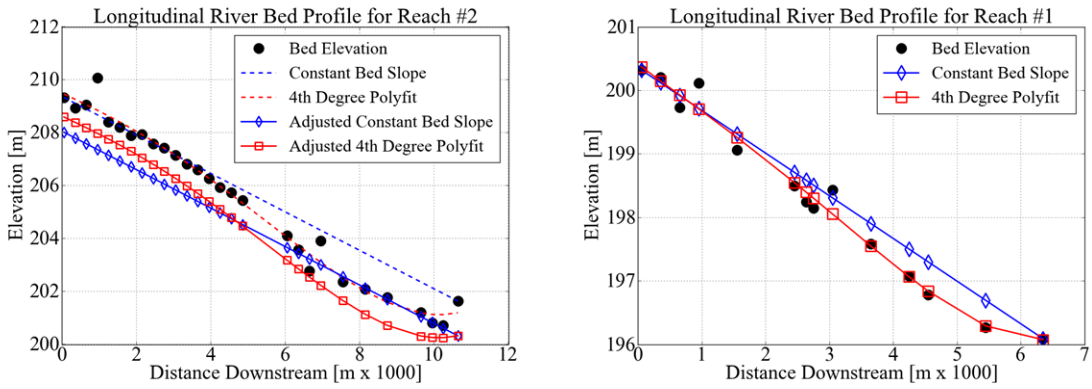

Figure 4.6. Bed elevation approximation of reach #2 (left) and reach #1 (right)

All of the sites with stage measurements have surveyed cross sections (11 in total). These surveys provide accurate description of channel bathymetry at these locations. Since the surveyed cross sections do not cover the floodplain, an arbitrary extension on both ends was imposed with a constant value of the upward side-slope (~0.03). The width of the surveyed cross-section widths are set to be equal to that of the nearby cross section (=400 m). This method is then implemented to all eleven cross sections. Two cross-section profiles at Oxford and Coralville gauge are depicted (Fig 4.7).

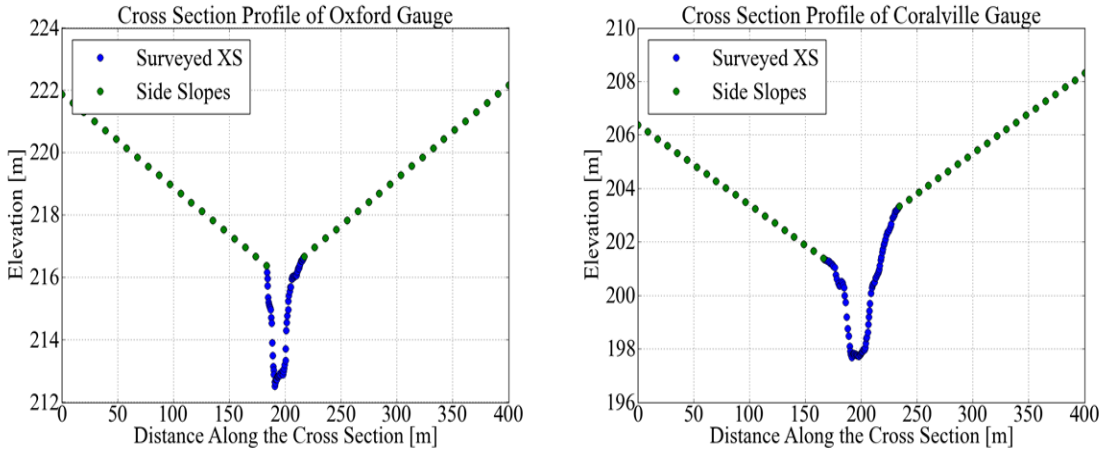

Figure 4.7. Modified cross section profiles at Oxford (left) and Coralville gauge stations (right)

4.4 Calibration of Coupled H-H Models

To better understand the effect of the spatial variability of the hydrological model parameters (e.g. channel velocity and runoff coefficients), a zoning of Clear Creek Watershed based on the spatial distribution of the gauge stations locations is created. Each zone represents the upstream contributing drainage for that particular gauge stations. A zoning sequence is determined based on the independency of the gauge stations, locations along the main stem and the streams order of a river network (Fig 4.8). Hydrological model calibration should follow the zoning map and the zoned sequence.

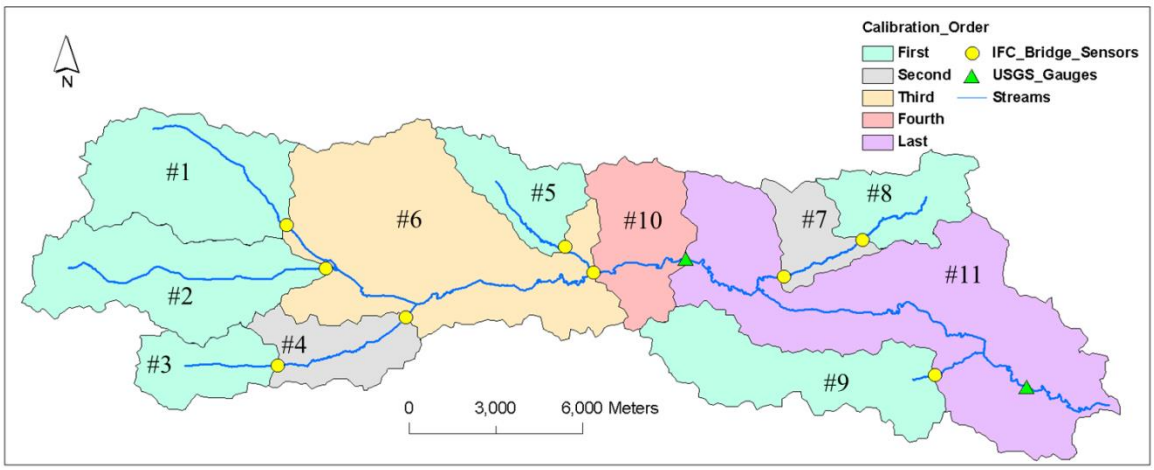

Figure 4.8. Schematic diagram showing the zoning of 11 gauge stations and the calibration sequence order

Runoff coefficients (RC) are defined as the ratio of the amount of runoff to the amount of precipitation. A preliminary estimate of runoff coefficients is performed for 11 zones derived above. First, runoff coefficients are assigned to 15 NLCD land cover classes based on the recommended value proposed by Dhakal et al. (2001) (see Table 4.3 and 4.4)

Table 4.3. Runoff coefficients for various land cover type

NLCD description	Land use or description in the source
Developed, open space	Residential: single family (0.3-0.5)
Developed, low intensity	50% of area impervious (0.55)
Developed, medium intensity	70% of area impervious (0.65)
Developed, high intensity	Business: downtown areas (0.7-0.95)
Barren land	Sand or sandy loam soil, 0-5% (0.15-0.25); black or lessial soil, 0-5% (0.18-0.3); heavy clay soils; shallow soils over bedrock: pasture (0.45)
Deciduous forest	Deciduous forest (Tennessee (0.52)
Evergreen forest	Forest (UK) (0.28-0.68); Forest (Germany) (0.33-0.59)
Mixed forest	Forest (UK) (0.28-0.68); Forest (Germany) (0.33-0.59)
Shrub/scrub	Woodland, sandy and gravel soils (0.1); loam soils (0.3); heavy clay soils (0.4); shallow soil on rock (0.4)
Grassland/herbaceous	Pasture, grazing HSG A (0.1); HSG B (0.2); HSG C (0.25); HSG D (0.3);
Pasture/hay	Pasture, sandy and gravel soils (0.15); loam soils (0.35); heavy clay soils (0.45); shallow soil on rock (0.45)
Cultivated crops	Cultivated, sandy and gravel soils (0.2); loam soils (0.4); heavy clay soils (0.5); shallow soil on rock (0.5)

Source: Dhakal, Nirajan, et al. "Estimation of volumetric runoff coefficients for Texas watersheds using land-use and rainfall-runoff data." Journal of Irrigation and Drainage Engineering 138.1 (2011): 43-54.

Table 4.4. Assigning runoff coefficients based on land cover type NLCD 2001

NLCD description	NLCD description (Table before)	Runoff coefficient, C
Unclassified	NA	NA
Water	NA	0.01 (Assumed)
Wetland	NA	0.05 (Assumed)
Bottom Forest	Mixed forest	0.48
Coniferous Forest	Mixed forest	0.48
Deciduous Forest	Deciduous forest	0.52
Ungrazed Grassland	Grassland/herbaceous	0.22
Grazed Grassland	Grassland/herbaceous	0.22
Planted Grassland	Grassland/herbaceous	0.22
Alfalfa/hay	Pasture/hay	0.35
Corn	Cultivated crops	0.4
Soybeans	Cultivated crops	0.4
Other Rowcrop	Cultivated crops	0.4
Road	Developed, high intensity	0.83
Commercial Industrial	Developed, high intensity	0.83
Residential	Developed, open space	0.4
Barren	Barren land	0.3
Clouds / No data	NA	NA

The area-weighted runoff coefficients for 11 sub-watersheds (C) are calculated as follows,

$$C = \frac{\sum_{i=1}^{n} C_i A_i}{\sum_{i=1}^{n} A_i} \tag{4.10}$$

where i = i^{th} land cover type with i^{th} area

The computed area-weighted runoff coefficients for 11 zones range from 0.32 to 0.42 (Fig. 4.9). Zone 11 has the largest runoff coefficient (0.42) because these areas include more residential and commercial use, while the remaining zones are mainly consisted of cropland and forest that have higher permeation capability.

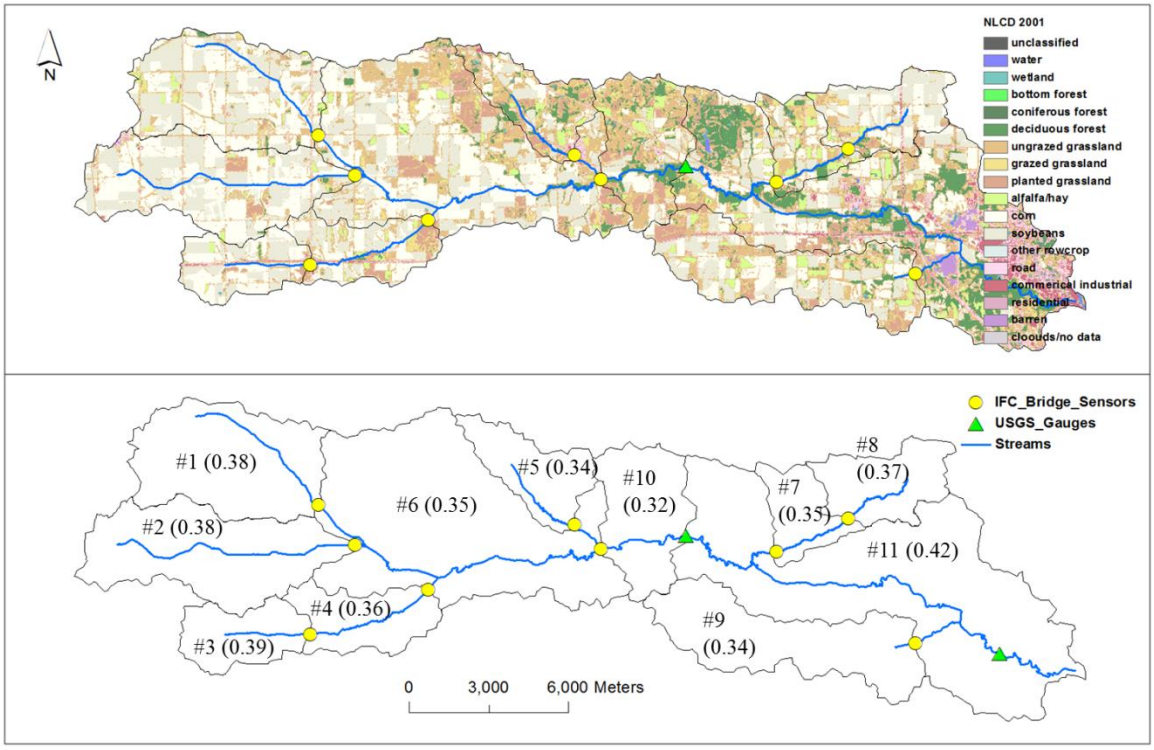

Figure 4.9. Schematic river diagram and zoning maps and runoff coefficients

Note that these calculated values are only used for reference during the calibration of the hydrological model. The spatially and temporal variability of runoff coefficients are subject to rainfall characteristics (e.g. intensity, duration), land cover type, soil properties and most importantly antecedent moisture conditions. Therefore, the main hypothesis of the calibration of the hydrological model is relied on the observed stage measurements which dedicate the amount of runoff generated for one particular storm

event, and the estimated runoff coefficients stay constant during one particular event. The calibration of the runoff coefficients are proceeded spatially through the zoning maps and zoning sequence. The aim of the calibration of the runoff coefficient for the hydrological model is to provide a better agreement of predicting the timing of the peak, peak value and the volume of a hydrograph with the measurement, and the selected runoff coefficient should be within the reasonable range as compared to the computed values before.

The calibration of the channel/floodplain roughness coefficients for the 1D-SVE model is essential because it can be used to compensate the uncertainty of river cross-sectional geometries, river morphology, bed elevation approximation and inflow boundary conditions. First, a trial simulation with some typical roughness coefficients is performed. The Manning's roughness coefficients for all the channels are set as constant value of 0.045 and the floodplain roughness coefficients are based on the Manning's roughness coefficients derived from NLCD 2002. A trial and error method is used to adjust the floodplain roughness to best fit the observed stage and discharge measurements.

The baseflow of the outlet reach is approximately equal to 4 CMS that matches the observed value of the USGS streamflow gauge at Coralville. This value is used to assign the baseflow for all the modeled reaches. In this study, it is assumed that 80% (3.2 CMS) of the baseflow comes from the inflow drained from the upstream of all the exterior reaches, and the remaining (0.8 CMS) comes from the lateral inflow drained for all the reaches. These inflow boundary conditions are adjusted spatially so as to match the initial stage level predicted by the IFC bridge sensors as close as possible. The initial stage hydrographs prediction for all stations is close to the measured value within 0.5 m.

4.5 Results and Discussion

Three case scenarios are run with two different set of model parameters for the hydrological and hydraulics models: (1) CUENCAS: Constant runoff coefficients (RC=0.5) over the entire watershed and two different channel velocities (i.e. v_0=0.3 and 0.2 m/s); 1D-SVE Model: Manning's roughness coefficient for channel (n=0.045) and NLCD-derived floodplain roughness coefficients (Fig. 4.15, left). (2) Constant runoff coefficients (RC=0.5) over the entire watershed and a channel velocities of v_0=0.2 m/s; 1D-SVE Model: Manning's roughness coefficient for channel (n=0.045) and calibrated floodplain roughness coefficients (Fig. 4.15, right); Artificial channelization by 0.5 m for two reaches containing USGS gauge stations at Oxford and Coralville. (3) Spatial varied runoff coefficients (RC=0.25 to 0.6) over the entire watershed and a channel velocities of v_0=0.2 m/s; 1D-SVE Model: Channel roughness (n=0.045) and calibrated floodplain roughness coefficients (Figure 4.15, right); Artificial channelization by 0.5 m for two reaches containing USGS gauge stations at Oxford and Coralville.

4.5.1 Results of case #1 (un-calibrated roughness coefficients; constant runoff coefficients)

According to the results from the case #1, the timing of the peak and shape of the stage hydrographs are captured for all of the tributaries, but not for the main stem of a river network (#6, Oxford and Coralville gauge stations). The peak arrival time of gauge station #6 is ahead of the observed peak by almost a day. The discrepancy between the stage observed and the simulated can be attributed to the inaccurate inflow generated from the hydrological model.

In addition, the simulated stage hydrographs from the coupled H-H models are compared with the discharge hydrographs provided from CUENCAS for two different channel velocities. Results indicate that the change of the channel velocities for the hydrological model affect the timing and shape of the hydrographs significantly, while these varied inflow boundary conditions does not results in significant change for the coupled H-H models results (Fig. 4.10 and 4.11). In addition, the amounts of runoff predicted from CUENCAS at multiple locations are underestimated which the second peak of discharge hydrograph generated from CUENCAS are much less than the first peak of discharge (Fig. 4.11). The simulated discharge hydrograph at Oxford and Coralville are compared with the USGS measured discharge hydrograph and with the hydrograph from CUENCAS (Fig. 4.12). The simulated rating curves are also compared with the historical and observed rating curve at Oxford and Coralville gauge stations (Fig. 4.13). The cause of the underestimated stage prediction during the timing of peak can be attributed to (1) uncertainty of runoff generated from hydrological model, (2) uncertainty of measurements in river topography and stage, (3) uncertainty of LiDAR-derived bed profiles.

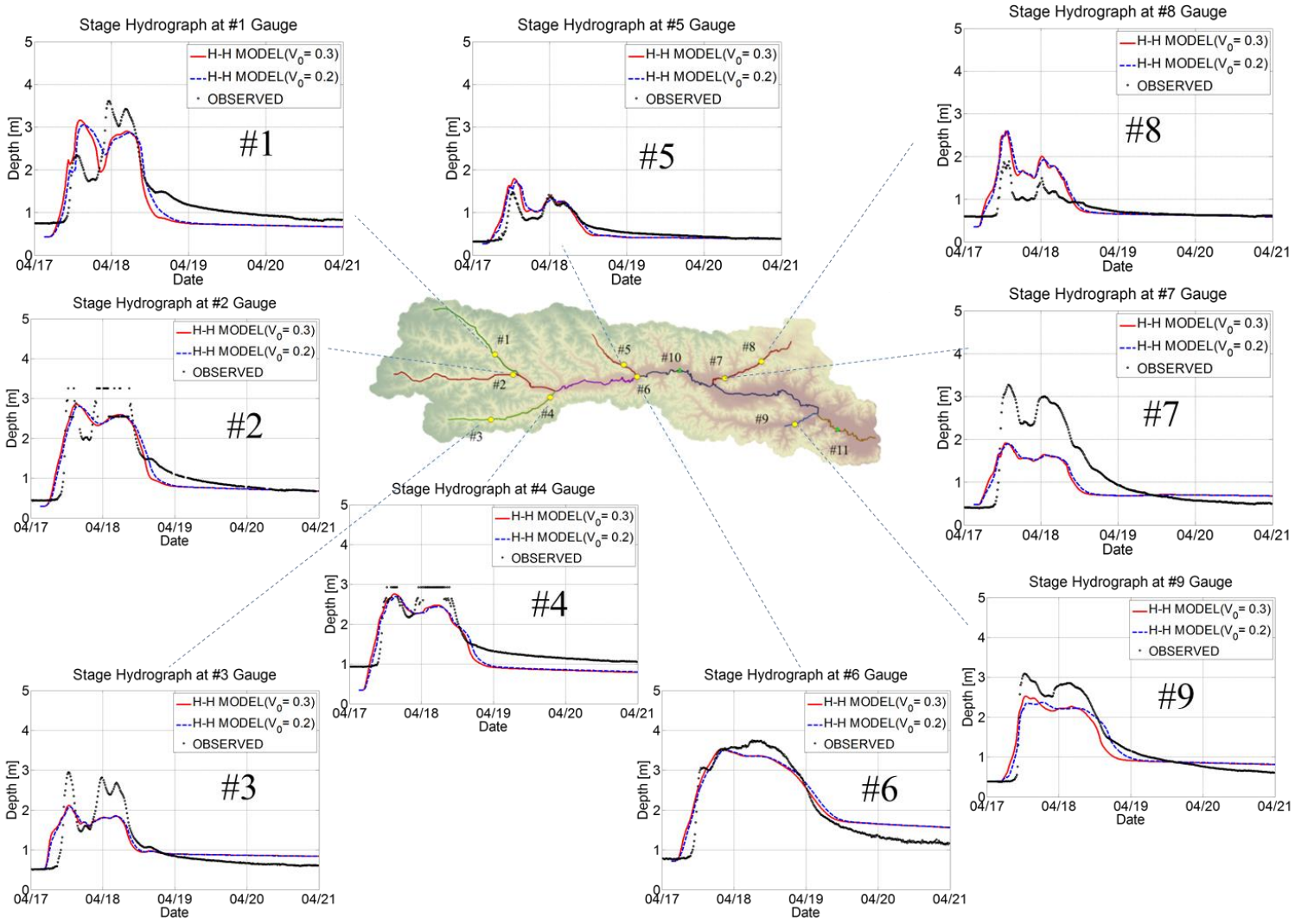

Figure 4.10. Simulated and observed stage hydrographs of the nine stations where IFC stage hydrograph were measured and comparison of discharge hydrograph from CUENCAS for case #1

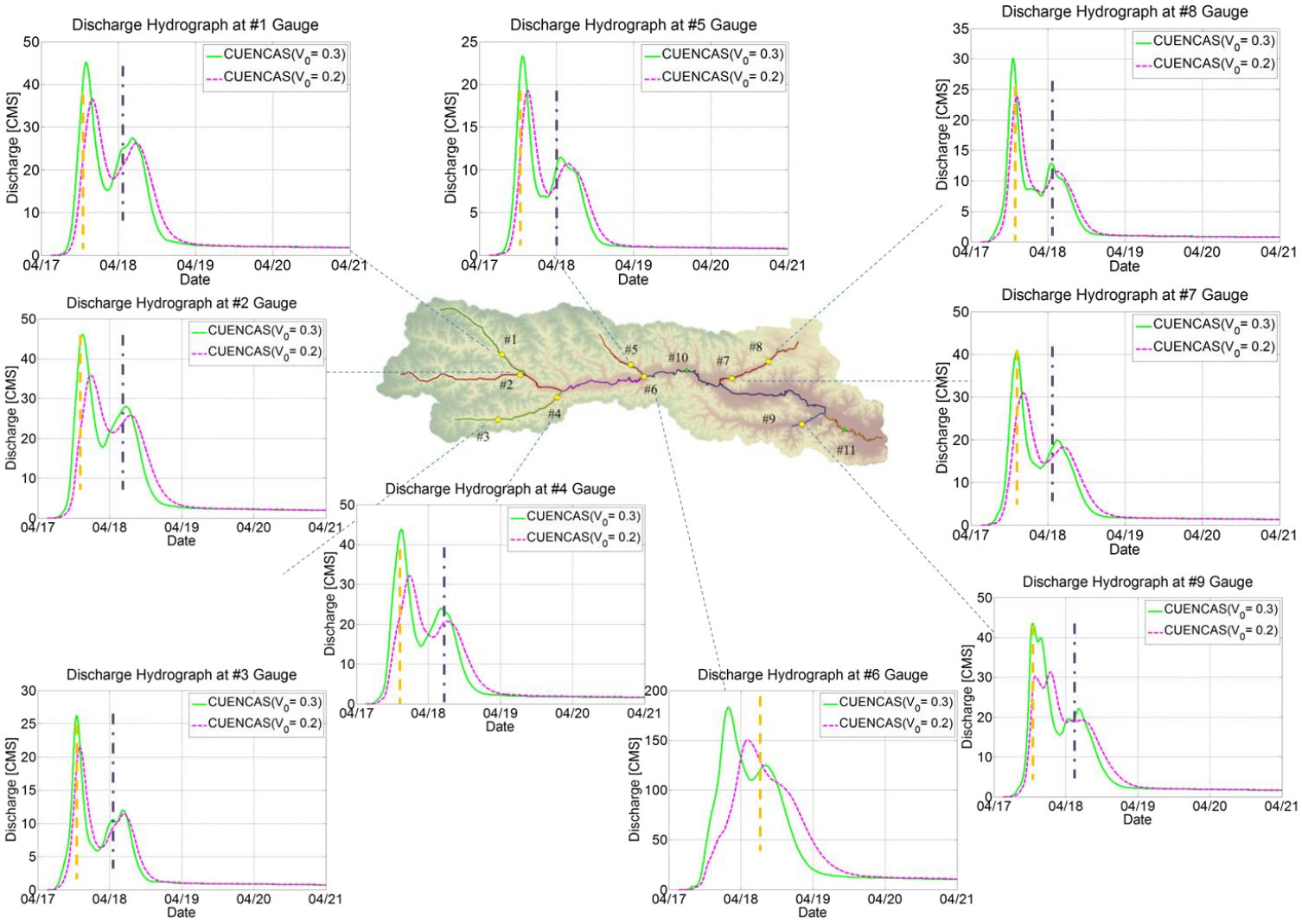

Figure 4.11. Comparisons of discharge hydrographs from CUENCAS with different channel velocities (v_0=0.3 and 0.2 m/s) to the nine stations where IFC stage hydrograph were measured. The first peak arrival time of the nine measured stage (yellow dotted lines) and the second peak arrival time of the nine measured stage (purple dotted-dash lines)

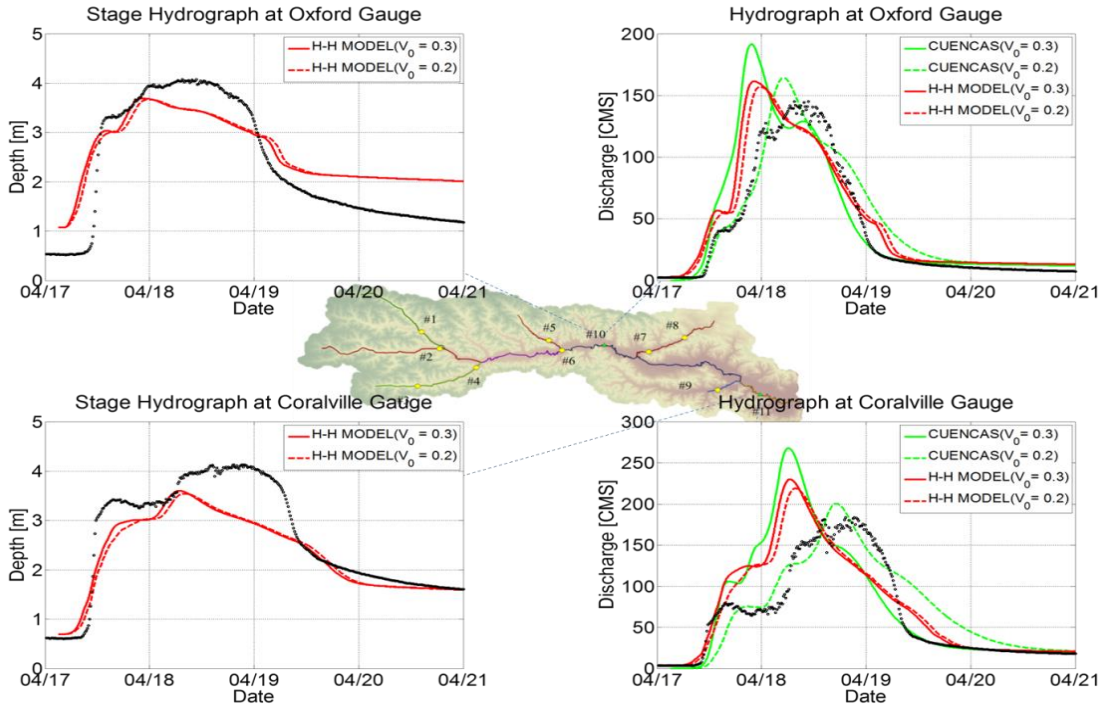

Figure 4.12. Simulated and observed stage and discharge hydrographs at Oxford (top panel) and Coralville (bottom panel) for case #1

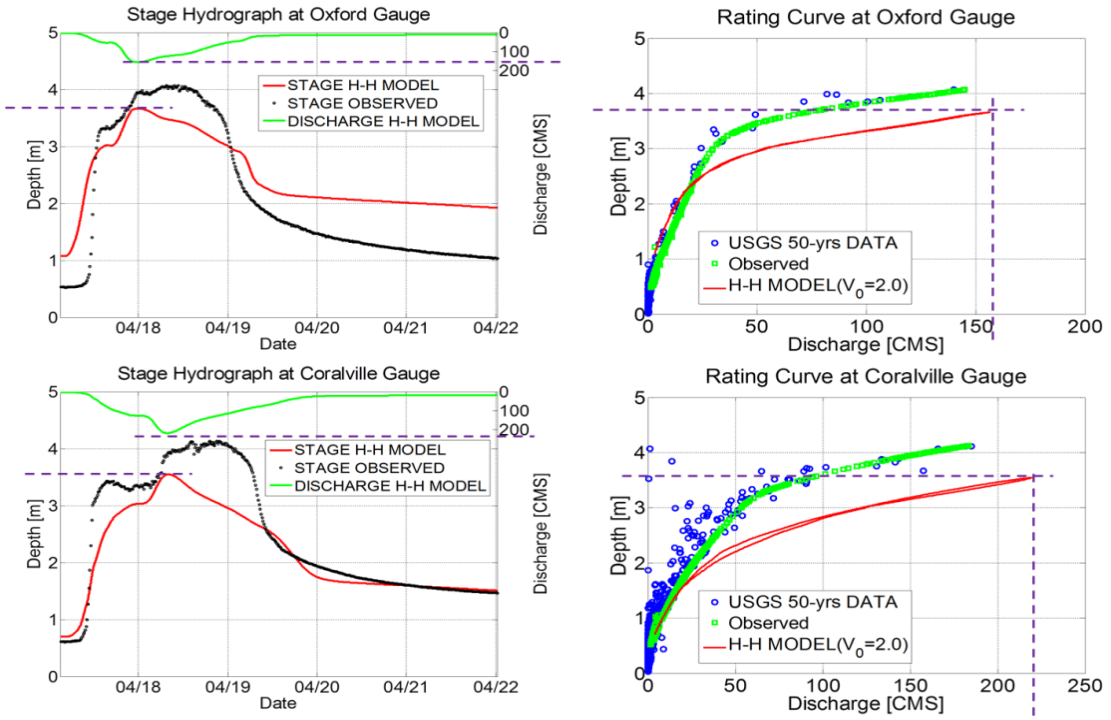

Figure 4.13. Comparison of simulated rating curve to the historical and observed rating curve at Oxford and Coralville gauge stations for case #1

4.5.2 Results of case #2 (calibrated roughness coefficients; constant runoff coefficients and artificial channelization)

The difference in channel bottom elevations between the LiDAR-derived DEM and the surveyed cross sections (Lee, personal communication) for eleven measured sites in Clear Creek Watershed ranges from 0.1 to 1.8 meter (Fig. 4.14). To minimize the effect of these factors, an artificial channelization of 0.5 m is applied for two reaches containing USGS gauge stations at Oxford and Coralville. Only two reaches with the USGS measurements are implemented because these locations provide sufficiently historical field measurements of river stage and discharge for model validation. Two 20-m width stream buffer polygons are created for these reaches. An artificial channelization means that the channel bathymetry within the polygons is deepen by an artificial value of 0.5 m, while the topography data outside the polygons remain the same (Fig. 4.15).

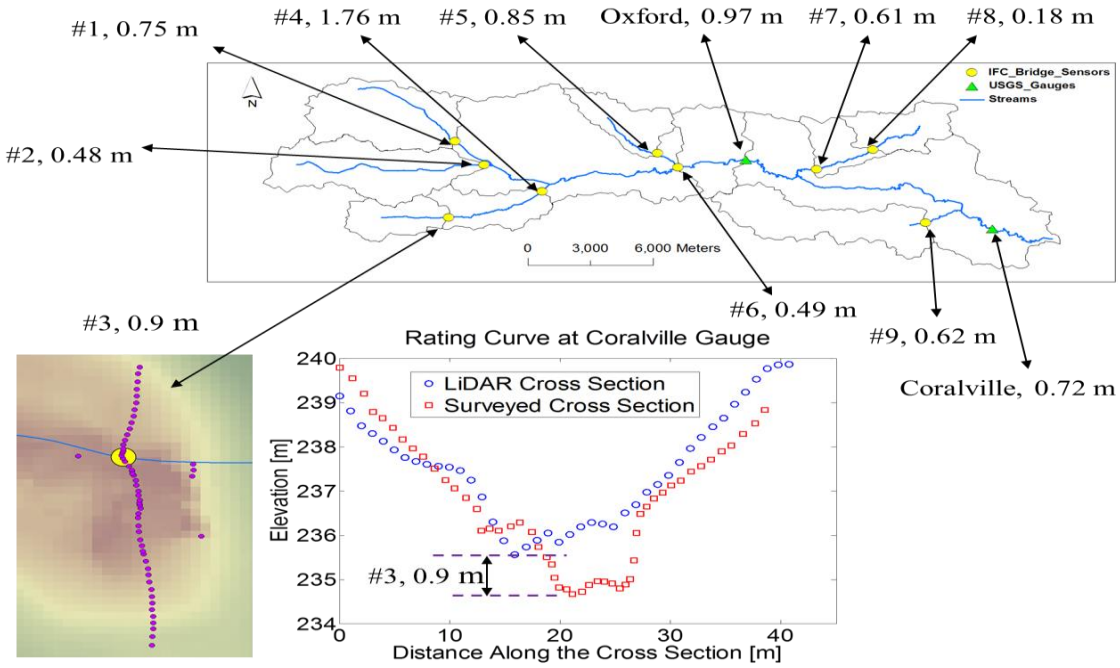

Figure 4.14. Comparison of LiDAR extracted channel bed elevations and surveyed river cross sections for 11 sites in Clear Creek Watershed, Iowa

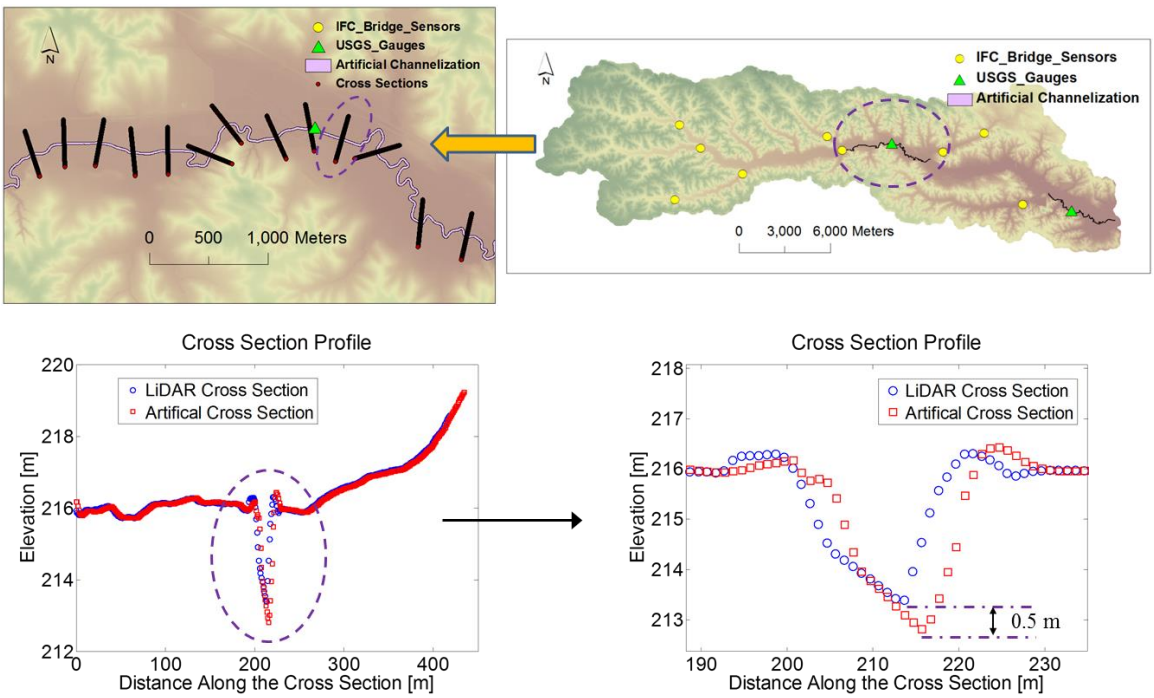

Figure 4.15. Artificial channelization of two reaches containing Oxford and Coralville gauges

According to results from the case #1, the timing of peak is matched for tributaries and appears earlier for the main stem of the river network (Fig. 4.10 and 4.12). Therefore, the floodplain roughness for the main stems (#1, #2, #5 and #7) were adjusted to slow down the flow speed for the main stem of the river networks. Figure 4.16 shows the floodplain roughness of all the reaches (#1 to #11) for case #1 (left), and the adjusted values of the floodplain roughness of all the reaches for cases #2 and #3 (right). Note that the selections of the floodplain roughness coefficients are within the reasonable ranges (i.e. 0.02 to 0.2).

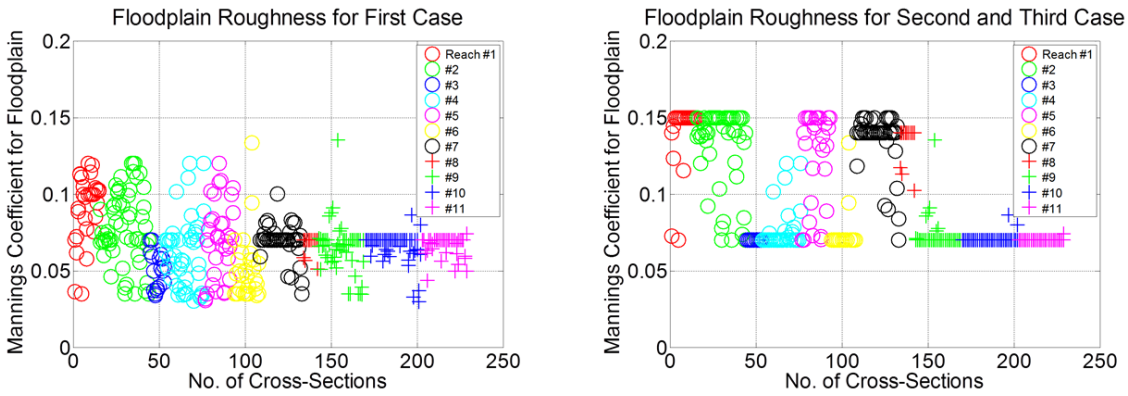

Figure 4.16. Floodplain roughness coefficients for case #1 (left) and cases # 2 and #3 (right)

By comparing the results between cases #1 and #2, the simulated hydrographs from case #2 agree better with the observed data in terms of timing of peak and peak value than case #1. In particular, the simulated hydrographs among the main stem of a river network (#6, Oxford and Coralville gauge stations) are improved (Fig 4.17 and 4.18). First, the improvement of the simulated results can be accounted by the increase of floodplain roughness coefficients among the main stem of a river network for case #1. This effect implies that the flow among the main stem of a river network tends to reach the floodplain during the period of rapid rising limb for this storm event. However, the long recession tail of the hydrograph cannot be alternated since the shape of recession limb of the hydrographs is controlled by the shape of the inflow generated from the hydrological model. In addition, the simulated rating curves of the case #2 are much closer to the historical and observed rating curve at Oxford and Coralville gauge stations than the case #1 (Fig. 4.18). Another factor that can be attributed to the improvement of the simulated results is the impact of the artificial channelization. It provides more accurate channel bed profiles that are closer to the surveyed bed elevations.

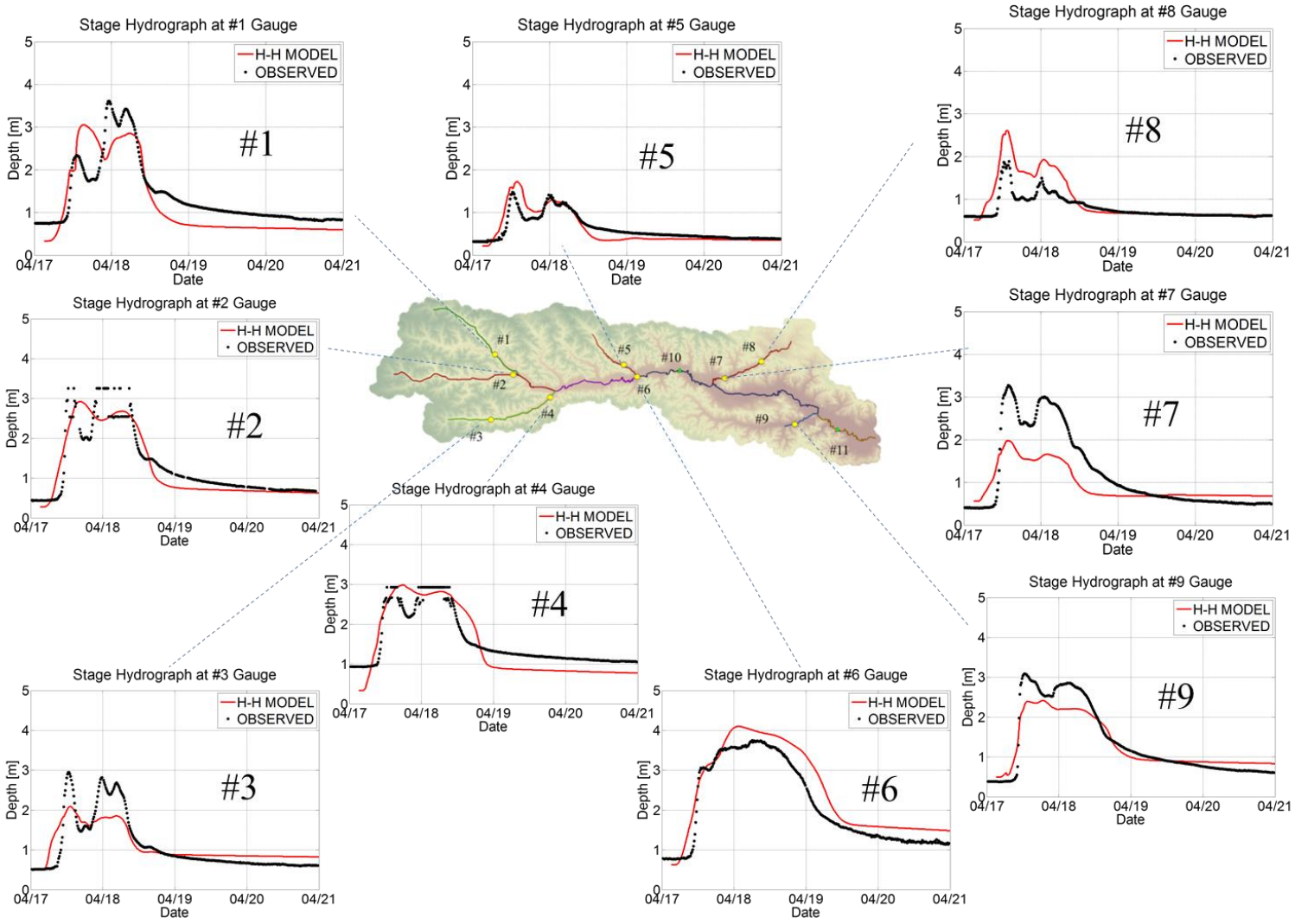

Figure 4.17. Simulated and observed stage hydrographs of the nine stations where IFC stage hydrograph were measured for case #2

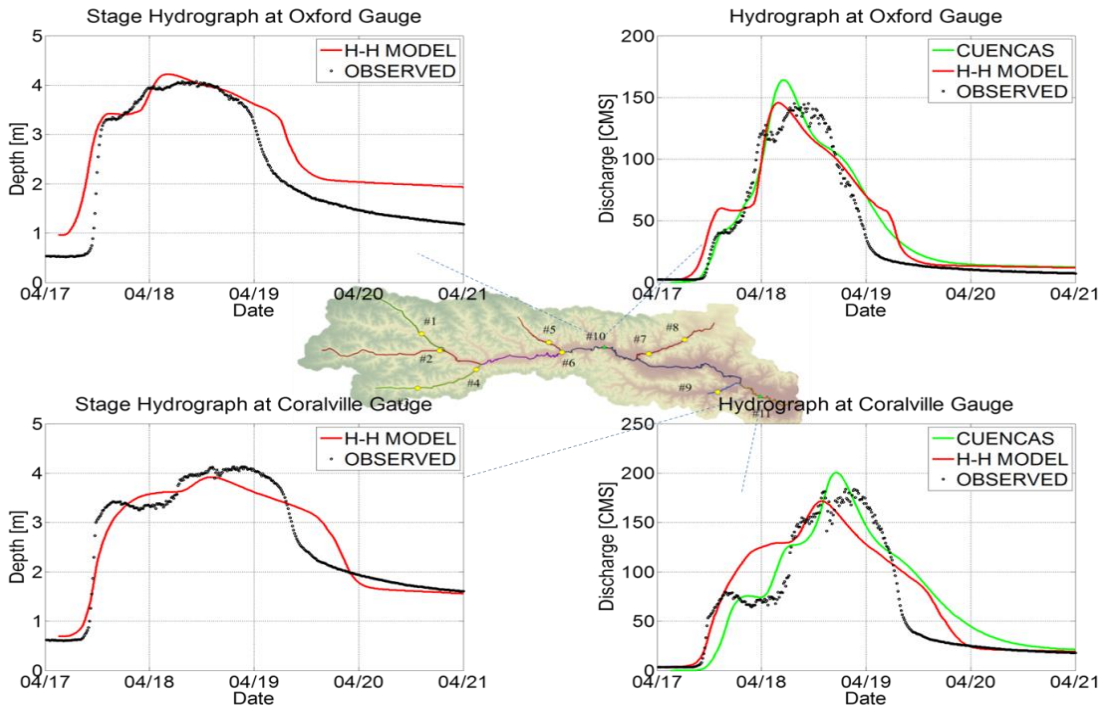

Figure 4.18. Simulated and observed stage and discharge hydrographs at Oxford (top panel) and Coralville (bottom panel) for case #2

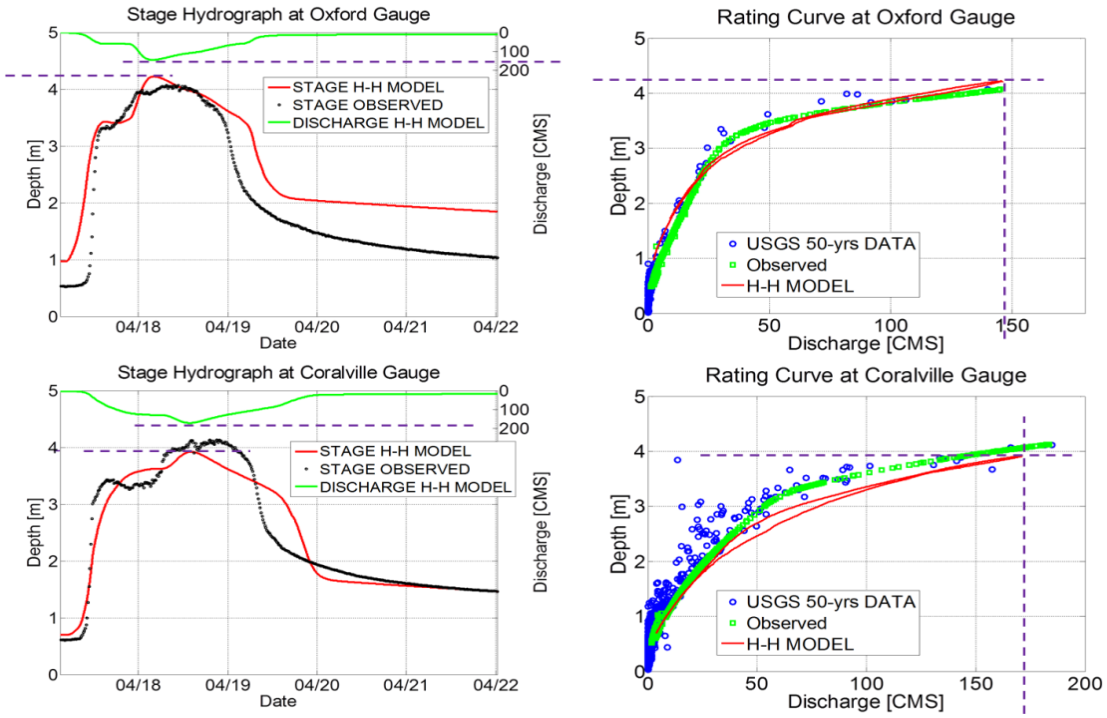

Figure 4.19. Comparison of simulated rating curve to the historical and observed rating curve at Oxford and Coralville gauge stations for case #2

4.5.3 Results of case #3 (calibrated roughness coefficients; spatial varied runoff coefficients and artificial channelization)

For case #3, results from the coupled H-H models are used to evaluate the spatial accuracy of the runoff field produced by the hydrological model. By comparing the simulated results with the measurements at multiple measured sites for the case #2, one can infer the adjustment of the spatial runoff coefficients of the hydrological model to better match the simulated stage and discharge hydrograph with the measurements at multiple locations. The adjustment sequential order follows the zoning map and the zoned sequence described in Chapter 4.4. Figure 4.20 depicts the adjusted runoff coefficients of the hydrological model used for case #3.

By comparing the results between cases #2 and #3, the simulated hydrographs from case #3 are better than case #2. Although there is slightly improvement compared with the results from the case #2, the effect of spatial varied runoff coefficients can be significant at local scale. For example, the decrease of runoff coefficient at zone #8 (0.5 to 0.25) results in peak stage reduction at gauge station #8. Similarly, the increase of runoff coefficients at zones #3, #4, #7, #9, #10 and #11 results in a small increase of peak discharge and stage at Oxford and Coralville gauge stations which are better matched with the measurements (Fig. 4.21 and 4.22). In addition, the simulated rating curves of the case #3 are even better than the one obtained in case #2 (Fig. 4.23).

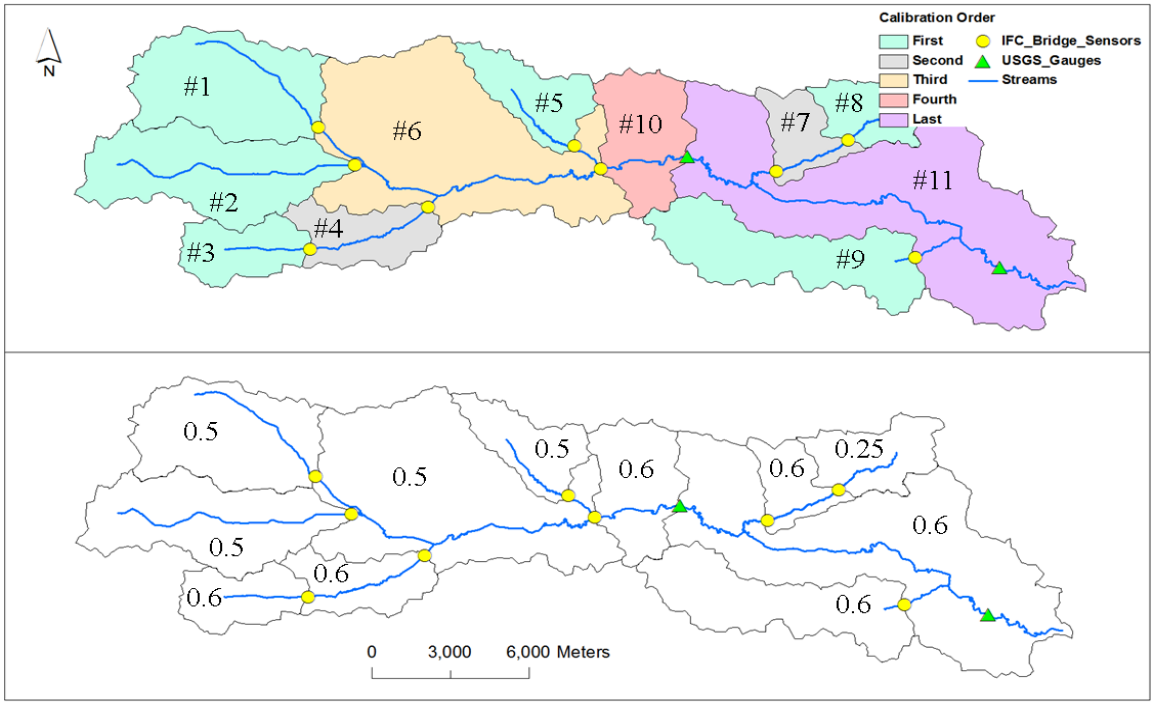

Figure 4.20. Spatial varied runoff coefficient of CUENCAS generated runoff input to coupled H-H models

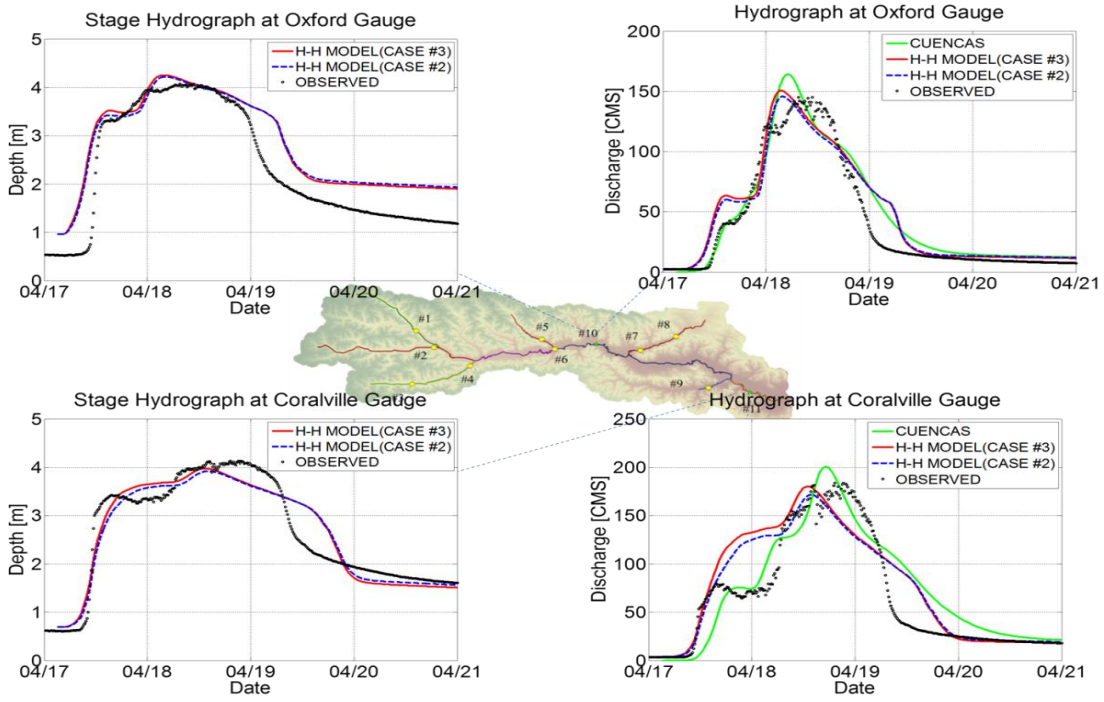

Figure 4.21. Simulated and observed stage and discharge hydrographs at Oxford (top panel) and Coralville (bottom panel) for cases #2 and #3

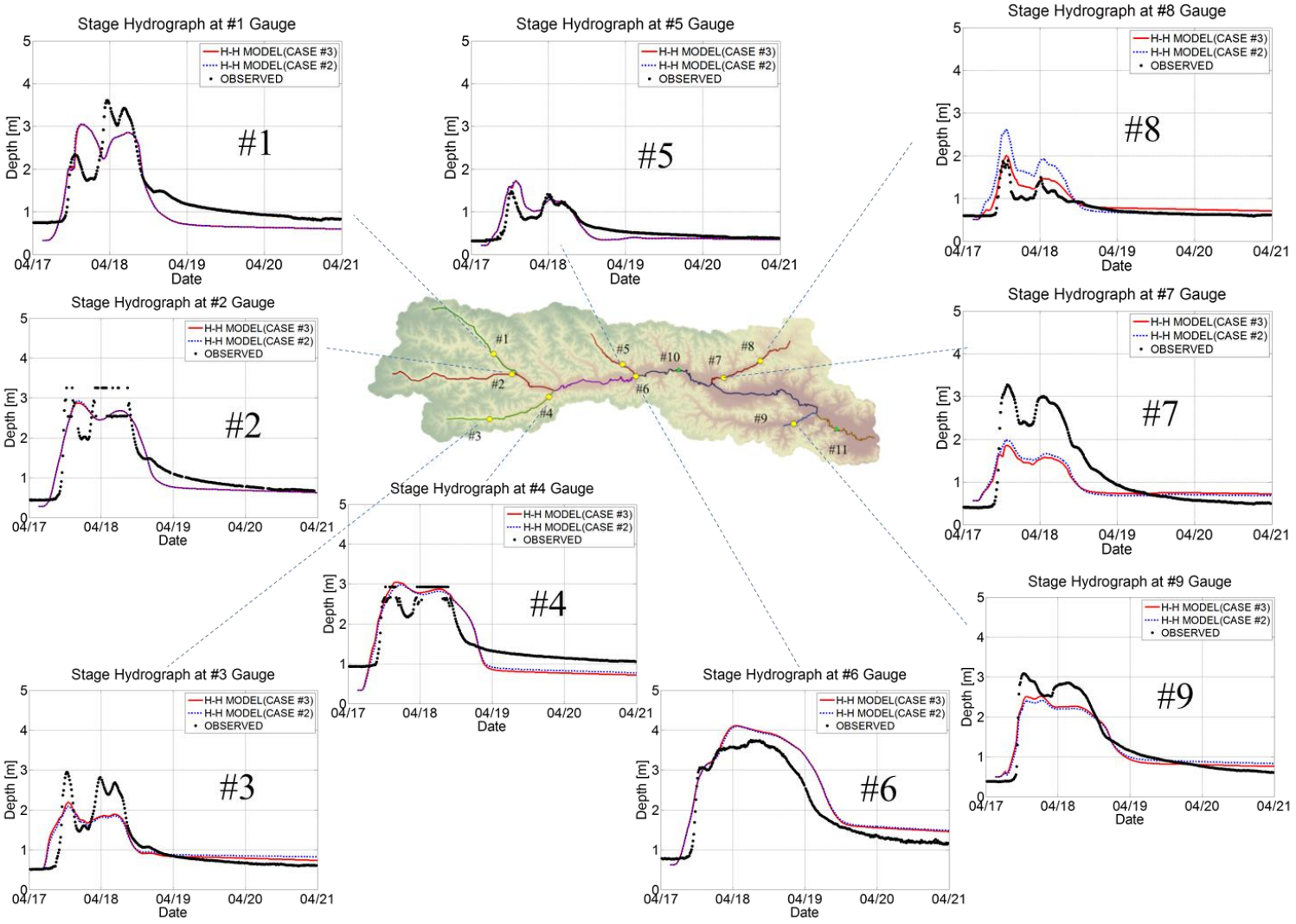

Figure 4.22. Simulated and observed stage hydrographs of the nine stations where IFC stage hydrograph were measured for cases #2 and #3

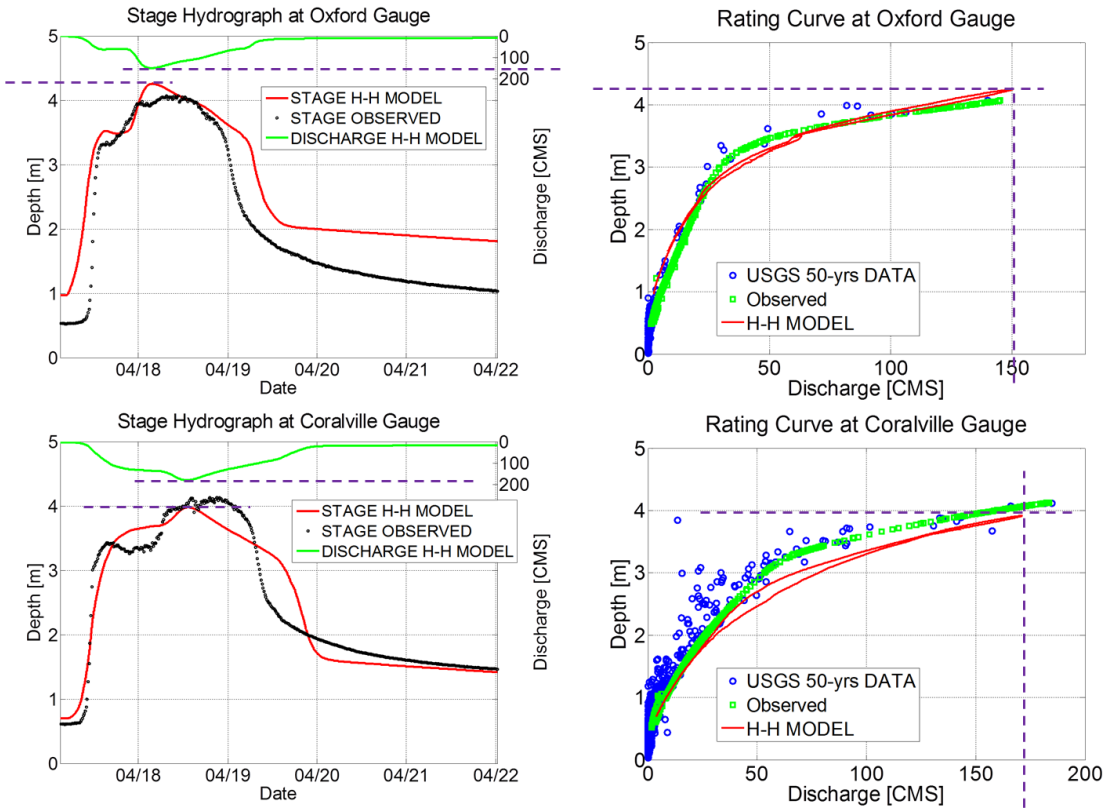

Figure 4.23. Comparison of simulated rating curve to the historical and observed rating curve at Oxford and Coralville gauge stations for case #3

4.5.4 Comparison of results for case #1, #2 and #3

By comparing the results among all three cases, the simulated hydrographs from case #3 agree the best with the observed data than cases #2 and #3 (Fig. 4.24 and 4.25). It can be accounted by the increase of floodplain roughness from cases #2 and #3. It slows down the overall flow speed so that the timing of peak of the simulated hydrographs for cases #2 and #3 agree better with the observed data than case #1 (un-calibrated floodplain roughness). The impact of the artificial channelization from cases #2 and #3 improves the stage prediction significantly at two USGS gauge stations (Oxford and Coralville) where the artificial channelization are implemented (Fig. 4.24). This result verifies that accurate stage prediction requires accurate channel bed profiles. The effect of spatial varied runoff

coefficients for case #3 improves the stage prediction locally (Fig. 4.25). The adjustment of the spatial runoff coefficients of the hydrological model is to better match the simulated stage and discharge hydrograph with the measurements at multiple locations. It controls the spatial variation of the runoff generated from the hydrological model.

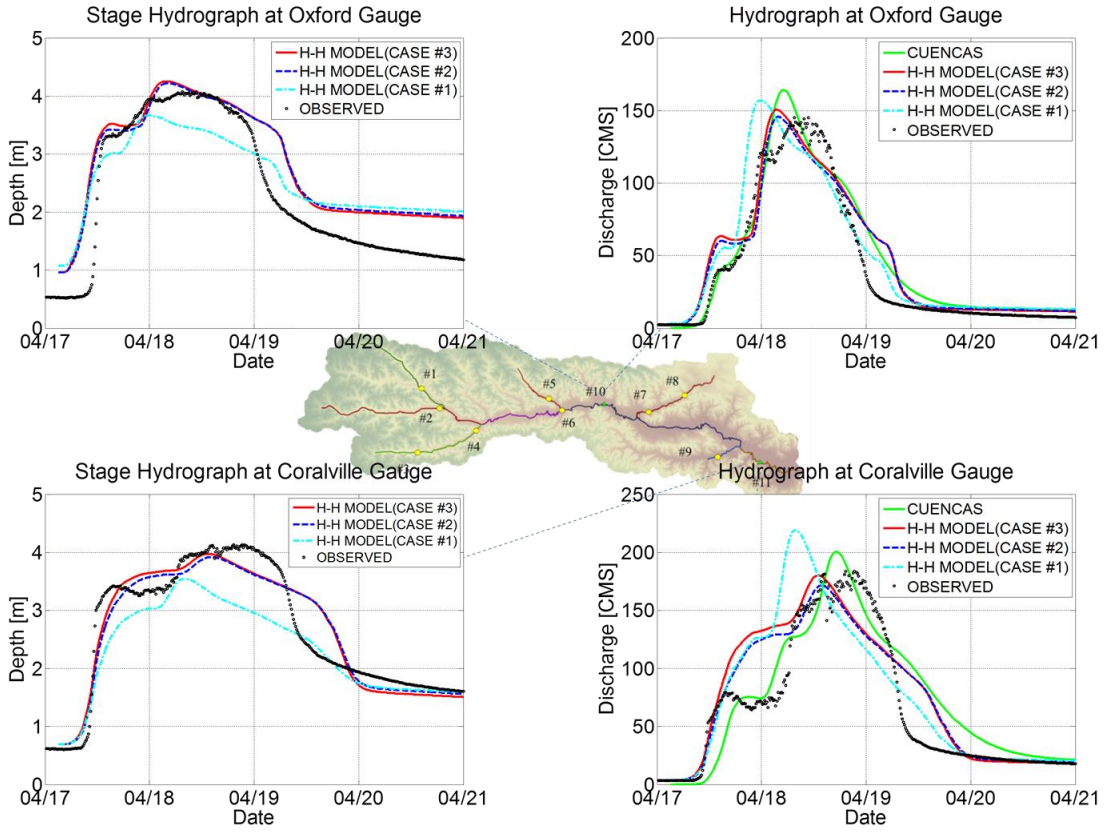

Figure 4.24. Comparison of simulated and observed stage and discharge at Oxford (top panel) and Coralville (bottom panel) for all three cases

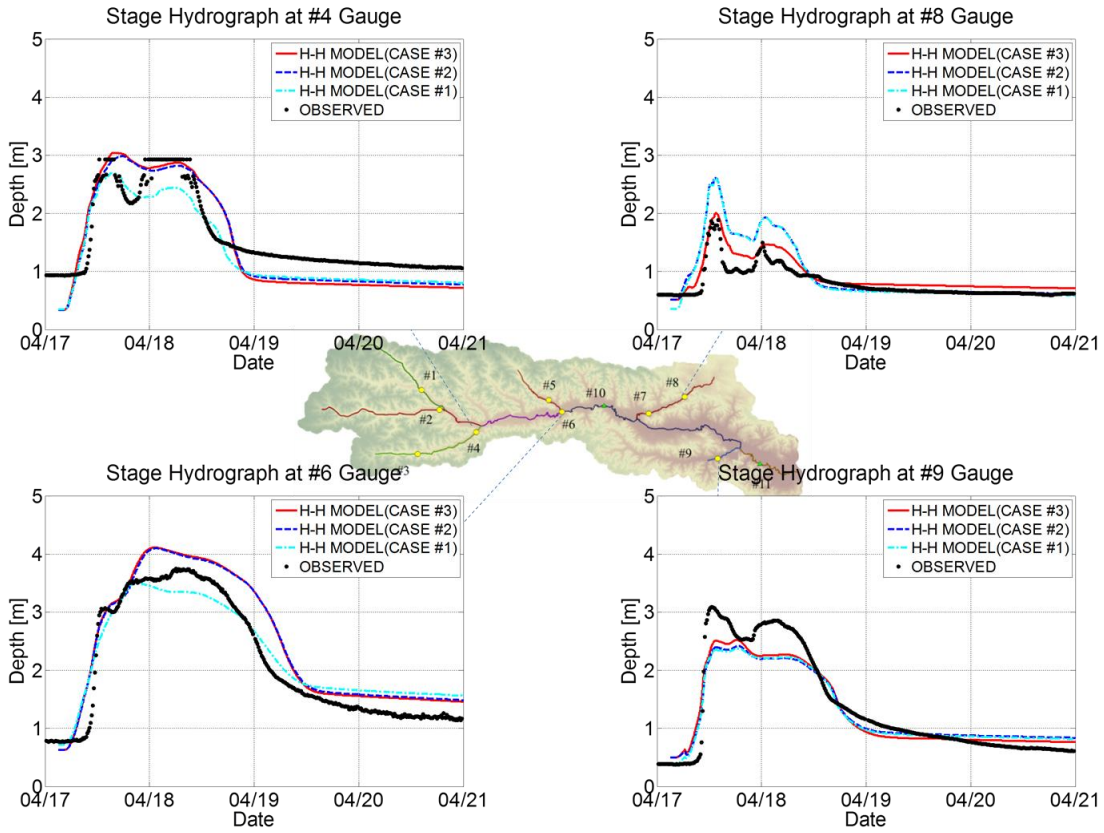

Figure 4.25. Comparison of simulated and observed stage hydrographs of the nine stations where IFC stage hydrograph were measured for all three cases

4.5.5 Parameterization of channel velocity

The empirically based storage-discharge relations (equation 4.3) used in CUENCAS are based on the non-linear flow velocity approximation as a function of the instantaneous discharge $q(e,t)$ and the upstream drainage area A_e as follows, According to equation 4.3, the flow velocity for the links can be written as,

$$v_e(t) = v_0 q(e,t)^{\lambda_1} {A_e}^{\lambda_2}$$

where v_0 is the initial velocity, λ_1 and λ_2 are the scaling exponents.

Substituting $v_e(t)$ from equation 4.3 into equation 4.2, and rewrite the expression as a function of $q(e,t)$,

$$q(e,t) = \left(v_0 C_A A^{\lambda_2}\right)^{\frac{1}{1-\lambda_1}} = K_c {C_A}^{\lambda_3} \quad (4.11)$$

where $\lambda_3 = \dfrac{1}{1-\lambda_1}$

and $K_c = \left(v_0 A^{\lambda_2}\right)^{\lambda_3}$ (4.12)

Taking the logarithms of both sides of equations 4.11 and 4.12, they become,

$$\log\left(q(e,t)\right) = \log(K_c) + \lambda_3 \log(C_A) \quad (4.13)$$

and

$$\log(K_c) = \lambda_3 \log(v_0) + \lambda_5 \log(A) \quad (4.14)$$

where $\lambda_5 = \lambda_2 \lambda_3$

To understand the difference of flow behaviour between CUENCAS and the coupled H-H models, the simulation results from 1D-SVE routing model (case #1 in previous section) are used to derive the flow velocity exponent (i.e. v_0, λ_1 and λ_2) of the ODEs system. First, 11 river cross sections relatively close to the 11 gauge stations are selected. According to equation 4.11, one can use the log-log relations between the discharge and cross-sectional area for each cross section to estimate the value of K_c, λ_3 and λ_1 by fitting the data to a linear polynomial function (Fig 4.26).

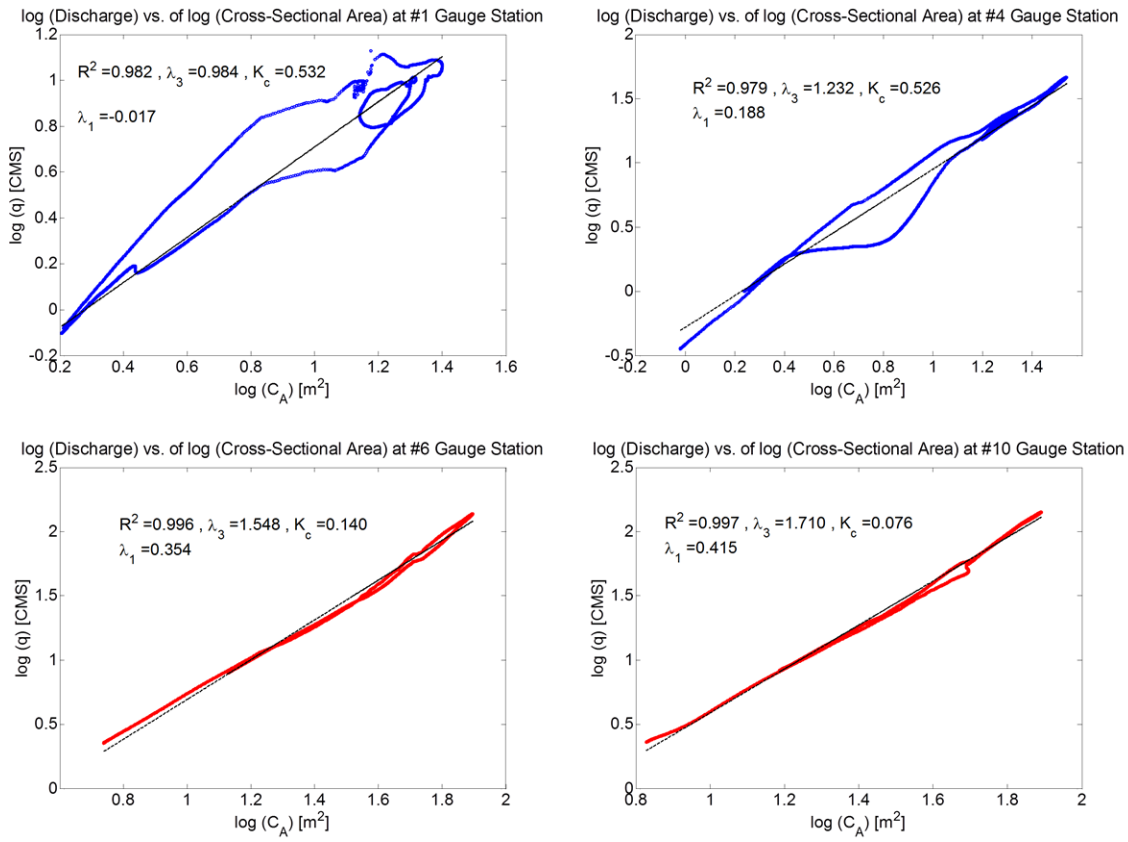

Figure 4.26. Log-log plots of discharge versus cross-sectional area for gauge stations #1, #4 (top panel), #6, #10 (bottom panel)

According to equation 4.9, one can use the log-log relations between K_c and A_e for each cross section to estimate the value of v_0, λ_1 and λ_2 by fitting the data to a linear polynomial function. The trend of the whole data set can be classified into two groups (i.e. [#1, #2, #3, #4, #5, #7, #8 and #9] and [#6, #10 and #11]). By considering the first group of the data, one can obtain a different value set of v_0, λ_1 and λ_2 (Fig 4.27 and Fig 4.28).

Results indicate that the kinematic routing assumption from CUENCAS do not totally agree with the routing solution from the 1D-SVE models. The difference between two routing approaches is more significant along the main stem of a river network rather than the tributaries. The next step is to establish a mechanism to connect direct data

observations to ODE based model parameters. By using the zoning map and zoning sequence methods described, the model parameters of the hydrological model (i.e. v_0, λ_1 and λ_2) can be adjusted through an trial and error process so as to have a better agreement between the observed and simulated stage and discharge at multiples locations. Once the calibration and validation of the coupled H-H models is finished, the derived model parameters from the coupled H-H models results are then substituted back to the links that cover the streams network from the coupled H-H models and re-run the hydrological simulation. Theoretically, the discrepancy between two different routing mechanisms can be reduced through the proposed method. The proposed mechanisms are the preliminary results that require more effort to implement for real application.

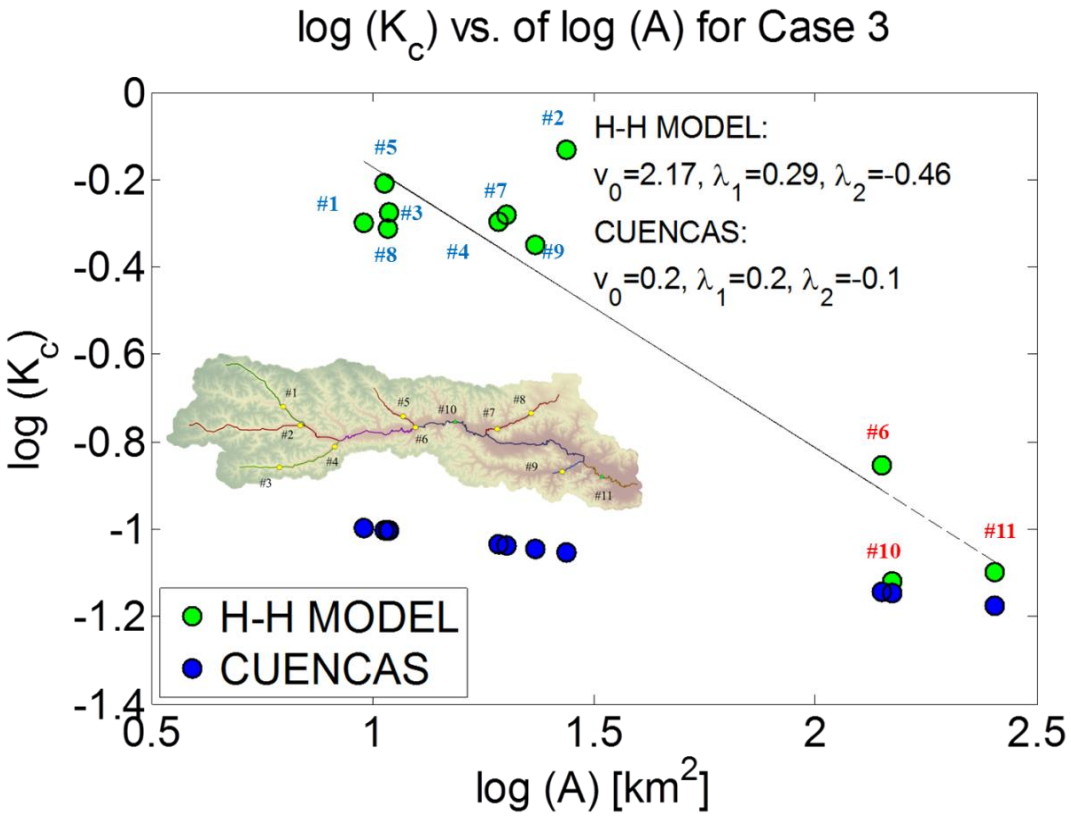

Figure 4.27. Log-log plot of K_c versus upstream drainage area, A from H-H model and CUENCAS for 11 gauge station in Clear Creek Watershed for case #3

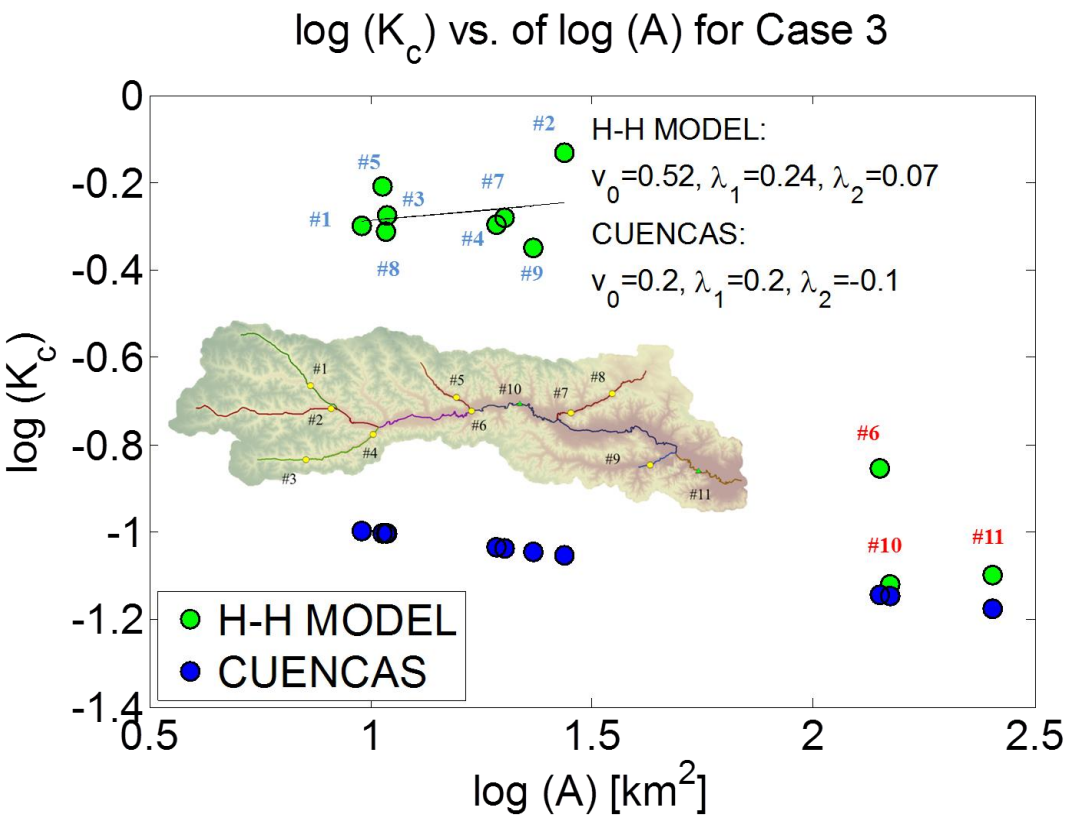

Figure 4.28. Log-log plot of K_c versus upstream drainage area, A from H-H model and CUENCAS for 8 gauge station (#1, #2, #3, #4, #5, #7, and #9) in Clear Creek Watershed for case #3

CHAPTER 5

SUMMARY

5.1 Summary

This study presents the development of a 1D-SVE solver with its own set of geo-processing tools to simulate 1D unsteady flow through a dendritic river networks. The 1D-SVE solver uses the standard four-point weighted Preissmann scheme to solve the dynamic wave form of the 1D-SVE which the channel/floodplain interaction and backwater effects due to downstream constriction can be accurately modeled. Automated GIS-based geo-processing tools are developed to streamline the process of preparing river bathymetric and model parameters for the 1D-SVE simulation. The accuracy of the 1D-SVE model is validated by comparing the simulated outflow hydrograph with a test case obtained by Choi et al. (1993) and HEC-RAS under the same model setting. Results show that the 1D-SVE models can perform comparatively accurate with other similar models (e.g. HEC-RAS).

The 1D-SVE model is externally coupled with the hillslope-based hydrological model, CUENCAS, for simulating unsteady open channel flow through a river network. The hillslope runoff generated from CUENCAS is re-distributed as the lateral inflows to the 1D-SVE model through the use of geo-processing tools. An application of the coupled H-H models is demonstrated in Clear Creek watershed, Iowa. In order to determine the spatial extent of the streams network that needed to be modeled by 1D-SVE model, the calculated average bed slopes for all the reaches within the watershed are classified into three different flood wave model types (i.e. kinematic, diffusive and dynamic) based on the NWS slope regimes classification method. A river network (11

reaches in total) comprised of streams that have diffusive/dynamic flow characteristic are delineated. It includes two USGS measurements of stage and discharges at stations (Oxford, 05404220, upstream), (Coralville, 05454300, downstream) and nine IFC river stage measurement are used for model validation and calibration. Composite river cross sections (surveyed channel bathymetry data and an arbitrary extension for the floodplain) are created for all the measured sites (11 in total). The bed elevations of the river cross sections per each reach are approximated by a 4^h degree polynomial fit method since it can better retains original bed elevation curvature.

Three case scenarios with different model parameters of the coupled H-H models are created to achieve the objectives described in Chapter 1: (1) Show that the results from the coupled H-H models can enhance hydrological model validation by providing a better spatial description of runoff field; (2) Develop a calibration/validation strategy for the coupled H-H models in the presence of dense networks of stage and discharge measurements.

The accuracy of the coupled H-H models is evaluated based on the agreement between simulated and observed stage and discharge for all the measured sites (11 in total). Moreover, the simulated rating curves are also compared with the historical and observed rating curve at Oxford and Coralville gauge stations. Results from these case scenarios indicate that the change of the channel velocities for the hydrological model does not results in significant change for the coupled H-H models results. However, the accuracy of the spatial and temporal variation of the runoff field generated from the hydrological model affect the accuracy of the results from coupled H-H models significantly. By adding more measured sites for hydrological model validation, one can

infer how accurate the spatial description of runoff field generated through the hydrologic simulation and better capture the interior flow dynamic via a dense river networks. One of the uncertainties in predicting river stage is the discrepancy of channel bed elevations estimated from the LiDAR-derived DEM and actual surveyed bed elevations which are ranged from 0.2 to 1.8 m. Therefore, artificial channelization of 0.5 m is imposed to minimize this uncertainty.

The calibration of the channel/floodplain roughness coefficients for the 1D-SVE model are used to compensate the uncertainty of river cross-sectional geometries, river morphology, bed elevation approximation and inflow boundary conditions. A trial and error method is used to adjust the floodplain roughness to best fit the observed stage and discharge measurements at multiple measured sites. After the calibration of 1D-SVE model is completed, the runoff coefficients of the hydrological model are adjusted to further match the simulated stage and discharge hydrograph with the measurements at multiple locations. The parameterization of the channel velocity for the ODE-based hydrological derived from the solutions obtained by the 1D-SVE models are investigated. Results indicate that the kinematic routing assumption from CUENCAS do not totally agree with the routing solution from the 1D-SVE models. The difference between the hydrological routing from CUENCAS and the hydraulic routing from the 1D-SVE models becomes more significant along the main stem of a river network than the tributaries that mainly comprised of kinematic wave characteristics.

5.2 Future Work

This section provides some insight on how the 1D-SVE models can be implemented and what further development can be considered. Further implementation can be considered for a watershed with more validation stage and discharge measurements and complex branching river networks. A proposed study is the implementation of the coupled H-H models on Squaw Creek in Ames with more validation stage and discharge measurements and complex branching river networks (e.g. 19 IFC bridge sensors & 3 USGS gauges, and about 20 reaches). The goal is to demonstrate that the increase of validation data enhances the hydrological model validation and the results from the coupled H-H models can provide guidance for setting up the hydrological model parameters and thus improve the flood predicative capability by better describing the interior flow dynamics over the entire basin.

The coupled H-H models can be embedded into the IFC based flood prediction model. The 1D-SVE solver is written in MATLAB and the geo-processing tools are written in PYTHON. To enhance the model performance for high computation requirement, there is a need to convert the 1D-SVE code into low-level language (e.g. C or FORTRAN language). In addition, the efficiency of the 1D-SVE solver can be improved by adjusting the developed solution algorithm to better manage the size of the active matrix storage and the banded matrix structure for system of linear equations. Throughout the modification of the proposed 1D-SVE solver, the code can be executed in parallel computing environment. Therefore, the coupled H-H models be compatible with the existing hydrological models and improve the computational efficiency of the coupled H-H models.

The coupled H-H models can be used to improve the flood predictive capability of the hydrological model where the backwater effects, flow unsteadiness and floodplain storage effects are dominant. The streams with the calculated average bed slopes can be superimposed with the streams modeled by the hydrological model to evaluate the model performance of the hydrological model for the streams that have flow dynamics characteristics. If the model performance is unsatisfactory, one can suspect that the hydrological model cannot perform well for the abovementioned situations.

Parametric studies on the effect of the model parameters of the 1D-SVE models (e.g. channel bed elevations, channel bed slope, floodplain storage dimension and channel/floodplain roughness etc.) on the coupled H-H models performance can be conducted in future. For example, what is the strategy for selecting the extent of river cross sections (200 m to 500 m?), bed slope approximation (constant bed slope or nth degree polynomial fit?) and roughness coefficients to optimize the coupled H-H models performance? Hence, the model parameters can be standardized for different watershed characteristics (e.g. watershed scale, stream size and river morphology)

REFERENCES

Abbot, M. B. "*Computational Hydraulics*: Elements of the theory of free surface flows." Pitman, London (1979).

Abbott, Michael Barry, and David R. Basco. "*Computational fluid dynamics-an introduction for engineers."* NASA STI/Recon Technical Report A 90 (1989): 51377.

Abbott, Michael B., Karsten Havno, and Sten Lindberg. "The fourth generation of numerical modelling in hydraulics." *Journal of Hydraulic Research* 29.5 (1991): 581-600.

Abshire, Kate Elizabeth. Impacts of Hydrologic and Hydraulic Model Connection Schemes on Flood Simulation and Inundation Mapping in the Tar River Basin. Diss. Duke University, 2012.

Acreman, M. C., R. Riddington, and D. J. Booker. "Hydrological impacts of floodplain restoration: a case study of the River Cherwell, UK." *Hydrology and Earth System Sciences* 7.1 (1999): 75-85.

Anderson, B. G., I. D. Rutherfurd, and A. W. Western. "An analysis of the influence of riparian vegetation on the propagation of flood waves." *Environmental Modelling & Software* 21.9 (2006): 1290-1296.

Blackburn, J., and F. E. Hicks. "Combined flood routing and flood level forecasting." *Canadian Journal of Civil Engineering* 29.1 (2002): 64-75.

Bravo, J. M., et al. "Coupled hydrologic-hydraulic modeling of the Upper Paraguay River basin." *Journal of hydrologic engineering* 17.5 (2011): 635-646.

Brunner, G.W., 2010a. HEC-RAS, River Analysis System Hydraulic Reference Manual. US Army Corps of Engineers. Hydrologic Engineering Center, Davis, 417pp.

Brunner, G.W., 2010b. HEC-RAS, River Analysis System User's Manual. US Army Corps of Engineers. Hydrologic Engineering Center, Davis, 790pp

Campbell, K. L., Kumar, S., and Johnson, H. P. 1972. "Stream straightening effects on flood-runoff characteristics." *Trans. Am. Soc. Agr. Egr.,* 151, 94–98.

Choi, G. W., and A. Molinas. "Simultaneous solution algorithm for channel network modeling." *Water resources research* 29.2 (1993): 321-328.

Cook, Aaron, and Venkatesh Merwade. "Effect of topographic data, geometric configuration and modeling approach on flood inundation mapping." *Journal of Hydrology* 377.1 (2009): 131-142.

Cunge, Jan Andrzej, Forrest M. Holly, and Adri Verwey. *Practical aspects of computational river hydraulics*. Vol. 3. 1980.

Dhakal, Nirajan, et al. "Estimation of volumetric runoff coefficients for Texas watersheds using land-use and rainfall-runoff data." *Journal of Irrigation and Drainage Engineering* 138.1 (2011): 43-54.

Di Baldassarre, Giuliano, and Pierluigi Claps. "A hydraulic study on the applicability of flood rating curves." *Hydrology Research* 42.1 (2010): 10-19.

Djordjevic, Slobodan, Dušan Prodanovic, and Godfrey A. Walters. "Simulation of transcritical flow in pipe/channel networks." *Journal of hydraulic engineering* 130.12 (2004): 1167-1178.

Fread, D. L. "Computation of stage-discharge relationships affected by unsteady flow1." JAWRA *Journal of the American Water Resources Association* 11.2 (1975): 213-228.

Fread, D. L. (1974). ‘‘Numerical properties of implicit four-point finite difference equations of unsteady flow.’’ *NOAA Technical Memorandum*

NWS HYDRO-18.Fread, D. L. "Flood routing in meandering rivers with flood plains." 3. *Symposium on Inland Waterways for Navigation, Flood Control, and Water Diversions*, Ft. Collins, Colo.(USA), 10-12 Aug 1976. ASCE, 1976.

Fread, D.L. and Smith, G.F. (1978), “Calibration Technique for 1-D Unsteady Flow Models,” *Journal Hydraulic Engr*., Vol. 104, No. HY7, pp. 1027-1044

Fread, D.L. (1985), “Channel Routing,” Chapter 14, Hydrological Forecasting, (Ed.: M.G. Anderson and T.P. Burt) John Wiley & Sons, pp. 437-503.

Freitag, Melina A., and K. W. Morton. "The Preissmann box scheme and its modification for transcritical flows." *International journal for numerical methods in engineering* 70.7 (2007): 791-811.

Getirana, Augusto CV, and Rodrigo CD Paiva. "Mapping large-scale river flow hydraulics in the Amazon Basin." *Water Resources Research* (2013).

Ghavasieh, Ahmad-Reza, Christine Poulard, and André Paquier. "Effect of roughened strips on flood propagation: Assessment on representative virtual cases and validation." *Journal of Hydrology* 318.1 (2006): 121-137.

Havno, K. and Brorsen, M., (1985), Generalised mathematical modelling system for flood analysis and flood control design, Papers 2. *International Conference on Hydraulics of Floods and Flood Control*, Cambridge, UK, BHRA, Stevenage.

Hicks, Faye E. "Hydraulic flood routing with minimal channel data: Peace River, Canada." *Canadian Journal of Civil Engineering* 23.2 (1996): 524-535.

Hicks, F. E., and T. Peacock. "Suitability of HEC-RAS for flood forecasting." *Canadian Water Resources Journal* 30.2 (2005): 159-174.

Islam, Adlul, et al. "Comparison of gradually varied flow computation algorithms for open-channel network." *Journal of irrigation and drainage engineering* 131.5 (2005): 457-465.

Johnson, T. C., M. J. Baines, and P. K. Sweby. "A box scheme for transcritical flow." *International journal for numerical methods in engineering* 55.8 (2002): 895-912.

Knebl, M. R., et al. "Regional scale flood modeling using NEXRAD rainfall, GIS, and HEC-HMS/RAS: a case study for the San Antonio River Basin Summer 2002 storm event." *Journal of Environmental Management* 75.4 (2005): 325-336.

Kutija, Vedrana. "On the numerical modelling of supercritical flow." *Journal of Hydraulic Research* 31.6 (1993): 841-858.

Kutija, Vedrana, and Caspar Jm Hewett. "Modelling of supercritical flow conditions revisited; NewC scheme." *Journal of hydraulic research* 40.2 (2002): 145-152.

Lai, Chintu. "Numerical modeling of unsteady open-channel flow." *Advances in hydroscience* 14 (1986): 161-333.

Liggett, James A., and Jean A. Cunge. "Numerical methods of solution of the unsteady flow equations." Unsteady flow in open channels 1 (1975): 89-178.

Liu, Y. B., et al. "Simulation of flood reduction by natural river rehabilitation using a distributed hydrological model." *Hydrology and Earth System Sciences* Discussions 8.6 (2004): 1129-1140.

Thomas, Nicholas Wayne. "Standard methods for the Iowa statewide floodplain mapping program." (2011).

Cunha, Luciana Kindl da. "Exploring the benefits of satellite remote sensing for flood prediction across scales." (2012).

Mantilla, Ricardo, Vijay K. Gupta, and Oscar J Mesa. "Role of coupled flow dynamics and real network structures on Hortonian scaling of peak flows." *Journal of Hydrology* 322.1 (2006): 155-167.

Meselhe, E. A., and FM Holly Jr. "Invalidity of Preissmann scheme for transcritical flow." *Journal of Hydraulic Engineering* 123.7 (1997): 652-655.

Nguyen, Quang Kim, and Hiroshi Kawano. "Simultaneous solution for flood routing in channel networks." *Journal of Hydraulic Engineering* 121.10 (1995): 744-750.

NWS: 2012, Hydrologic Information Center - Flood Loss Data, http://nws.noaa.gov/oh/hic/flood_stats/Flood_loss_time_series.shtml. [Accessed 9/25/13.]

NWS, 2009, Service Assessment Report: Central United States flooding of June 2008; 65p at http://www.weather.gov/os/assessments/pdfs/central_flooding 09.pdf

Odgen, F.L., and P.Y Julien. Mathematical Models of Small Watershed Hydrology and Applications. 1st Ed. Colorado, US: *Water Resources Publication*, LLC, 2002. 90-91. eBook.

Pai, Naresh, and Dharmendra Saraswat. "A geospatial tool for delineating streambanks." *Environmental Modelling & Software* 40 (2013): 151-159.

Paiva, Rodrigo CD, Walter Collischonn, and Carlos EM Tucci. "Large scale hydrologic and hydrodynamic modeling using limited data and a GIS based approach." *Journal of Hydrology* 406.3 (2011): 170-181.

Paiva, Rodrigo CD, Walter Collischonn, and Diogo Costa Buarque. "Validation of a full hydrodynamic model for large-scale hydrologic modelling in the Amazon." *Hydrological Processes* 27.3 (2013a): 333-346.

Paiva, Rodrigo Cauduro Dias de, et al. "Large-scale hydrologic and hydrodynamic modeling of the Amazon River basin." *Water Resources Research* (2013b).

Paz, A. R., et al. "Large-scale hydrodynamic modeling of a complex river network and floodplains." *Journal of hydrologic engineering* 15.2 (2009): 152-165.

Paz, Adriano Rolim da, et al. "Large-scale modelling of channel flow and floodplain inundation dynamics and its application to the Pantanal (Brazil)." *Hydrological processes* 25.9 (2011): 1498-1516.

Pramanik, N., Panda, R., Sen, D., 2010. One dimensional hydrodynamic modeling of river flow using DEM extracted river cross-sections. *Water Resources Management* 24 (5), 835e852.

Ponce, Victor Miguel, Daryl B. Simons, and Ruh-Ming Li. "Applicability of kinematic and diffusion models." *Journal of the Hydraulics Division* 104.3 (1978): 353-360.

Ponce, Victor M. "Kinematic wave controversy." *Journal of Hydraulic Engineering* 117.4 (1991): 511-525.

Reed, S. (2010). Lessons Learned from Transitioning NWS Operational Hydraulic Models to HEC-RAS. Presented at the *ASCE-EWRI World Water Congress 2010*, Providence, RI.

Sart, Caroline, et al. "Adaptation of Preissmann's scheme for transcritical open channel flows." *Journal of Hydraulic Research* 48.4 (2010): 428-440.

Schaffarnek, R. W., Baltzer, R. A. and Goldberg, D. E. (1981). "A model for simulation of flows in singular and interconnected channels". *Techniques of Water-Resources Investigation Report, Book, Chapter C3*, U.S. Geological Survey, Denver

Sen, D. J., and N. K. Garg. "Efficient solution technique for dendritic channel networks using FEM." *Journal of Hydraulic Engineering* 124.8 (1998): 831-839.

Sen, D. J., and N. K. Garg. "Efficient algorithm for gradually varied flows in channel networks." *Journal of irrigation and drainage engineering* 128.6 (2002): 351-357.

Sholtes, Joel S., and Martin W. Doyle. "Effect of channel restoration on flood wave attenuation." *Journal of Hydraulic Engineering* 137.2 (2010): 196-208.

Strelkoff, Theodor. "Numerical solution of Saint-Venant equations." *Journal of the Hydraulics Division* 96.1 (1970): 223-252.

Strelkoff, T. S., and H. T. Falvey. "Numerical methods used to model unsteady canal flow." *Journal of irrigation and drainage engineering* 119.4 (1993): 637-655.

Thomas, N. (2011). Standard Methods for the Iowa Statewide Floodplain Mapping Program.

Turner-Gillespie, Daniel F., James A. Smith, and Paul D. Bates. "Attenuating reaches and the regional flood response of an urbanizing drainage basin." *Advances in Water Resources* 26.6 (2003): 673-684.

Vieira, D.A. and Wu, W. (2000), "One-dimensional channel network model CCHE1D 2.0 – User's manual," *Technical Report No. NCCHE-TR-2000-2*, National Center for Computational Hydroscience and Engineering, The University of Mississippi.

Wolff, C. Gary, and Stephen J. Burges. "An analysis of the influence of river channel properties on flood frequency." *Journal of Hydrology* 153.1 (1994): 317-337.

Woltemade, Christopher J., and Kenneth W. Potter. "A watershed modeling analysis of fluvial geomorphologic influences on flood peak attenuation." *Water Resources Research* 30.6 (1994): 1933-1942.

Zeng, J. " Development and Validation of a Fully Three-Dimensional Sediment Transport Numerical Model for Application to River Flows" (2006).